Dear Editor,

We would like to thank the two referees for their helpful comments, which have been fully taken into account upon manuscript revision. A point-by-point response to all the comments and a revised manuscript were uploaded.

Best Regards
Nan Ma and co-authors

Response to comments of referee #1

General comments

This paper presents a detailed analysis of instrumental measurements of particle physics and their cloud condensation parameters during an intensive field campaign in a highly polluted region of the North China Plain. The analysis focused on the CCN activity potential of the particles in the 20 to 200nm size range. CCN activation ratio data are unique for this region and provide results of value to the wider atmospheric sciences and cloud physics community. Chemical analysis for the size range of particles most important for CCN activity of the total particle population is lacking. The measurement of hygroscopic growth factor helps in understanding the CCN of the several events and indicated a chemical effect but the compounds or groups of compounds causing this effect cannot be identified with certainty. The data presentation via graphs is generally clear, quantitative and provides an excellent integral overview.

Reply:

Thanks for the comment.

It was a pity that we have no online measurement of chemical composition of nucleation mode particles during the NPF events. Actually, our collaborator did AMS measurement during the joint intensive campaign. Unfortunately, we met some problem during transporting of our mobile laboratory. Our measurement therefore started too late and has no overlap with AMS measurement in the campaign.

However, we did particle volatility measurement with a volatility tandem differential mobility analyzer (TROPOS-type VTDMA; Philippin et al., 2004) during the campaign. The hygroscopicity and volatility of nanoparticles as measured by the HTDMA and VTDMA is often invoked to provide insight into the particle composition (Zhang et al., 2011). We therefore decided to involve this dataset in our study, together with hygroscopicity data, to provide some additional information about the new particles.

Our study aimed at evaluating the variability of the CCN activity during NPF events in an anthropogenically polluted atmosphere and the applicability of some simplified CCN parameterization. The online measurements of hygroscopicity and volatility of new particles can already provide indication for distinguishing different NPF types. Without direct measurement of chemical composition, to be more accurate, in the revised manuscript, the two NPF types were termed MH-type NPF (more-hygroscopic type NPF) and LH-type NPF (less-hygroscopic NPF), instead of sulfate-dominant NPF and OM-dominant NPF. And we built most of the discussion in section 3.1 and 3.2 on the basis of HTDMA and VTDMA measurements, instead of on PM10 chemical composition data. In the response to the specific comments, there is more detailed information about this.

Specific comments

Reviewer:

Abstract and introduction: Mention of region and season is made. The data base of the study is different event types in one region, NCP, over one four week time period. Thus, it would be more accurate and

clear to refer to the results in terms of a case study of NPF type, i.e., based on your NCP PNSD and chemical composition data for the summertime campaign.

Reply:

Thanks for the comment.

We have revised the abstract as "…We investigated size-resolved activation ratio as well as particle number size distribution, hygroscopicity and volatility during a 4-week intensive field experiment in summertime at a regional atmospheric observatory at Xianghe. Interestingly, based on a case study, two types of NPF events were found, in which the newly formed particles exhibited either a higher or a lower hygroscopicity…". And in the introduction, we have revised the last sentence as "…we have therefore undertaken to investigate and understand the contribution and influence of NPF on particle CCN activity, based on a case study in summertime in the NCP"

Reviewer:

Page 2 line 18: i.e. at least up to 50 nm. This value of critical diameter depends on supersaturation in the parcel as it cools below the dew point temperature by lifting, radiation or mixing. For fog and low level stratus with limited vertical motion the Dcrit may be around 50 nm. For stratocumulus it may be closer to 30 nm. For cumulus, less than 30 nm. Your point about growth by condensation (and some coagulation) determining the relative organic vs. inorganic (with greater vs. lesser water solubility) chemical composition of the CCN is still valid. A volume growth factor of 10^4 to 10^5 is still needed.

Reply:

Thanks for the comment. The sentence has been revised as: "To become effective CCN, newly formed particles need to grow about 10^4 to 10^5 times in volume (i.e. to about 30 to 50 nm, depending on cloud types)"

Reviewer:

Line 20: It should be mentioned that, although particle size is the parameter of primary importance, chemical composition does modify the PNSD-based CCN determination by affecting the hygroscopicity or solubility of the potential CCN particle. But this effect is only significant for particles at or slightly greater than Dcrit . However, if the condensing vapor causing NP growth has a strong surfactant effect that lowers the water vapor accommodation coefficient or diffusion of condensed water during cloud droplet formation from the particle's surface into its volume, then the chemical composition effect on CCN fraction may extend to Dp much larger than Dcrit .

Reply:

Many thanks for the comprehensive explanation. The sentence has been expanded as: "Although particle size is the parameter of primary importance, chemical composition does modify the PNSD-based CCN determination by affecting the hygroscopicity or solubility of the potential CCN particles. But this effect is

only significant for particles at or slightly greater than $D_{P,cri}$. However, if the condensing vapor causing particle growth has a strong surfactant effect that lowers the water vapor accommodation coefficient or diffusion of condensed water during cloud droplet formation from the particle's surface into its volume, then the chemical composition effect on CCN fraction may extend to diameter much larger than $D_{P,cri}$."

Reviewer:

Page 3, line 9: State the particle size range. ... particle size range from xx to xxx nm.

Reply:

The sentence has been revised as "…microphysical and optical properties of aerosol particles over the size range from 10 nm to 10 μm were measured at Xianghe station…"

Reviewer:

line 12: Was the data during locally influenced time periods eliminated from the analysis? What hours constituted daytime? Does it match the chemical sampling schedule? Was this simply determined by hour of the day or was there meteorological input such as inversion height, thermal stability, wind speed?

Reply:

The daytime period is roughly defined as from 09:00 to 18:00, i.e. between the morning rush hour and evening rush hour. This definition is actually based on aerosol measurements. Figure R1 shows the campaign-average diurnal variation of particle number size distribution, BC mass concentration (m_{BC}) and single scattering albedo (ω). We can see during the time period between 09:00 and 18:00 LT, the average PNSD is basically dominated by the new particle formation without indication of local emission. BC mass concentration stays in a relatively low level and single scattering albedo is around 0.9. Since the anthropogenic emission is low and the boundary layer is well mixed in daytime in summer, the daytime measurements are assumed to be more representative of the background of the region.

In the 5 days used in this study, we did not find visible influence of local anthropogenic emission on our measurements during daytime. But the influence is always obvious in the evening, as shown in Fig.3 and 6 in manuscript. Since we mainly focused on the new particle formation in daytime, the locally influenced time periods (in nighttime) was not eliminated in the figures.

The chemical sampling always started at 06:00 and 18:00, and lasted for 12 hours. Considering the PM10 chemical composition data is not appropriate for this analysis, we decided to remove most of the content about PM10 data.

The hours constituting daytime and nighttime are now given in the text.

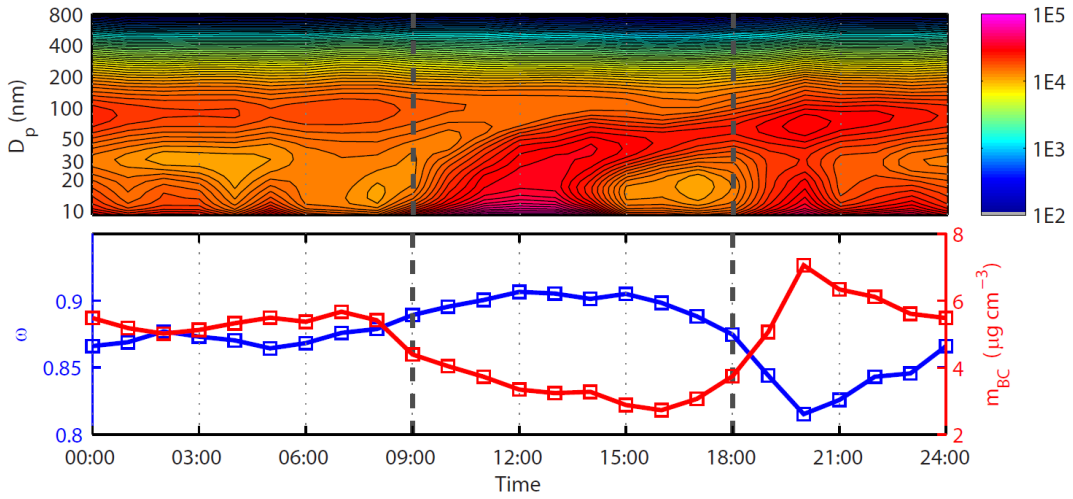

Figure R1. Average diurnal variation of particle number size distribution (upper), single scattering albedo and mass concentration of black carbon (lower).

Reviewer:

Line 15: Does "Inc., Thermo," refer to the nafion dryer?

Reply:

"Rupprecht & Patashnick Co., Inc., Thermo" refers to the PM10 impactor inlet. The Nafion dryer is made by Leibniz-Institute for Tropospheric Research. This information has been added in the text: "…three in-line Nafion dryers (Leibniz-Institute for Tropospheric Research, Germany; Wiedensohler et al., 2013) and…"

Reviewer:

Page 4, line 4: What was the particle diameter range of the DMA-CCNC system? Does it match the SMPS system? What was the time resolution of the AR measurement system? Was it operated in a scanning or stepping mode? If the latter, what was the step interval?

Reply:

The diameter range of the DMA-CCNC system is about from 9 to 300 nm. The diameter range of SMPS (TROPOS-type, for the measurement of PNSD) is from 9 to 800 nm. The reason we only measured up to 300 nm for DMA-CCNC is listed as following.

1) The aerosol flow in DMA is 1.5 lpm. To keep a proper aerosol to sheath flow ratio, the sheath flow is high. Therefore the upper limit of the size range is about 300 nm.

2) We mainly focused on the ascending part of the activation curve. Most particles larger than 300 nm were activated at the applied supersaturation.

The DMA-CCNC system is operated in a size-scanning mode. The time resolution of a full scan (5 supersaturaitons, 2 full-size scan for each supersaturation) is about 1 hour. In the text we have added: "The system is operated in a size-scanning mode" and "The time resolution of a full scan (size-resolved activation ratios at 5 SS) is 1 hour"

Reviewer:

Line 11 "The size-resolved particle activation ratio was then inverted ... " I understand the general idea here but not the details. You have AR for specific SS and Dp values. Eventually you determine the activation ratio curve, as the function AR(Dp,SS) used in Eqn. 2. The inversion operation is not clear; maybe it is not needed if explained in Deng 2011.

Reply:

The inversion algorithm applied in this study is similar like that given in Deng et al. (2011), but some improvement was made. The algorithm in Deng et al. (2011) only corrects the effect of multiple charges. The algorithm applied in this study also considered the width of the DMA transfer function. The improved algorithm has been published in Acta Scientiarum Naturalium Universitatis Pekinensis (in Chinese), this paper (Deng et al., 2012) has been added in the reference. In the following we provide a brief description of the new algorithm.

Assuming the voltage of a DMA is set to V_i $(i=1,2,...,I)$ to select particles with electrical mobility of Z_{pi} $(i=1,2,...,I)$. The CCN number concentrations measured by CCNC are

$$R_i = \int_0^\infty G(i,x)A(x)n(x)dx \quad (1)$$

where, $x=\log D_p$, $A(x)$ is activation ratio, $n(x)$ is the inverted PNSD. Kernel function $G(i,x)$ can be expressed as

$$G(i,x) = \sum_{\upsilon=1}^{\infty} \phi(x,\upsilon)\Omega(x,\upsilon,i) \quad (2)$$

where, $\phi(x,\upsilon)$ is the probability of a *x*-size particle taking υ elementary charges, and $\Omega(x,\upsilon,i)$ is DMA transfer function (i.e. probability of *x*-size particle with υ elementary charges "surviving" in the output aerosol flow of DMA with voltage of V_i).

Now we need to solve equation (1) to get $A(x)$ from measured R_i and $n(x)$. To solve equation (1), the integration is discretized into *j*-1 intervals ($x_{\text{int},j}$ $(j=1,2,...,J)$) which are much finer than the measured size bins (about 1/50). The activation ratio at $x_{\text{int},j}$ can be expressed with the activation ratio at measured sizes:

$$A(x_{\text{int},j}) = A(x_{i(j)}) + P_{i(j)}(x_{\text{int},j} - x_{i(j)}) \quad (3)$$

$i(j)$ is the ordinal of the measured size closest to $x_{\text{int},j}$. $P_{i(j)}$ can be derived with linear fitting of the 5 activation ratios at sizes close to $x_{\text{int},j}$. Then, equation (1) can be written as

$$R_i = \Delta x_{\text{int}} \sum_{j=1}^{J} G\left(i, x_{\text{int},j}\right) A\left(x_{\text{int},j}\right) n\left(x_{\text{int},j}\right) \quad (4)$$

We can set $H_{ij} = \Delta x_{\text{int}} G\left(i, x_{\text{int},j}\right) n\left(x_{\text{int},j}\right)$. Then equation (4) can be written as

$$R_i = \sum_{j=1}^{J} H_{ij} A\left(x_{\text{int},j}\right) \quad (5)$$

Considering equation (3), equation (5) can be expressed as

$$\begin{aligned} R_i &= \sum_{j=1}^{J} H_{ij} \left[A\left(x_{i(j)}\right) + P_{i(j)} \left(x_{\text{int},j} - x_{i(j)}\right) \right] \\ &= \sum_{j=1}^{J} H_{ij} A\left(x_{i(j)}\right) + \sum_{j=1}^{J} H_{ij} P_{i(j)} x_{\text{int},j} - \sum_{j=1}^{J} H_{ij} P_{i(j)} x_{i(j)} \quad (6) \\ &= \sum_{k=1}^{I} Q_{ik} A\left(x_k\right) + \sum_{k=1}^{I} T_{ik} P_k - \sum_{k=1}^{I} Q_{ik} P_k x_k \end{aligned}$$

where,

$$Q_{ik} = \sum_{j=1}^{J} H_{ij} \delta\left(i(j) - k\right) \quad (7)$$

$$T_{ik} = \sum_{j=1}^{J} H_{ij} x_{\text{int},j} \delta\left(i(j) - k\right) \quad (8)$$

$$\delta(x) = \begin{cases} 0, & x \neq 0 \\ 1, & x = 0 \end{cases} \quad (9)$$

We can set $S_i = R_i - \sum_{k=1}^{I} T_{ik} P_k + \sum_{k=1}^{I} Q_{ik} P_k x_k$ which is known. Then equation (6) can be written as

$$S_i = \sum_{k=1}^{I} Q_{ik} A\left(x_k\right) \quad (10)$$

Equation set (10) then can be solved by applying nonnegative least squares to minimize $\|\mathbf{S} - \mathbf{QA}\|$.

Reviewer:

Line 14: Was the SS calibration done with monodisperse particles of known chemical composition?

Reply:

Yes. To make it clear, the sentence has been rewritten as "The SS of CCN counter were calibrated before the campaign and checked at the end of the campaign with monodisperse ammonium sulfate particles (Rose et al., 2008)"

Reviewer:

Line 23: Were the TDMA calibration ammonium sulfate particles monodisperse?

Reply:

Yes. The effective RH of HTDMA was calibrated with monodisperse ammonium sulfate particles automatically every 6 hours. We have revised the corresponding sentence in section 2.4 as "Calibration with monodisperse ammonium sulfate particles was automatically conducted every 6 hours".

Reviewer:

Page 5, Figure 2: The details of the PNSD data that are discussed are not clear to this reader even at 300% magnification due to the high time and size variability of the data. This could perhaps improved by smoothing of the contours. The fine structure in the data is not needed to convey the general features such as "nucleation mode did not start at the lower detection limit of our SMPS", and the beginning and end of particle growth by condensation of vapors. A quantitative label for color scale is needed for panels 1 and 2. The hygroscopic growth at 50 nm is most germane to understanding CCN activation; however -PDF at other diameters would be of interest, perhaps as a supplement to the manuscript.

Reply:

Thanks for the suggestions. We have smoothed the PNSD data before making the contour plot. It looks much clearer now. We have also added the PDF of 50 nm particle shrink factor (at 300 °C) in this figure, as shown in Fig. R2. The labels of color bar for panels of PNSD, κ-PDF and f_s-PDF (PDF of shrink factor at 300 ℃) have been added.

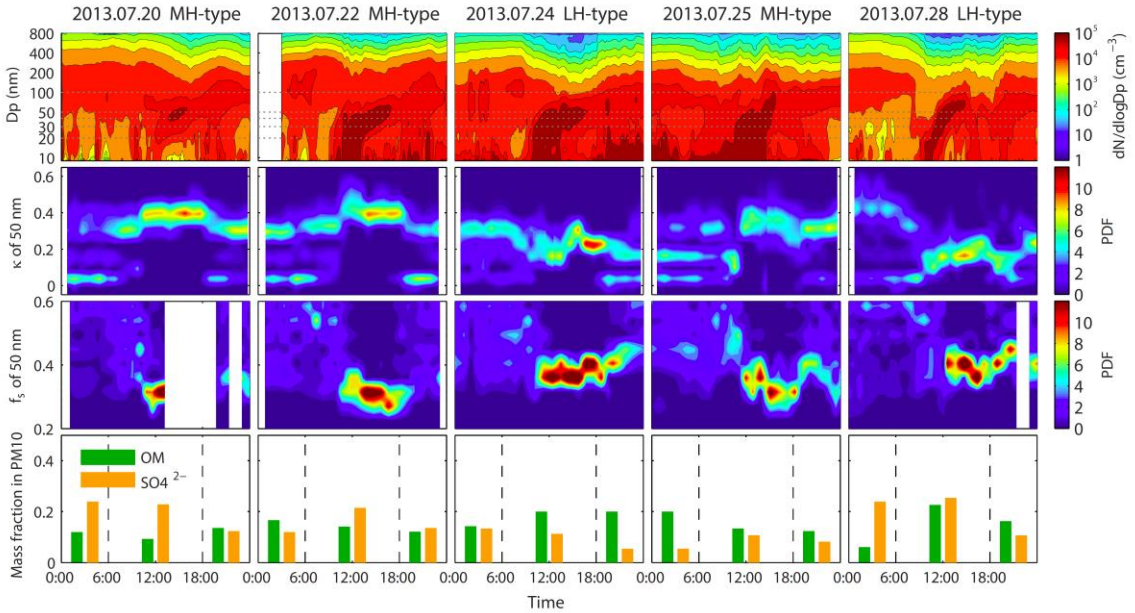

Fig. R2 (Fig. 2 in manuscript). 5 NPF events observed during the campaign period. Subplots show the time series of particles number size distribution, κ-PDF of 50 and f_s-PDF of 50 nm particles, and mass fraction of organics and sulfate from PM10 HV-sample analysis.

And we have also added two figures of κ-PDF and f_s-PDF for 50, 100, 150 and 250 nm in supplement (Fig. R2 and R3). We can see the variations of κ-PDF and f_s-PDF for the four sizes are different, since particle with different sizes may have different origin and undergo different aging processes. During NPF events, new particles mainly dominated up to about 80 nm (sometimes also up to 100 nm). The temporal variation of hygroscopicity and volatility of larger particles (150 and 250 nm) may reflect the air mass changes, as can be seen on July 24th and 28th in Fig. R3.

As answering the general comment of reviewer #2, we agreed that the composition of the new particles may also depend on the air masses, since the air mass routes determine the concentration of precursors to a large extent. In the north NCP, air masses coming from the south are usually more polluted and with high concentration of SO_2; while air masses coming from the north are much cleaner (Xu et al., 2011; Ma et al., 2011). During the three MH-type NPF events (July 20th, 22nd and 25th), the wind direction was mainly in south section and/or the wind speed was low. The polluted air mass might contain high concentration of SO_2, promoting the production of sulfate in particle phase. This might be also the reason of the high stable κ of 100 – 250 nm particles on those days. During the two LH-type NPF events (July 24th and 28th), the wind direction was N/NW and the air mass was clean. The relative contribution of sulfuric acid to the particle growth might be therefore lower. Larger particles also exhibited lower κ on the two days, since secondary production might also contribute much on their mass.

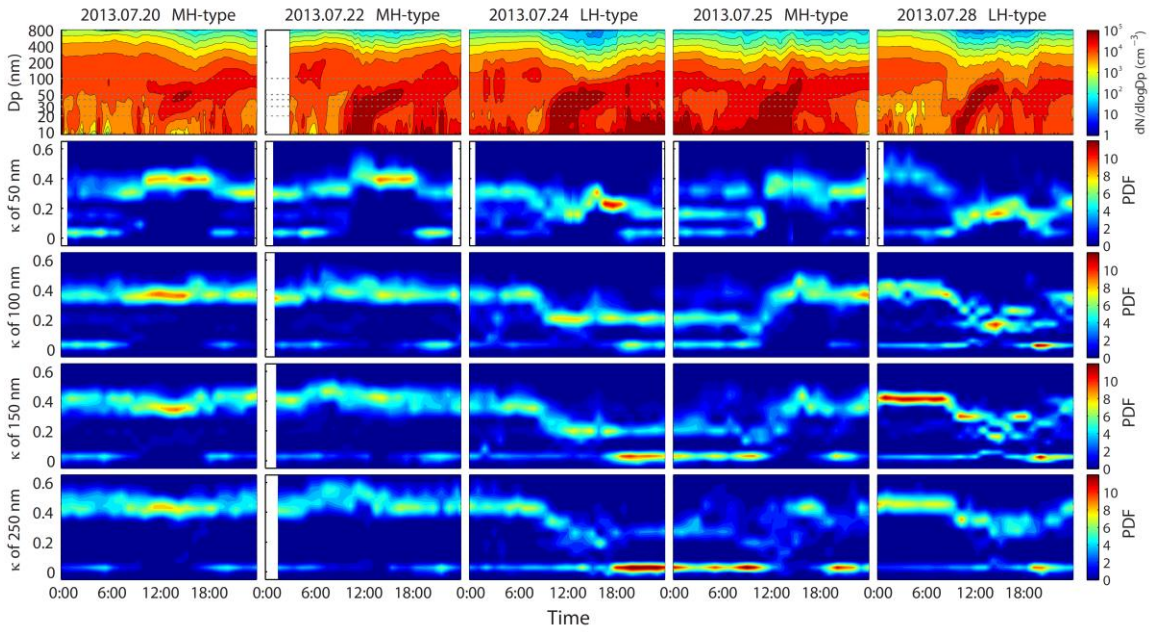

Fig. R3 (Fig. S2 in supplement). 5 NPF events observed during the campaign period. Subplots show the time series of particles number size distribution, and κ-PDF of 50, 100, 150 and 250 nm particles.

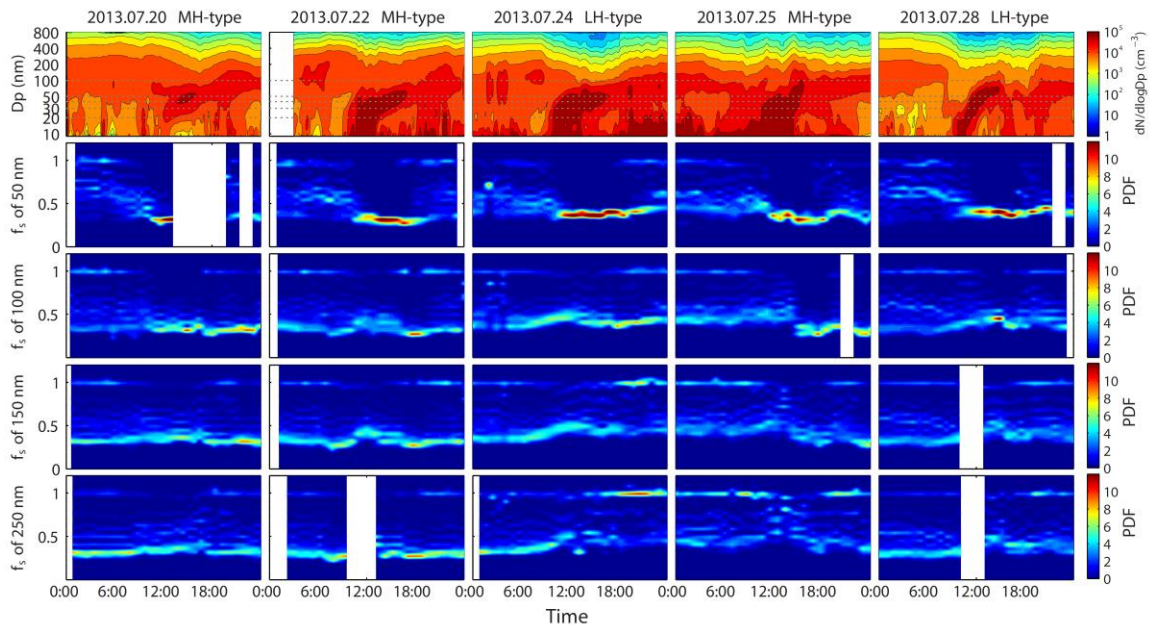

Fig. R4 (Fig. S3 in supplement). 5 NPF events observed during the campaign period. Subplots show the time series of particles number size distribution, and f_s-PDF of 50, 100, 150 and 250 nm particles.

Reviewer:

Page 6, line 10: The inference of the chemistry of nuclei mode particles from PM10 chemical analysis leaves a lot to be desired. Is there data from previous experiments in the NCP when mass spectrometric analysis was done to aid in the understanding of what the size dependence of sulfate and organic compounds might have been in this field study?

Reply:

We also realized that it was improper to use PM10 chemical composition in our analysis. But we did not find any study which reports the online measurements of chemical composition of sub-100 nm particles in the NCP. Actually our collaborator did AMS measurement during the joint intensive campaign. Unfortunately, we met some problem during transporting of our mobile laboratory. Our measurement therefore started too late and has no overlap with AMS measurement in the campaign. Figure R5 displays the average mass fraction and size-resolved mass distribution of different compounds measured with AMS for the period June 9th to July 9th. We can see organics and sulfate dominates the mass of submicron particles.

Actually, we also did particle volatility measurement with a volatility tandem differential mobility analyzer (TROPOS-type VTDMA; Philippin et al., 2004) during the campaign. The hygroscopicity and volatility of nanoparticles as measured by the HTDMA and VTDMA is often invoked to provide insight into the particle composition (Zhang et al., 2011). We therefore decided to involve this dataset in our study, together with hygroscopicity data, to provide some additional information about the new particles. In the revised manuscript, we built most of the discussion in section 3.1 and 3.2 on the basis of HTDMA

and VTDMA measurements, instead of on PM10 chemical composition data. More details will be show in the response to another comment below (Page 9, line 29 …).

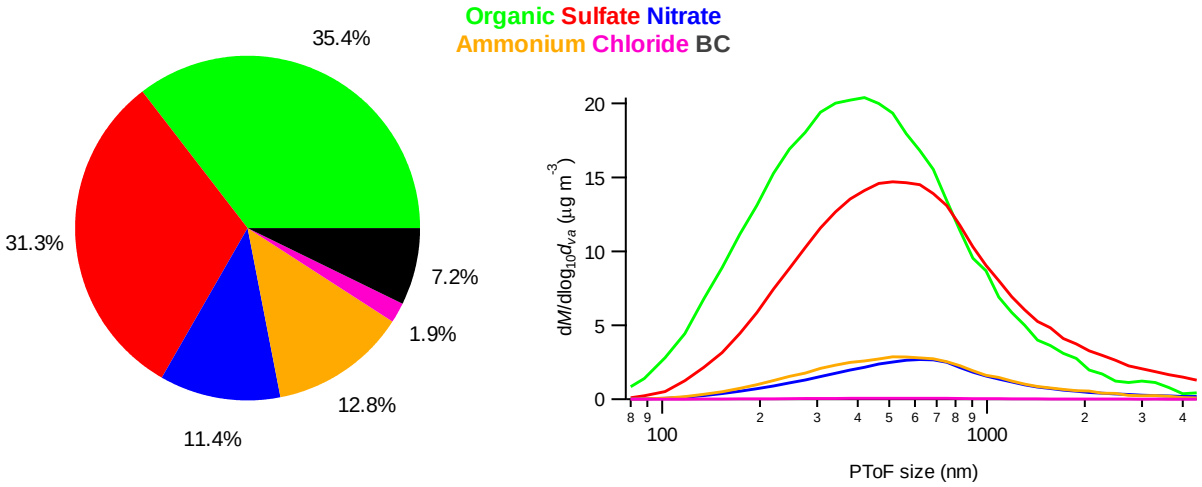

Fig. R5. Average mass fraction (left) and size-resolved mass distribution (right) of different compounds measured with AMS for the period June 9th to July 9th (this figure is from our collaborator: Key Laboratory for Urban Habitat Environmental Science and Technology, Shenzhen Graduate School of Peking University)

Reviewer:

Line 17: I don't understand "production activity". Do you mean rate of condensation?

Reply:

The sentence has been deleted.

Reviewer:

Line 24: It would be useful in this figure to identify the two events, the sulfate-dominant NPF event and OM-dominant NPF events, either in the caption or under the dates at the top of panel 1.

Reply:

Thanks for the suggestion. The types (MH/LH) of the five NPF events have been added in the title of Fig. 2, 3 and 6 in the manuscript.

Reviewer:

Line 25: "And two types of NPF ... " Does this refer to Yue's work? If yes, then I suggest, "Furthermore, they observed two types of NPF .... "

Reply:

We have deleted this sentence in the revised manuscript.

Reviewer:

Line 31: You present BC mass concentrations. Do you have similar mass concentration data for sulfate and OM? Total sub 800nm and sub 80 nm mass derived from the SMPS volume and an assumed density would be useful as well.

Reply:

Unfortunately, we had no online measurements of sulfate and organic mass concentration during the NPF events.

Following your suggestion, we calculated the mass concentration of sub-80 nm and sub-800 nm, from PNSD and an assumed density 1.6 gcm^{-3}. This data has been added in panel B of Fig. 3 and 6 (as shown below). We have also added some description of this data in section 3.2.1 and 3.2.2.

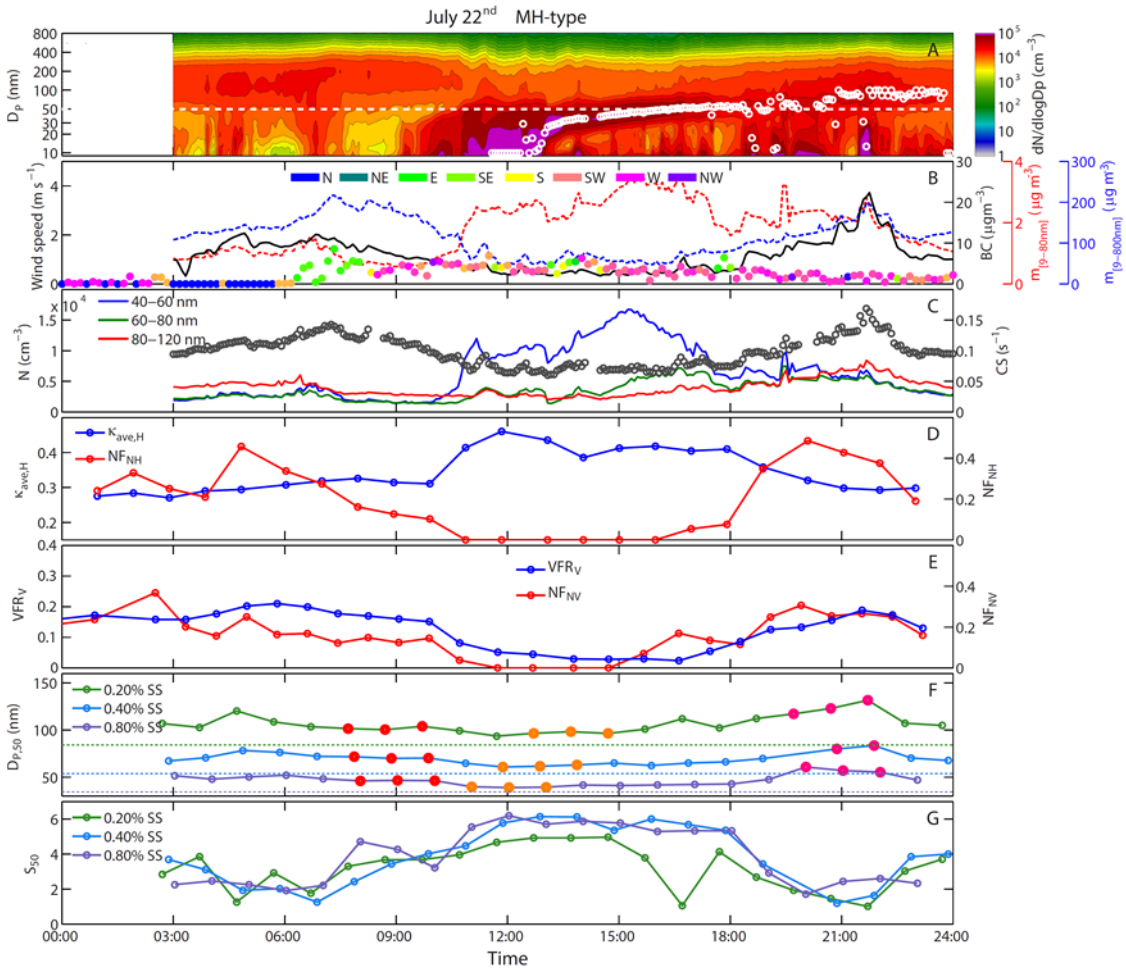

Fig. R6 (Fig. 3 in manuscript). MH-type NPF event on July 22nd. Time series of (A) particle number size distribution and geometric mean diameter of nucleation mode, (B) wind speed/direction and the mass concentration of BC, sub-80 nm and sub-800 nm particles, (C) condensational sink (CS) and number concentration of particles in defined size ranges, (D) average κ of hygroscopic mode and number fraction of nearly-hydrophobic mode for 50 nm particles, (E) volume fraction remaining of volatile mode and number fraction of non-volatile mode for 50 nm particles, (F) $D_{P,50}$ for 0.20%, 0.40% and 0.80% SS, as well as (G) S_{50} for the three SS. The dashed lines in panel F show the theoretical critical diameters for ammonium sulfate at the three SS. Points filled with color in panel G show the records selected to calculate the average size-resolved activation ratio shown in Fig. 5.

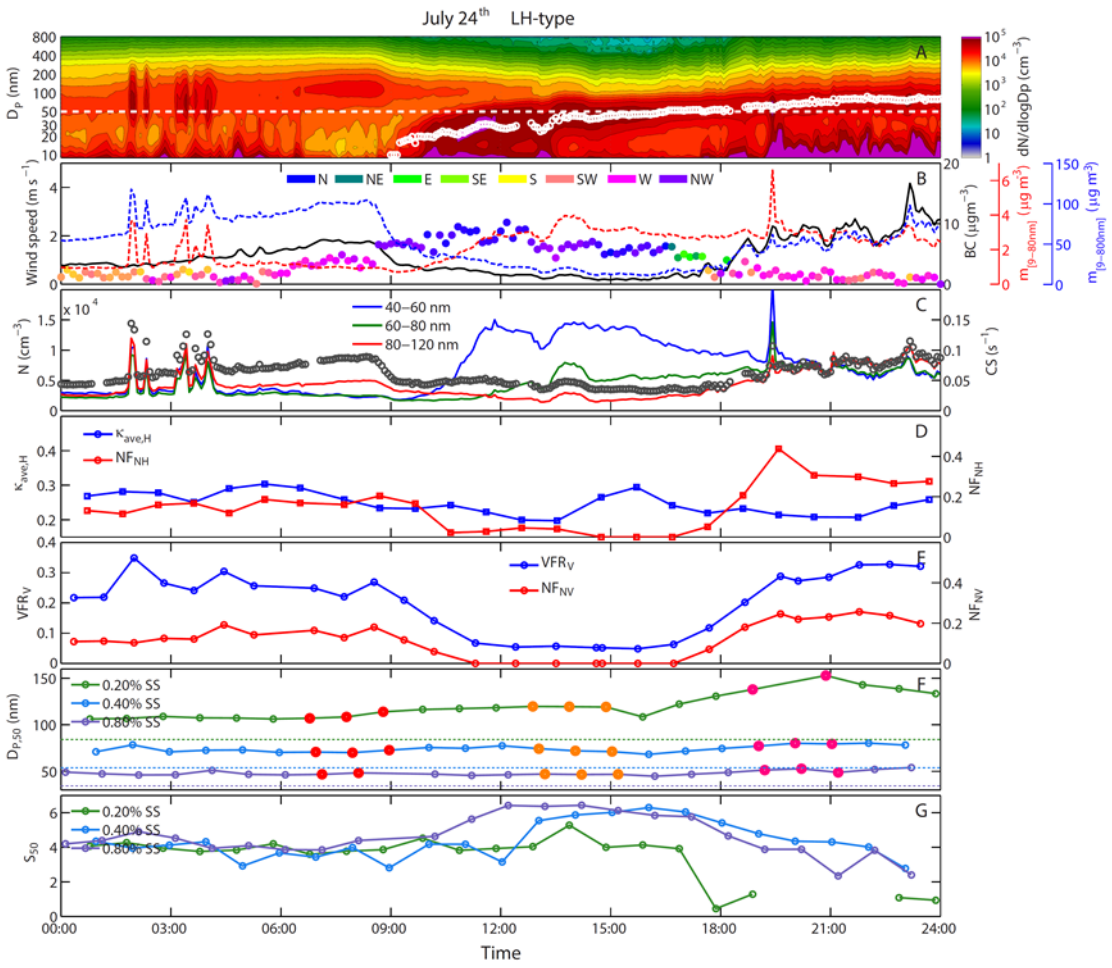

Figure R7 (Fig. 6 in manuscript). LH-type NPF event on July 24th. Time series of (A) particle number size distribution and geometric mean diameter of nucleation mode, (B) wind speed/direction and the mass concentration of BC, sub-80 nm and sub-800 nm particles, (C) condensational sink (CS) and number concentration of particles in defined size ranges, (D) average κ of hygroscopic mode and number fraction of nearly-hydrophobic mode for 50 nm particles, (E) volume fraction remaining of volatile mode and number fraction of non-volatile mode for 50 nm particles, (F) $D_{P,50}$ for 0.20%, 0.40% and 0.80% SS, as well as (G) S_{50} for the three SS. The dashed lines in panel F show the theoretical critical diameters for ammonium sulfate at the three SS. Points filled with color in panel G show the records selected to calculate the average size-resolved activation ratio shown in Fig. 5.

Reviewer:

Page 7, line 4, Figure 3A The label on the ordinate should be Dp, particle diameter. The color scale label should be placed next to the color scale bar.

Reply:

Thanks for point out this error. It has been corrected. The color scale bar and label for the PNSD contour plot has also been added in Fig. 3 and 6, as shown in Fig. R6 and R7.

Reviewer:

Figure 3 overall: The timing of the appearance of NFP varies depending on the parameter. NFP appear sporadically beginning at 900, Fig 3A. N(40,60) and increases sharply at about 1030. Nuclei mode reaches 50nm about 1200LT. The condensational sink does not decrease sharply over time in the morning. Of course there are other parameters not quantified and presented such as advection or mixing from more polluted layers aloft or actinic flux and photochemical precursor gas formation. These are beyond the scope of the observations and discussion. Simply mention that the indicatory parameters for NFP, Dp,nuclei, N(40,60) and , increase more or less in coincidence over a three hour period.

Reply:

Many thanks for the comment. We fully agreed that the nucleation and growth during this event might be influenced or controlled by some more factors besides condensational sink. To understand the whole process is not the aim of this study, and requires additional observations which are not available. Following your suggestion, we have added "The indicatory parameters for NPF, $N_{[40\text{-}60nm]}$ and the geometric mean diameter of nucleation mode, increase in coincidence over a three-hour period" in section 3.2.1.

Reviewer:

Figure 3 D: The legend shows NFH while the right hand label shows NFNH.

Reply:

Thanks for point out this error. It has been corrected in the new figure, as shown in Fig. R6 and R7.

Reviewer:

Line 27, Figure 3E: The highlighting of the points used for calculating the average sizeresolved activation ratio shown in Figure 5 is difficult to see and the change in color is not clear. A larger circle for those points would help the reader at a glance. Also, a theoretical critical Dp line for ammonium sulfate as a reference for the three SS values would be useful for comparison.

Reply:

Thanks for the suggestion. A larger colored circle is now used in panel F in Fig. 3 and 6. And the theoretical critical diameters for ammonium sulfate at the three SS are also marked as dashed lines, as shown in Fig. R6 and R7.

Reviewer:

Page 8, line 30, Figure 5: What is the SS for the campaign average curve? It is difficult to follow all the curves and colors on this plot. I suggest breaking the single plot into three panels, one for each SS. The

information in Figure 5 is summarized in Figure 3 panels E and F, but, these do not show the OM vs. sulfate differences or that activation ratios remain below 1.0 even at sizes much larger than Dcrit,SS, so figure 5 is of value for showing this result.

Reply:

Thanks for the suggestion. We have broken Fig. 5 into three panels, one for each SS, as shown in Fig R8. The campaign average activation curves at the three SS are shown as solid black lines in each panel.

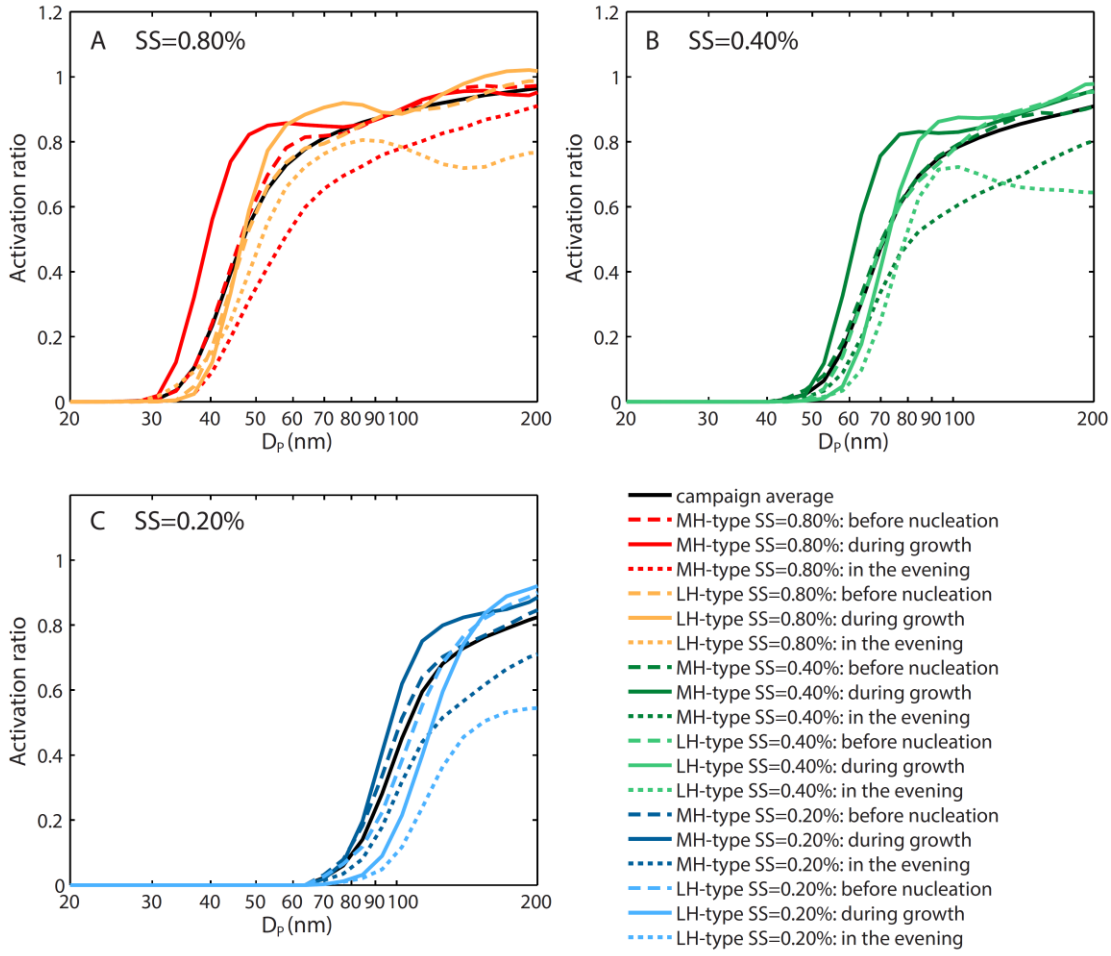

Fig. R8: Average size-resolved activation ratio for the selected periods on July 22nd and 24th

Reviewer:

This last point, AR < 1 at Dp»Dp,crit, needs explanation. Certainly size plays the dominant role as you point out since approximately 80% of the particles activate at Dp50 plus about 5 nm. However, on average only about 85% activation ratio is reached at twice the Dp50. In two cases the maximum AR is only about 60%. Do you have an explanation, e.g., truly insoluble, non-wettable primary particles, or organic surfactants?

Reply:

We thought this relatively low activation ratio at sizes much larger than $D_{p,50}$ was caused by the externally mixed BC particles which is completely hydrophobic, because 1) emission of BC particles from fossil fuel and bio fuel consuming usually increased in the evening due to increased traffic and cooking, 2) the vertical mixing and photochemical aging process were inhibited in the nocturnal boundary layer. It can be seen in Fig. R9 that the number fraction of non-volatile and nearly-hydrophobic particles had very similar variation as the BC mass concentration in the afternoon and evening, especially for 100 and 150 nm.

July 24th is actually a kind of extremely case of BC influence. We can see the BC mass concentration in the evening of July 24th is similar as that in the evening of July 22nd. However, the air mass was very clean in the daytime of July 24th (can be seen also from the $m_{[9\text{-}800nm]}$ in panel B of Fig. R6 and R7). Due to the low concentration of background aerosol particles, the relative contribution of BC in the evening was higher than in the other days. Thus the number fraction of externally mixed BC particles is higher, resulting in a low activation ratio (Fig. R8) and high number fraction of non-volatile and nearly hydrophobic mode (Fig. R9). The decrease of the activation ratio at size range of 100 – 200 nm for 0.80% and 0.40% SS is probably because the number fraction of externally mixed BC particles at 150 nm is higher than at 100 nm, which is also reflected in NF_{NV} and NF_{NH} (Fig. R9).

To make it clear, we have added "And the activation ratio reaches only about 80% even at the size of $D_{P,50}$ ×2, which is probably due to the high concentration of externally mixed BC particles (also shown as a clear near-hydrophobic and non-volatile mode at 100 and 150 nm in Fig. S2 and S3)." in section 3.2.1, and "The increasing anthropogenic emission caused a decrease in particle hygroscopicity and CCN activity (Figure 6D, F and G). However, the activation ratio at size range of 100 – 200 nm is much lower than that in the nighttime of July 22nd (Fig. 5). This is probably because the concentration of background aerosol particles was lower on July 24th (also can be seen from the $m_{[9\text{-}800nm]}$ in panel B of Fig. 3 and 6). The relative contribution of BC particles in the evening was therefore higher, resulting in a high number fraction of externally mixed BC particles." in section 3.2.2.

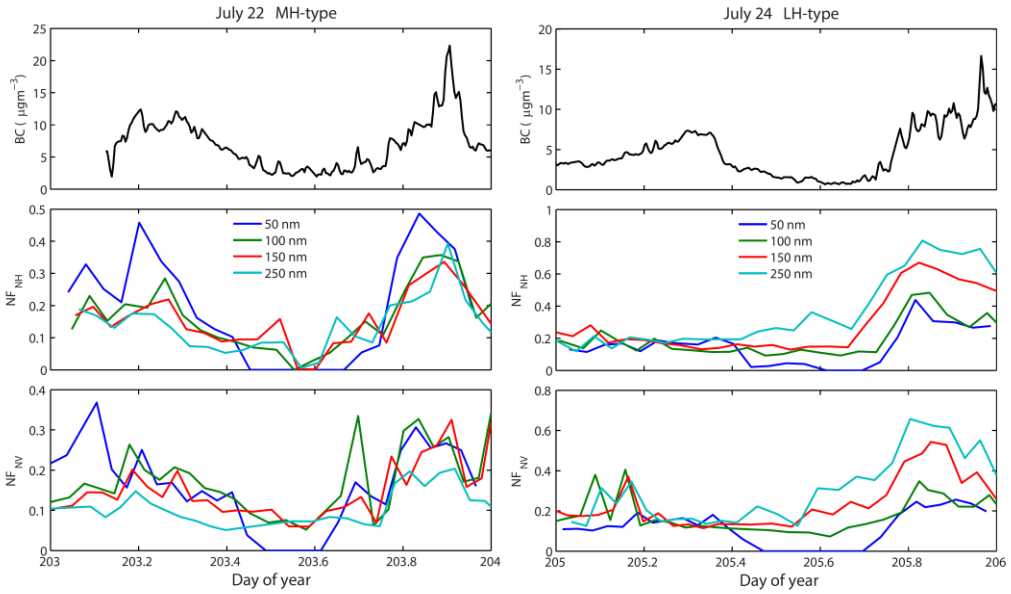

Fig. R9. Temporal variation of BC mass concentration, NF_{NH} and NF_{NV} on July 22nd and July 24th

Reviewer:

Page 8, line 11, Figure 6: Change caption and legends and plotting in figure 6 as suggested for figure 3. See Word changes in figure 3 caption.

Reply:

Figure 6 has been improved in the same way as Fig. 3.

Reviewer:

Page 9, line 29: Do you know from chemical measurement that sulfate dominated the particle growth size mode, i.e., nuclei and Aitken modes? From PM10 sulfate analysis alone that cannot be supported. The best evidence you have is for sulfate vs. OM is from your and NFNH.

Reply:

Many thanks for this comment.

We have also realized that it was improper to use PM10 chemical composition in our analysis. Most of the OM and sulfate mass is in accumulation mode which is dominated not only by secondary production but also by horizontal and vertical transportation. The mass fractions of sulfate and OM in nucleation mode are therefore not necessarily proportional to their mass fractions in PM10. Unfortunately, we have no measurement about size-resolved particle chemical composition in ultrafine size range.

However, we did particle volatility measurement with a volatility tandem differential mobility analyzer (TROPOS-type VTDMA; Philippin et al., 2004) during the campaign. The hygroscopicity and volatility of nanoparticles as measured by the HTDMA and VTDMA is often invoked to provide insight into the particle composition (Zhang et al., 2011). We therefore decided to involve this dataset in our study, together with hygroscopicity data, to provide some additional information about the new particles.

Non-volatile cores were found in 50 nm newly formed particles in all the five NPF events (Fig. R6 and R7). This phenomenon was also observed in Melpitz, Germany (Wehner et al., 2005) and Hyytiälä, Finland (Ehn et al., 2007). The sizes of the non-volatile residues of 50 nm new particles were however different in the five NPF events. In the NPF event on July 20th, 22nd and 25th, the majority of 50 nm new particles exhibited a shrink factor of about 0.3; while on July 24th and 28th, the shrink factor is a slightly higher, about 0.4. It means more polymer-type organics were formed during the growth of new particles on July 24th and 28th. In another study in the same region, Yue et al. (2010) found that sulfuric acid was the major contributor of the growth of newly formed particles, and organic compounds might also play a major role in some cases. Combining all the information above and the result of particle hygroscopicity, it is very likely that condensation and neutralization of sulfuric acid dominated the growth of the new particles on July 20th, 22nd and 25th; while its contribution was much lower on July 24th and 28th and organic compounds had an important contribution to particle growth. However, since we have no direct measurement of nanoparticle chemical composition, to be more accurate, we have modified the name of the two types of NPF events. The events on July 20th, 22nd and 25th were termed MH-type NPF (NPF with More Hygroscopic particles); while the events on July 24th and 28th were termed LH-type NPF (NPF with Less Hygroscopic particles).

Our study aimed at evaluating the variability of the CCN activity during NPF events in an anthropogenically polluted atmosphere and the applicability of some simplified CCN parameterization. Although the chemical composition measurement of ultrafine particles was not available, the online measurements of hygroscopicity and volatility can provide some indication for distinguishing different NPF types. In the revised manuscript, we built most of the discussion in section 3.1 and 3.2 on the basis of HTDMA and VTDMA measurements, instead of on PM10 chemical composition data.

We have deleted most of the content about PM10 composition data, added a new section to introduce VTDMA measurement, revised section 3.1 and 3.2, added VTDMA data in figure 2, 3 and 6 (shown as Fig. R2, R6 and R7), and replaced figure 4 with a new figure of average κ-PDF and f_s-PDF during NPF (Fig. R10). In the following we list the major new content which has been added in the revised manuscript (in dark blue color).

In section 2.5:

Particle shrink factor (f_s), defined as the ratio between the diameter of a particle after being heated at a certain temperature and its original diameter, was measured with a volatility tandem differential mobility analyzer (TROPOS-type VTDMA; Philippin et al., 2004) at 300 °C. The same dry particle diameters as HTDMA measurement (50, 100, 150, 200, 250, 300 and 350 nm) was selected for VTDMA measurement. The time resolution of full scans was about 50 minutes.

The VTDMA has a similar structure as the HTDMA with the only difference in the conditioning unit – the humidifier is replaced with a volatilization column, where volatile compounds would evaporate at 300 °C revealing non-volatile particles or cores (Burtscher et al., 2001). The residence time of the particles in the heating column was 0.5 s, which is sufficient to evaporate the volatile fraction of particles in a narrow size range (Philippin et al., 2004). The TDMA inversion algorithm developed by Gysel et al. (2009) was used for data inversion. Ambient temperature (25 °C) scans were used to correct the size shift between the two DMAs and define the width of the transfer function (Gysel et al., 2009). 203 nm PSL particles were used to calibrate the offset in sizing of the two DMAs on weekly basis.

The probability density function of f_s (f_s-PDF) was used in this study. We simply define the particles with f_s<0.8 as non-volatile mode particles, and the rest as volatile mode particles. The volume fraction remain of volatile mode particles at 300 °C was calculated with $VFR_V = \frac{\int_{f_s=0}^{0.8} f_s \cdot c(f_s)\, df_s}{\int_{f_s=0}^{0.8} c(f_s)\, df_s}$, where $c(f_s)$ is the probability density function of f_s.

In section 3.1:

The hygroscopicity and volatility of nanoparticles as measured by the HTDMA and VTDMA is often invoked to provide insight into the particle composition (Zhang et al., 2011). It is interesting to see in Fig. 2 that the hygroscopicity of newly formed particles is largely different in the five events. On July 20th, 22nd and 25th, after the nucleation mode grew to 50 nm, the κ-PDF at 50 nm exhibited a dominant hygroscopic mode at κ around 0.4 until 18:00 LT. However, the newly formed, 50 nm, particles exhibited a much lower κ on July 24th and 28th. In the late afternoon on July 24th, the hygroscopic mode was located between 0.1 and 0.2. On July 28, the average κ of hygroscopic mode was also lower than 0.2. The hygroscopicity

parameter κ of a particle is mainly determined by its chemical composition (Petters and Kreidenweis, 2007). Therefore, it can be assumed that the particulate matter produced during the growth process was dominated by different species in different NPF events.

The difference in chemical composition of new particles was also reflected by the VTDMA measurement. Non-volatile residual at 300 ℃ can be found in 50 nm newly formed particles in all the five NPF events. This phenomenon was also observed in Melpitz, Germany (Wehner et al., 2005) and Hyytiälä, Finland (Ehn et al., 2007). And the non-volatile cores were presumed to be polymer-type organics (Wehner et al., 2005; Ehn et al., 2007). In our measurements, the sizes of the non-volatile cores of 50 nm new particles were however different in the five NPF events. In the event on July 20th, 22nd and 25th, the majority of 50 nm new particles exhibited a shrink factor of about 0.3; while on July 24th and 28th, the shrink factor is a slightly higher, about 0.4. This means more polymer-type organics were formed during the growth of new particles on July 24th and 28th.

In a study combining in-situ measurements and aerosol dynamic model, sulfuric acid was found to be the major contributor of the growth of newly formed particles in the north NCP, and organic compounds were also found to play a major role in some cases (Yue et al., 2010). Yue et al. (2010) classified NPF events in the north NCP into two types, i.e. sulfur-rich and sulfur-poor events, in which the growth of the new particles is respectively dominated by sulfates and organics. Observed in the same region, our measurements of particle hygroscopicity and volatility can be also well explained by the two NPF types as in Yue et al. (2010). The NPF events on July 20th, 22nd and 25th are very like the sulfur-rich type NPF, i.e., condensation and neutralization of sulfuric acid contributed most to the growth of the new particles, and resulted in a high particle hygroscopicity. The NPF events on July 24th and 28th are like the sulfur-poor event, i.e., condensation of organic compounds had a higher contribution to the growth, resulting in a lower particle hygroscopicity, and more polymers might be produced (Kalberer et al., 2004), resulting in a higher shrink factor.

As a reference, the mass fraction of organic and sulfate compounds in PM10 obtained from offline analysis of 12-h DIGITEL HV-samples are shown in the bottom subplots of Fig. 2. It should be noted that the ultrafine particles account for only a minor fraction in PM10 total mass and the mass fractions of organics and sulfate are determined not only by the activity of secondary production, but also the long range transportation and vertical mixing. It can be seen that the average mass fraction of organics during the daytime of July 20th, 22nd and 25th was lower than the average of the previous nighttime, while the mass fraction of sulfate obviously increased (July 22nd and 25th) or at least stayed at the same level (July 20th). And the opposite variation can be found on July 24th and 28th. This is basically consistent with the measurements of particle hygroscopicity and volatility.

The possible difference in the chemical composition of new particles might be cause by several factors, e.g. the concentration of precursors and the activity of some reactions. Furthermore, these factors might be determined or influenced by other parameters, e.g. ambient temperature, radiation, air mass origin, and vertical mixing. To find out the reason of the composition variation of the new particles is out of the scope of this study, and needs some additional measurements which are not available. In the following sections, we will focus on the CCN activity of new particles in the two types of NPF event. Since we have no direct measurement of the chemical composition of ultrafine particles, to be accurate, the events on July 20th, 22nd and 25th are termed MH-type NPF (NPF with More Hygroscopic particles), while the events on July 24th and 28th are termed LH-type NPF (NPF with Less Hygroscopic particles).

In section 3.2.1:

As the boundary layer developed in the morning, the particulate condensational sink (Kulmala et al., 2001) and the mass concentration of BC and sub-800 nm particles started to decrease at 07:00 LT. The newly formed particles started to be visible in our SMPS record at around 09:00 LT. The indicatory parameters for NPF, $N_{[40\text{-}60nm]}$ and the geometric mean diameter of nucleation mode, increase in coincidence over a three-hour period. Large amount of secondary particulate matter was produced during the growth of new particles, shown as a sharp increase in sub-80 nm particle mass concentration. The new particles continued growing until the end of the day with an average growth rate of 6.3 nm h^{-1} (Fig. 3A). The newly formed particles reached 50 nm at around 10:30 LT, resulting in a sharp elevation of $N_{[40\text{-}60nm]}$ from about 2×10^3 cm^{-3} to 1×10^4 cm^{-3}. Correspondingly, the number fraction of nearly hydrophobic mode particles (NF_{NH}) and non-volatile mode particles (NF_{NV}) decreased from about 0.2 to 0, meaning that the newly formed particles grew to 50 nm and dominated the nuclei mode number. This can also be confirmed by the average κ-PDF and f_s-PDF during the NPF event (Fig. 4). Both κ-PDF and f_s-PDF exhibited narrow unimodal patterns, indicating that the majority of 50 nm particles originated from the same source, NPF. Identifying as MH type, during the NPF event, the 50 nm new particles exhibited a much higher $\kappa_{ave,H}$ than the pre-existing particles (about 0.45 vs. 0.3). As discussed in section 3.1, it is very likely that the condensation and neutralization of sulfuric acid contributed most to the growth of the new particles.

In section 3.2.2:

The NPF event started at around 09:00 LT. The growth of newly formed particles continued throughout the day with an average growth rate of 6.3 nm h-1 (Fig. 6A). It can be seen that N[40-60nm] increased from about 2×103 cm-3 to 1.4×104 cm-3 in a few hours, N[60-80nm] also increased during the daytime. As the newly formed particles grew to 50 nm and become the majority at this size, the number fraction of nearly-hydrophobic mode and non-volatile mode particles decreased to almost 0 within 1 hour. The κ-PDF and fs-PDF also exhibited narrow unimodal patterns (Fig. 4). It is interesting to note that, unlike the event on July 22nd, the average κ for the hygroscopic mode of 50 nm particles decreased a bit after the nucleation, and stayed below 0.3 for the rest of the day. Such low hygroscopicity of newly formed particles implies that the driving mechanism of particle growth in daytime for this event was somehow different from the event on July 22nd. It very likely that sulfuric acid played a less important role in the growth process, and organics had a higher contribution, compared with the MH-type NPF. It can be also seen in Fig. 6E that VFRV during this NPF event is higher than that during the event on July 22nd, meaning that the more polymer-type organics was produced during the growth of the new particles in this event.

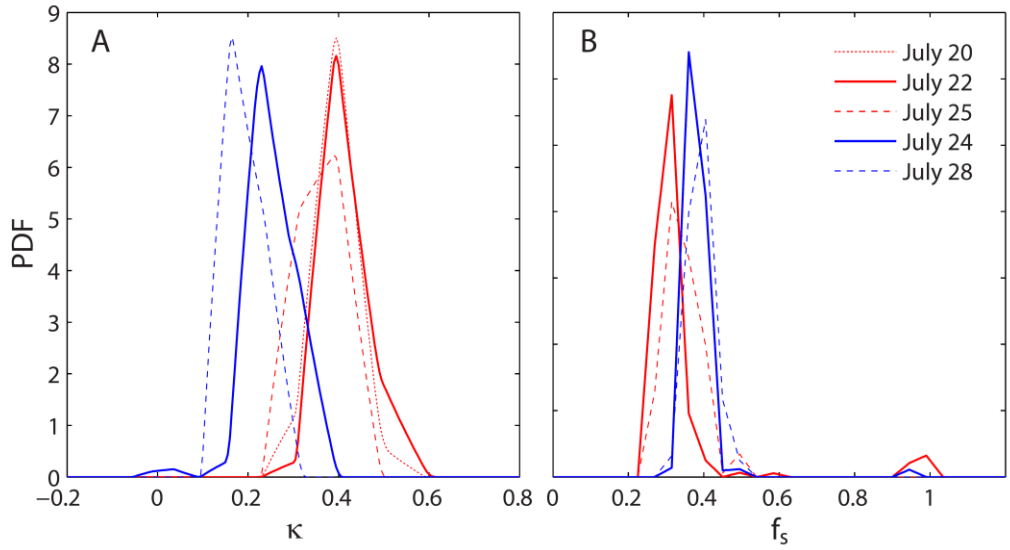

Fig. R10 (Fig. 4 in manuscript). Average κ-PDF (A) and f_s-PDF (B) of 50 nm particles during the 5 NPF events.

Reviewer:

Page 10, lines 1 through 3: It is not clear how the difference ratio plotted in Figure 7 was calculated, what NCCN ref and NCCN Aravg are. The text and figure caption and x-scale label symbols are not consistent. Provide an equation (4) in the text for the bias parameter used in the figure e.g. CCNbias = ...

Reply:

Thanks for the comment.

$N_{CCN,AR\text{-}ave}$, $N_{CCN,D\text{-}ave}$ and $N_{CCN,ref}$ are defined before equation (3): "To answer this question, the CCN number concentration was calculated with eq. (2) based on the campaign average activation ratio shown as the solid black line in panel A of Fig. 5 (the calculated CCN number concentration is termed $N_{CCN,AR\text{-}ave}$), campaign average critical diameter (termed $N_{CCN,D\text{-}ave}$) and real-time activation ratio (termed $N_{CCN,ref}$) at 0.80% SS."

We have added two equations to define the relative difference plotted in Fig. 7: "The relative difference between $N_{CCN,AR\text{-}ave}$ and $N_{CCN,ref}$ (termed CCNbiasA), and between $N_{CCN,D\text{-}ave}$ and $N_{CCN,ref}$ (termed CCNbiasB), was then evaluated. CCNbiasA and CCNbiasB were respectively calculated as

$$CCNbiasA = \frac{N_{CCN,AR-ave} - N_{CCN,ref}}{N_{CCN,ref}} \quad (4)$$

$$CCNbiasB = \frac{N_{CCN,D-ave} - N_{CCN,ref}}{N_{CCN,ref}} \quad (5)"$$

And the caption of Fig. 7 has been revised.

Reviewer:

Line 13, Figure 7: The caption should the time period of average, i.e., afternoons of July 22nd and July 24th. I assume the frequency statistics are number of occurrences per interval of relative ratio, and for the 2 dim, number of occurrences per interval of relative ratio and time. Mention this in the caption.

Reply:

Fig. 7 in the manuscript is based on the data of the entire campaign period, not only the two NPF days. The caption of Fig. 7 has been revised as "Fig. 7. 2 dimensional frequency distribution (number of occurrences per interval of CCNbias and time of day, shown as contour plot) and overall frequency distribution (number of occurrences per interval of CCNbias, shown as red line) of CCNbiasA (panel A) and CCNbiasB (panel B) for the entire campaign period"

Reviewer:

Are there significant differences between the two parameters? To me they look very similar other than the left hand tail. You do not mention the chemistry or physics behind this tail. Nor can I imagine any.

Reply:

The frequency distributions of CCNbiasA and CCBbiasB are very similar since the average activation ratio curve and average critical dimeter used in the calculation are derived from the same dataset which was also used this sensitivity test. In other words, the average activation ratio curve and average critical diameter well represented the CCN activity during the campaign period. Therefore, the majority of the CCNbiasA and CCNbiasB are located around 0, within ±10%.

The left hand tails of the two distributions represent the data during NPF events. The campaign average activation ratio and critical diameter were not appropriate for N_{CCN} prediction during NPF events (especially during MH-type). Using average critical diameter may cause larger negative bias in N_{CCN}. Figure R11 shows the measured AR curve during the NPF event on July 22nd, and the campaign average AR curve and the critical diameter. Compared with the real-time AR curve (red line), using average critical diameter (a stepwise size-resolved activation ratio, blue line) overestimates N_{CCN} at $D_P > D_{P,cri}$ and underestimates N_{CCN} at $D_P < D_{P,cri}$. If PNSD and activation ratio curve are similar as the average ones (e.g. on non-NPF days), those overestimation and underestimation may compensate. However, during NPF events, the activation ratio curve may shift towards lower size (in MH-type NPF) and particle number concentration in ultrafine size range increases significantly. The underestimation in the left side of $D_{P,cri}$ is therefore much higher than the overestimation in the right side of $D_{P,cri}$, and resulting in a large negative CCNbiasB.

We had added some discussion about this in section 3.3: "This indicates that to use an average $D_{P,cri}$ may result in a larger underestimation of calculated N_{CCN} during NPF events in the NCP. This is because using such a stepwise size-resolved activation ratio overestimates N_{CCN} at $D_P > D_{P,cri}$ and underestimates N_{CCN} at $D_P < D_{P,cri}$. If real-time PNSD and activation ratio curve are similar as the average ones, those overestimation and underestimation may compensate. However, during NPF events, the activation ratio curve may shift towards lower size (in MH-type NPF) and particle number concentration in ultrafine size

range increases significantly. The underestimation of N_{CCN} in the left side of $D_{P,cri}$ is therefore much higher than the overestimation in the right side of $D_{P,cri}$, and resulting in a large negative CCNbiasB."

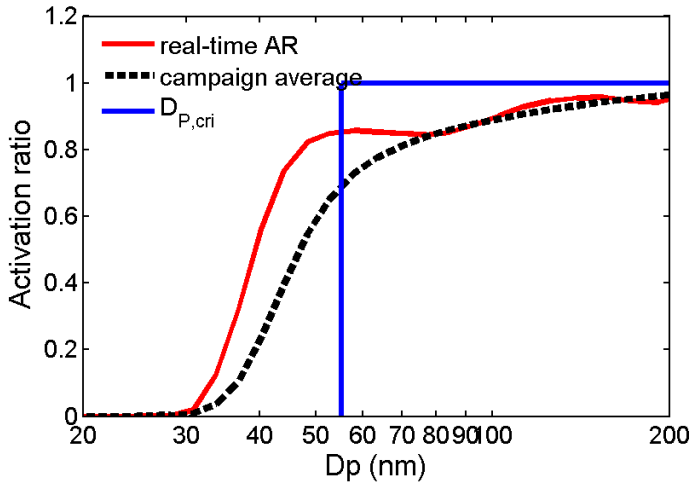

Fig. R11: measured AR curve during the NPF event on July 22nd, and the campaign average AR curve and the critical diameter

Reviewer:

In other plots and discussions you have presented and compared data from 22 July vs. 24 July. Were there significant differences in the frequency distribution plots for those two days?

Reply:

Fig. R12 shows the frequency distribution (number of occurrences per interval of CCNbias) of CCNbiasA (left panel) and CCNbiasB (right panel) for July 22nd and July 24th.

Calculated with campaign average AR curve, CCNbiasA has much more negative values (left tail) on July 22nd than on July 24th, due to the occurrence of MH-type NPF event on July 22nd. Calculated with campaign average critical diameter, CCNbiasB on both days shows big left tail in their frequency distributions. The number of negative values on July 22nd is also higher than that on July 24th.

Probably because NPF usually happens in an atmosphere which is not very polluted (low condensational sink), the influence of freshly emitted BC on CCN activity is quite large in the evening of the two NPF days. Positive CCNbias up to +30% can be seen on both days.

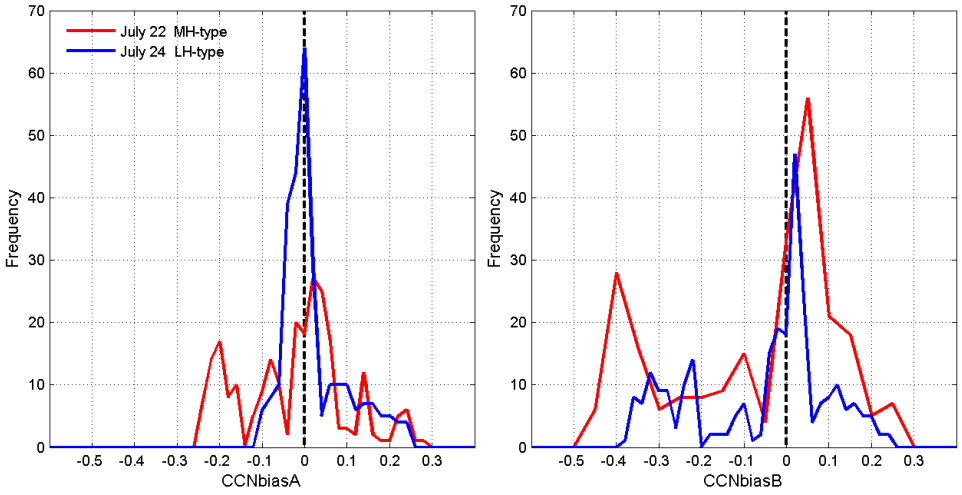

Fig. R12. Frequency distribution (number of occurrences per interval of CCNbias) of CCNbiasA (left panel) and CCNbiasB (right panel) on July 22nd and July 24th.

Reviewer:

Page 11, line 31: " ... bias of the estimated NCCN ranges from about 0 to 30% ... " From your frequency distribution plots in Figure 7, I would put the biases at 10%. That is my simple ocular analysis. Better would be the percent bias at one or two standard deviations of the of the data.

Reply:

The frequency distribution plot in Fig. 7 in the manuscript is for the entire campaign measurement. Therefore most of the bias values are within ±10%. The bias during NPF events is usually larger, especially during MH-type NPF (shown as the left tail of the frequency distribution in Fig. 7). To avoid confusion, the sentence has been revised as "From the discussion in section 3.3 we learned that the bias of the estimated N_{CCN} during NPF events can be up to 30% if a fixed activation ratio curve (best estimation, representative of the region and season) is used"

Reviewer:

Page 12, line 25: I would make a stronger statement. This means that during NPF in the NCP, the CCN activity of newly formed particles was different during these two events; the aerosol present during the organic dominated event was less hygroscopic and less active as CCN for a given diameter and supersaturation.

Reply:

Thanks for the suggestion. The sentence has been revised as "This means that during NPF in the NCP, the CCN activity of newly formed particles was different during these two events; the aerosol present during the LH-type event was less active as CCN for a given diameter and supersaturation"

Reviewer:

Line 29: Again your 0 to 30% values could be more accurately presented as I suggested above, page 11, line 31.

Reply:

Thanks for the suggestion. Similar as for P11L31, the sentence has been revised as "The bias of the estimated N_{CCN} during NPF events can be up to 30% if a fixed activation ratio curve is used"

Reference

Deng, Z. Z., Zhao, C. S., Ma, N., Zhang, Q., Huang, M. Y.: A Method for Measuring Aerosol Activation Ratios with High Size Resolution, Acta Scientiarum Naturalium Universitatis Pekinensis, 48(3), 2012 (in Chinese).

Ehn, M., Petäjä, T., Birmili, W., Junninen, H., Aalto, P., and Kulmala, M.: Non-volatile residuals of newly formed atmospheric particles in the boreal forest, Atmos. Chem. Phys., 7, 677-684, doi:10.5194/acp-7-677-2007, 2007.

Ma, N., Zhao, C. S., Nowak, A., Müller, T., Pfeifer, S., Cheng, Y. F., Deng, Z.Z., Liu, P. F., Xu, W. Y., Ran, L., Yan, P., Göbel, T., Hallbauer, E., Mildenberger, K., Henning, S., Yu, J., Chen, L. L., Zhou, X. J., Stratmann, F., and Wiedensohler, A.: Aerosol optical properties in the North China Plain during HaChi campaign: an in-situ optical closure study, Atmos. Chem. Phys., 11, 5959-5973, doi:10.5194/acp-11-5959-2011, 2011.

Philippin, S., Wiedensohler, A., and Stratmann, F.: Measurements of non-volatile fractions of pollution aerosols with an eight-tube volatility tandem differential mobility analyzer (VTDMA-8), J Aerosol Sci, 35, 185-203, DOI 10.1016/j.jaerosci.2003.07.004, 2004.

Wehner, B., Petäjä, T., Boy, M., Engler, C., Birmili, W., Tuch, T., Wiedensohler, A., and Kulmala, M.: The contribution of sulfuric acid and non-volatile compounds on the growth of freshly formed atmospheric aerosols, Geophys. Res. Lett., 32, L17810, doi:10.1029/2005gl023827, 2005.

Xu, W. Y., Zhao, C. S., Ran, L., Deng, Z. Z., Liu, P. F., Ma, N., Lin, W. L., Xu, X. B., Yan, P., He, X., Yu, J., Liang, W. D., and Chen, L. L.: Characteristics of pollutants and their correlation to meteorological conditions at a suburban site in the North China Plain, Atmos. Chem. Phys., 11, 4353-4369, doi:10.5194/acp-11-4353-2011, 2011.

Yue, D. L., Hu, M., Zhang, R. Y., Wang, Z. B., Zheng, J., Wu, Z. J., Wiedensohler, A., He, L. Y., Huang, X. F., and Zhu, T.: The roles of sulfuric acid in new particle formation and growth in the mega-city of Beijing, Atmos. Chem. Phys., 10, 4953-4960, doi:10.5194/acp-10-4953-2010, 2010.

Zhang, R., Khalizov, A., Wang, L, Hu, M., and Xu, W.: Nucleation and growth of nanoparticles in the atmosphere, Chem. Rev., 112, 1957–2011, 2012.

Response to comments of referee #2

General comments

This paper investigated the ability of aerosols acting as CCN during the new particle formation (NPF) events over North China Plain. The authors focused on two different NPF events and suggested that the possible deviation of simplified NCCN estimation might be significant for the NPF periods.

Overall comment: The authors differentiated two cased based on the sulfate fraction in PM10 to conclude the sulfate dominant and OM dominated cases. However, the sulfate fraction in PM10 cannot be representative for sub-micron sized particles and that was also stated by the authors. If sulfate fraction in PM10 can represents for the sulfate fraction in sub-micrometer sized particles, the authors should also expect the high sulfate fraction should correspond to higher kappa for all periods and this is not always true. For example, the kappa of 7/20 in the early morning showed a much lower value even though the sulfate fraction is similar to the daytime of 7/20. This analytical method might be suspicious without further validation. The composition variation might be due to the parcel source since the provided two cases has the source difference; i.e. west-southwest wind for 7/22 and northwest wind for 7/24. Could the radiation also play a role affecting the hygroscopicity because 7/22 is a hazy day while 7/24 is a sunny day? Overall, it is difficult to conclude the exact factor with only two cases.

Reply:

Many thanks for this comment.

We have also realized that it was improper to use PM10 chemical composition in our analysis. Most of the OM and sulfate mass is in accumulation mode which is dominated not only by secondary production but also by horizontal and vertical transportation. The mass fractions of sulfate and OM in nucleation mode are therefore not necessarily proportional to their mass fractions in PM10. Unfortunately, we have no measurement about size-resolved particle chemical composition in ultrafine size range. Actually, our collaborator did AMS measurement during the joint intensive campaign. But we met some problem during transporting of our mobile laboratory. Our measurement therefore started too late and has no overlap with AMS measurement in the campaign.

However, we did particle volatility measurement with a volatility tandem differential mobility analyzer (TROPOS-type VTDMA; Philippin et al., 2004) during the campaign. The hygroscopicity and volatility of nanoparticles as measured by the HTDMA and VTDMA is often invoked to provide insight into the particle composition (Zhang et al., 2011). We therefore decided to involve this dataset in our study, together with hygroscopicity data, to provide some additional information about the new particles.

Non-volatile cores were found in 50 nm newly formed particles in all the five NPF events (Fig. R1 and R2). This phenomenon was also observed in Melpitz, Germany (Wehner et al., 2005) and Hyytiälä, Finland (Ehn et al., 2007). The sizes of the non-volatile residues of 50 nm new particles were however different in the five NPF events. In the NPF event on July 20th, 22nd and 25th, the majority of 50 nm new particles exhibited a shrink factor of about 0.3; while on July 24th and 28th, the shrink factor is a slightly higher, about 0.4. It means more polymer-type organics were formed during the growth of new particles on July 24th and 28th. In another study in the same region, Yue et al. (2010) found that sulfuric acid was

the major contributor of the growth of newly formed particles, and organic compounds might also play a major role in some cases. Combining all the information above and the result of particle hygroscopicity, it is very likely that condensation and neutralization of sulfuric acid dominated the growth of the new particles on July 20th, 22nd and 25th; while its contribution was much lower on July 24th and 28th and organic compounds had an important contribution to particle growth.

The possible difference in the chemical composition of new particles might be cause by different factors, e.g. the concentration of precursors and the activity of some reactions. These factors might be determined or influenced by other parameters, e.g. ambient temperature, radiation, air mass origin, and vertical mixing. We agreed that the composition of the new particles may strongly depend on the route of air masses, since the air mass routes determine the concentration of precursors to a large extent. In the northern NCP, air masses coming from the south are usually more polluted and with high concentration of SO_2; while air masses coming from the north are much cleaner (Xu et al., 2011; Ma et al., 2011). During the three MH-type NPF events (July 20th, 22nd and 25th), the wind direction was mainly in south section and/or the wind speed was low. The polluted air mass might contain high concentration of SO_2, promoting the production of sulfate in particle phase. During the two LH-type NPF events (July 24th and 28th), the wind direction was N/NW and the air mass was clean. The relative contribution of organic compounds to the particle growth might be therefore higher. The radiation might also play some roles, but we have no radiation measurements during the campaign.

In this study, we aimed at evaluating the variability of the CCN activity during NPF events in an anthropogenically polluted atmosphere and the applicability of some simplified CCN parameterization. To find out the reason behind the composition variation of the new particles is out of the scope of this study, and needs more additional measurements which are not available. So we decided to focus on CCN activity and not go deep into questions about particle composition. Although the chemical composition measurement of ultrafine particles was not available, the online measurements of hygroscopicity and volatility can already provide information for distinguishing different NPF types and explaining the variation in CCN activity.

In the manuscript, we now build most of the discussion in section 3.1 and 3.2 on the basis of HTDMA and VTDMA measurements, instead of on PM10 chemical composition data. Since we have no direct measurement of nanoparticle chemical composition, to be more accurate, we have modified the name of the two types of NPF events. The events on July 20th, 22nd and 25th were termed MH-type NPF (NPF with More Hygroscopic particles); while the events on July 24th and 28th were termed LH-type NPF (NPF with Less Hygroscopic particles).

We have deleted most of the content about PM10 composition data, added a new section to introduce VTDMA measurement, revised section 3.1 and 3.2, added VTDMA data in figure 2, 3 and 6 (shown as Fig. R1, R2 and R3), and replaced figure 4 with a new figure of average κ-PDF and f_s-PDF during NPF (Fig. R4). In the following we list the major new content which has been added in the revised manuscript (in dark blue color).

In section 2.5:

Particle shrink factor (f_s), defined as the ratio between the diameter of a particle after being heated at a certain temperature and its original diameter, was measured with a volatility tandem differential mobility analyzer (TROPOS-type VTDMA; Philippin et al., 2004) at 300 °C. The same dry particle diameters as

HTDMA measurement (50, 100, 150, 200, 250, 300 and 350 nm) was selected for VTDMA measurement. The time resolution of full scans was about 50 minutes.

The VTDMA has a similar structure as the HTDMA with the only difference in the conditioning unit – the humidifier is replaced with a volatilization column, where volatile compounds would evaporate at 300 °C revealing non-volatile particles or cores (Burtscher et al., 2001). The residence time of the particles in the heating column was 0.5 s, which is sufficient to evaporate the volatile fraction of particles in a narrow size range (Philippin et al., 2004). The TDMA inversion algorithm developed by Gysel et al. (2009) was used for data inversion. Ambient temperature (25 °C) scans were used to correct the size shift between the two DMAs and define the width of the transfer function (Gysel et al., 2009). 203 nm PSL particles were used to calibrate the offset in sizing of the two DMAs on weekly basis.

The probability density function of f_s (f_s-PDF) was used in this study. We simply define the particles with f_s<0.8 as non-volatile mode particles, and the rest as volatile mode particles. The volume fraction remain of volatile mode particles at 300 °C was calculated with $VFR_V = \frac{\int_{f_s=0}^{0.8} f_s \cdot c(f_s)\, df_s}{\int_{f_s=0}^{0.8} c(f_s)\, df_s}$, where $c(f_s)$ is the probability density function of f_s.

In section 3.1:

The hygroscopicity and volatility of nanoparticles as measured by the HTDMA and VTDMA is often invoked to provide insight into the particle composition (Zhang et al., 2011). It is interesting to see in Fig. 2 that the hygroscopicity of newly formed particles is largely different in the five events. On July 20th, 22nd and 25th, after the nucleation mode grew to 50 nm, the κ-PDF at 50 nm exhibited a dominant hygroscopic mode at κ around 0.4 until 18:00 LT. However, the newly formed, 50 nm, particles exhibited a much lower κ on July 24th and 28th. In the late afternoon on July 24th, the hygroscopic mode was located between 0.1 and 0.2. On July 28, the average κ of hygroscopic mode was also lower than 0.2. The hygroscopicity parameter κ of a particle is mainly determined by its chemical composition (Petters and Kreidenweis, 2007). Therefore, it can be assumed that the particulate matter produced during the growth process was dominated by different species in different NPF events.

The difference in chemical composition of new particles was also reflected by the VTDMA measurement. Non-volatile residual at 300 ℃ can be found in 50 nm newly formed particles in all the five NPF events. This phenomenon was also observed in Melpitz, Germany (Wehner et al., 2005) and Hyytiälä, Finland (Ehn et al., 2007). And the non-volatile cores were presumed to be polymer-type organics (Wehner et al., 2005; Ehn et al., 2007). In our measurements, the sizes of the non-volatile cores of 50 nm new particles were however different in the five NPF events. In the event on July 20th, 22nd and 25th, the majority of 50 nm new particles exhibited a shrink factor of about 0.3; while on July 24th and 28th, the shrink factor is a slightly higher, about 0.4. This means more polymer-type organics were formed during the growth of new particles on July 24th and 28th.

In a study combining in-situ measurements and aerosol dynamic model, sulfuric acid was found to be the major contributor of the growth of newly formed particles in the north NCP, and organic compounds were also found to play a major role in some cases (Yue et al., 2010). Yue et al. (2010) classified NPF events in the north NCP into two types, i.e. sulfur-rich and sulfur-poor events, in which the growth of the new

particles is respectively dominated by sulfates and organics. Observed in the same region, our measurements of particle hygroscopicity and volatility can be also well explained by the two NPF types as in Yue et al. (2010). The NPF events on July 20th, 22nd and 25th are very like the sulfur-rich type NPF, i.e., condensation and neutralization of sulfuric acid contributed most to the growth of the new particles, and resulted in a high particle hygroscopicity. The NPF events on July 24th and 28th are like the sulfur-poor event, i.e., condensation of organic compounds had a higher contribution to the growth, resulting in a lower particle hygroscopicity, and more polymers might be produced (Kalberer et al., 2004), resulting in a higher shrink factor.

As a reference, the mass fraction of organic and sulfate compounds in PM10 obtained from offline analysis of 12-h DIGITEL HV-samples are shown in the bottom subplots of Fig. 2. It should be noted that the ultrafine particles account for only a minor fraction in PM10 total mass and the mass fractions of organics and sulfate are determined not only by the activity of secondary production, but also the long range transportation and vertical mixing. It can be seen that the average mass fraction of organics during the daytime of July 20th, 22nd and 25th was lower than the average of the previous nighttime, while the mass fraction of sulfate obviously increased (July 22nd and 25th) or at least stayed at the same level (July 20th). And the opposite variation can be found on July 24th and 28th. This is basically consistent with the measurements of particle hygroscopicity and volatility.

The possible difference in the chemical composition of new particles might be cause by several factors, e.g. the concentration of precursors and the activity of some reactions. Furthermore, these factors might be determined or influenced by other parameters, e.g. ambient temperature, radiation, air mass origin, and vertical mixing. To find out the reason of the composition variation of the new particles is out of the scope of this study, and needs some additional measurements which are not available. In the following sections, we will focus on the CCN activity of new particles in the two types of NPF event. Since we have no direct measurement of the chemical composition of ultrafine particles, to be accurate, the events on July 20th, 22nd and 25th are termed MH-type NPF (NPF with More Hygroscopic particles), while the events on July 24th and 28th are termed LH-type NPF (NPF with Less Hygroscopic particles).

In section 3.2.1:

As the boundary layer developed in the morning, the particulate condensational sink (Kulmala et al., 2001) and the mass concentration of BC and sub-800 nm particles started to decrease at 07:00 LT. The newly formed particles started to be visible in our SMPS record at around 09:00 LT. The indicatory parameters for NPF, $N_{[40\text{-}60nm]}$ and the geometric mean diameter of nucleation mode, increase in coincidence over a three-hour period. Large amount of secondary particulate matter was produced during the growth of new particles, shown as a sharp increase in sub-80 nm particle mass concentration. The new particles continued growing until the end of the day with an average growth rate of 6.3 nm h^{-1} (Fig. 3A). The newly formed particles reached 50 nm at around 10:30 LT, resulting in a sharp elevation of $N_{[40\text{-}60nm]}$ from about 2×10^3 cm^{-3} to 1×10^4 cm^{-3}. Correspondingly, the number fraction of nearly hydrophobic mode particles (NF_{NH}) and non-volatile mode particles (NF_{NV}) decreased from about 0.2 to 0, meaning that the newly formed particles grew to 50 nm and dominated the nuclei mode number. This can also be confirmed by the average κ-PDF and f_s-PDF during the NPF event (Fig. 4). Both κ-PDF and f_s-PDF exhibited narrow unimodal patterns, indicating that the majority of 50 nm particles originated from the same source, NPF. Identifying as MH type, during the NPF event, the 50 nm new particles exhibited a much higher $\kappa_{ave,H}$ than the pre-existing particles (about 0.45 vs. 0.3). As discussed in section 3.1, it is very likely that the condensation and neutralization of sulfuric acid contributed most to the growth of the new particles.

In section 3.2.2:

The NPF event started at around 09:00 LT. The growth of newly formed particles continued throughout the day with an average growth rate of 6.3 nm h-1 (Fig. 6A). It can be seen that N[40-60nm] increased from about 2×103 cm-3 to 1.4×104 cm-3 in a few hours, N[60-80nm] also increased during the daytime. As the newly formed particles grew to 50 nm and become the majority at this size, the number fraction of nearly-hydrophobic mode and non-volatile mode particles decreased to almost 0 within 1 hour. The κ-PDF and fs-PDF also exhibited narrow unimodal patterns (Fig. 4). It is interesting to note that, unlike the event on July 22nd, the average κ for the hygroscopic mode of 50 nm particles decreased a bit after the nucleation, and stayed below 0.3 for the rest of the day. Such low hygroscopicity of newly formed particles implies that the driving mechanism of particle growth in daytime for this event was somehow different from the event on July 22nd. It very likely that sulfuric acid played a less important role in the growth process, and organics had a higher contribution, compared with the MH-type NPF. It can be also seen in Fig. 6E that VFRV during this NPF event is higher than that during the event on July 22nd, meaning that the more polymer-type organics was produced during the growth of the new particles in this event.

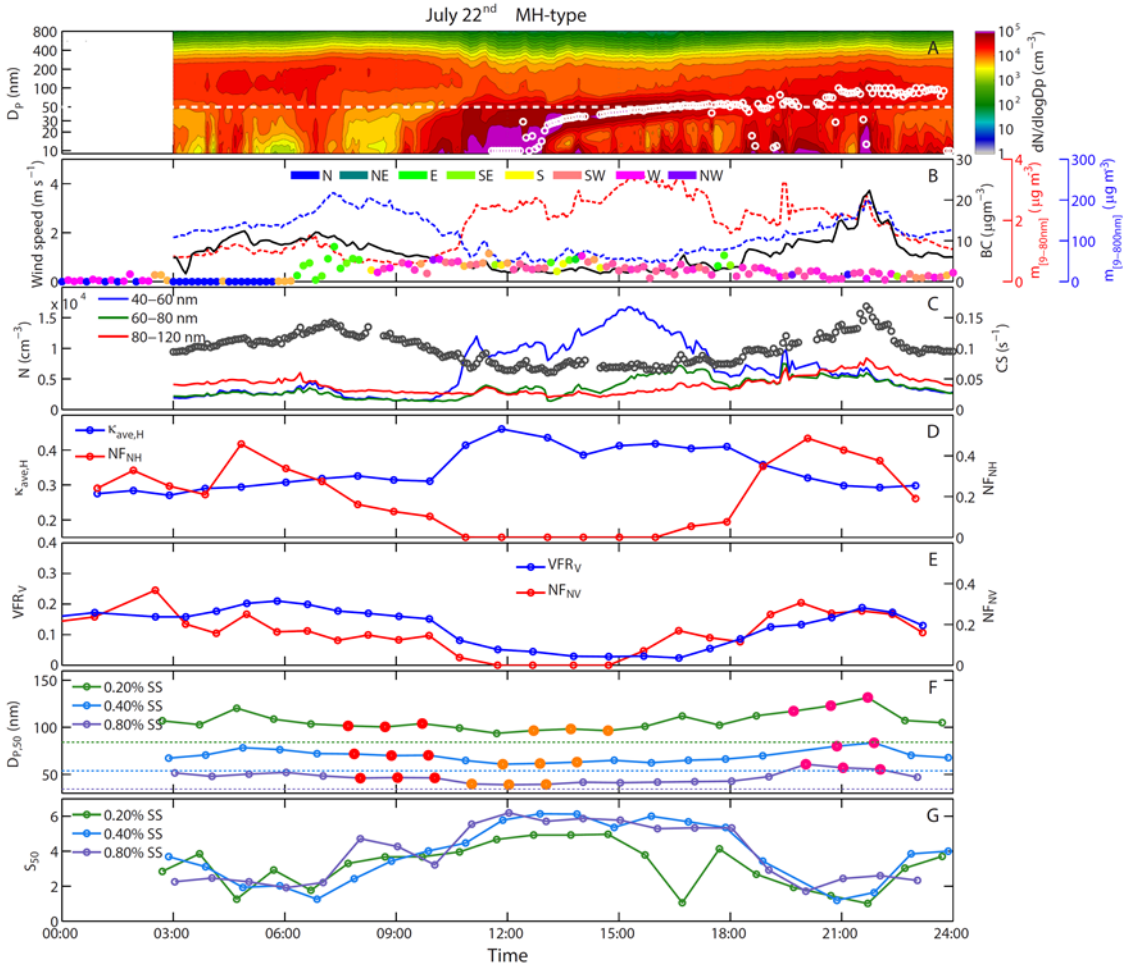

Fig. R1 (Fig. 3 in manuscript). MH-type NPF event on July 22nd. Time series of (A) particle number size distribution and geometric mean diameter of nucleation mode, (B) wind speed/direction and the mass

concentration of BC, sub-80 nm and sub-800 nm particles, (C) condensational sink (CS) and number concentration of particles in defined size ranges, (D) average κ of hygroscopic mode and number fraction of nearly-hydrophobic mode for 50 nm particles, (E) volume fraction remaining of volatile mode and number fraction of non-volatile mode for 50 nm particles, (F) $D_{P,50}$ for 0.20%, 0.40% and 0.80% SS, as well as (G) S_{50} for the three SS. The dashed lines in panel F show the theoretical critical diameters for ammonium sulfate at the three SS. Points filled with color in panel G show the records selected to calculate the average size-resolved activation ratio shown in Fig. 5.

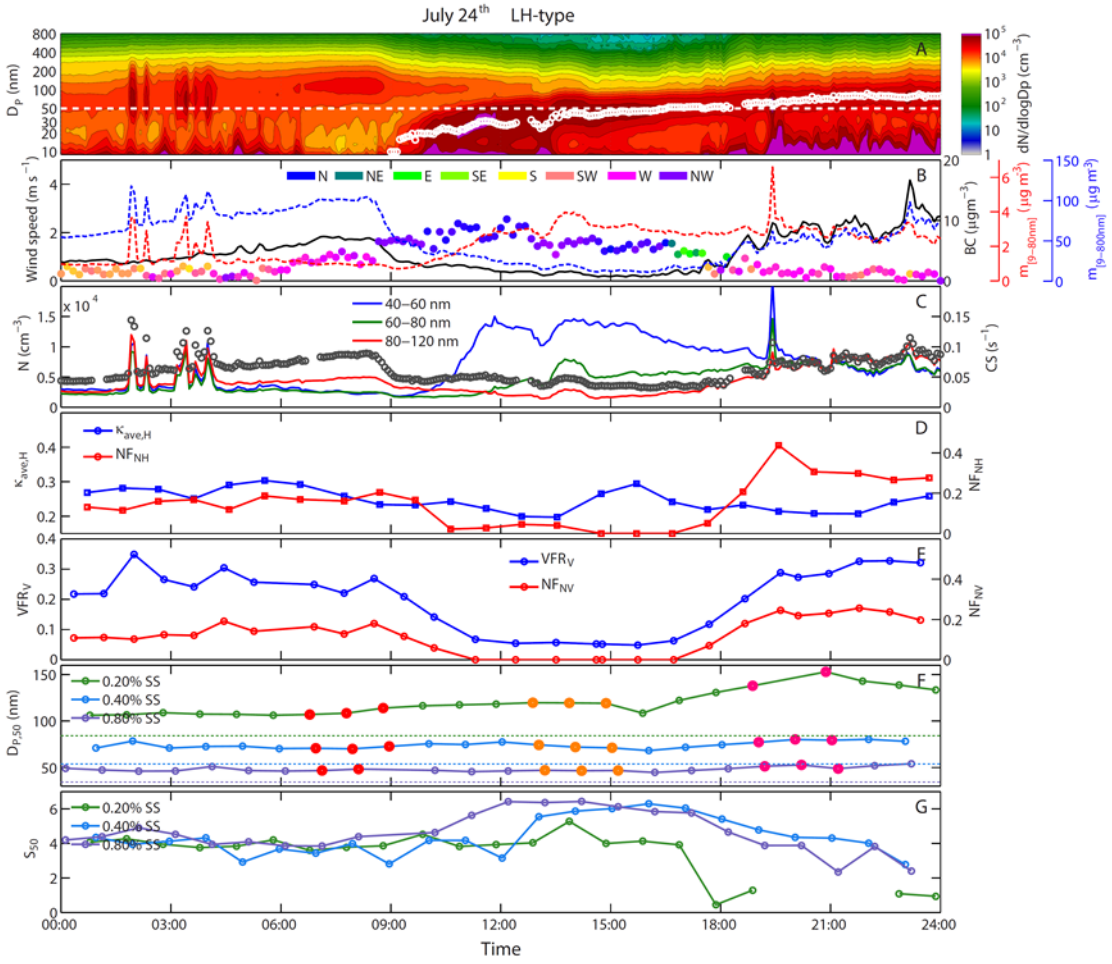

Figure R2 (Fig. 6 in manuscript). LH-type NPF event on July 24th. Time series of (A) particle number size distribution and geometric mean diameter of nucleation mode, (B) wind speed/direction and the mass concentration of BC, sub-80 nm and sub-800 nm particles, (C) condensational sink (CS) and number concentration of particles in defined size ranges, (D) average κ of hygroscopic mode and number fraction of nearly-hydrophobic mode for 50 nm particles, (E) volume fraction remaining of volatile mode and number fraction of non-volatile mode for 50 nm particles, (F) $D_{P,50}$ for 0.20%, 0.40% and 0.80% SS, as well as (G) S_{50} for the three SS. The dashed lines in panel F show the theoretical critical diameters for ammonium sulfate at the three SS. Points filled with color in panel G show the records selected to calculate the average size-resolved activation ratio shown in Fig. 5.

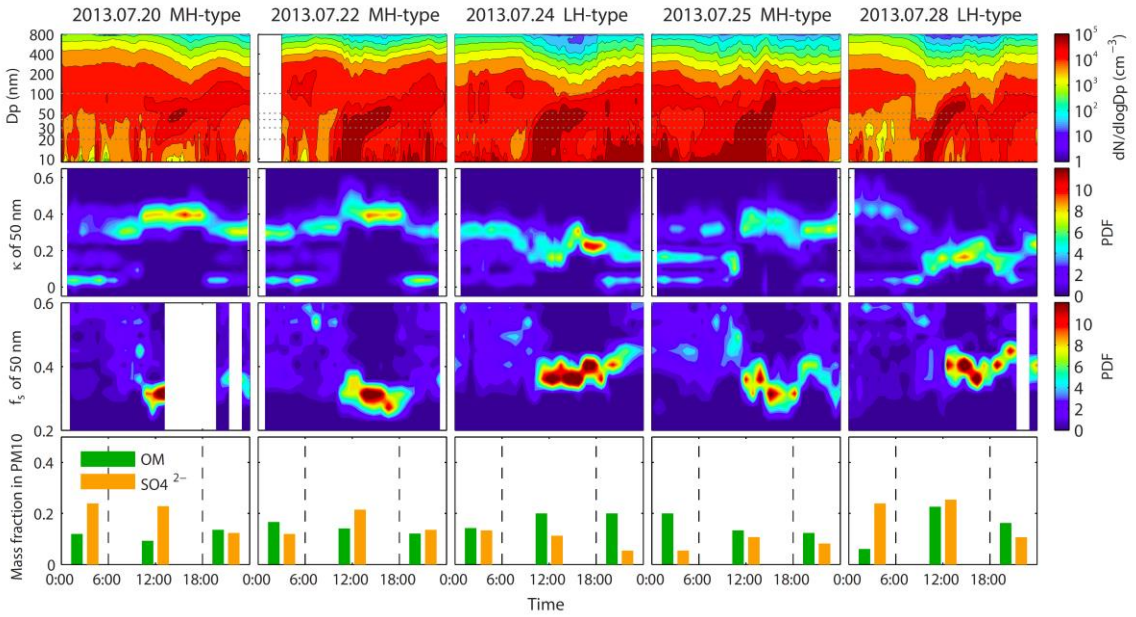

Fig. R3 (Fig. 2 in manuscript). 5 NPF events observed during the campaign period. Subplots show the time series of particles number size distribution, κ-PDF of 50 and f_s-PDF of 50 nm particles, and mass fraction of organics and sulfate from PM10 HV-sample analysis.

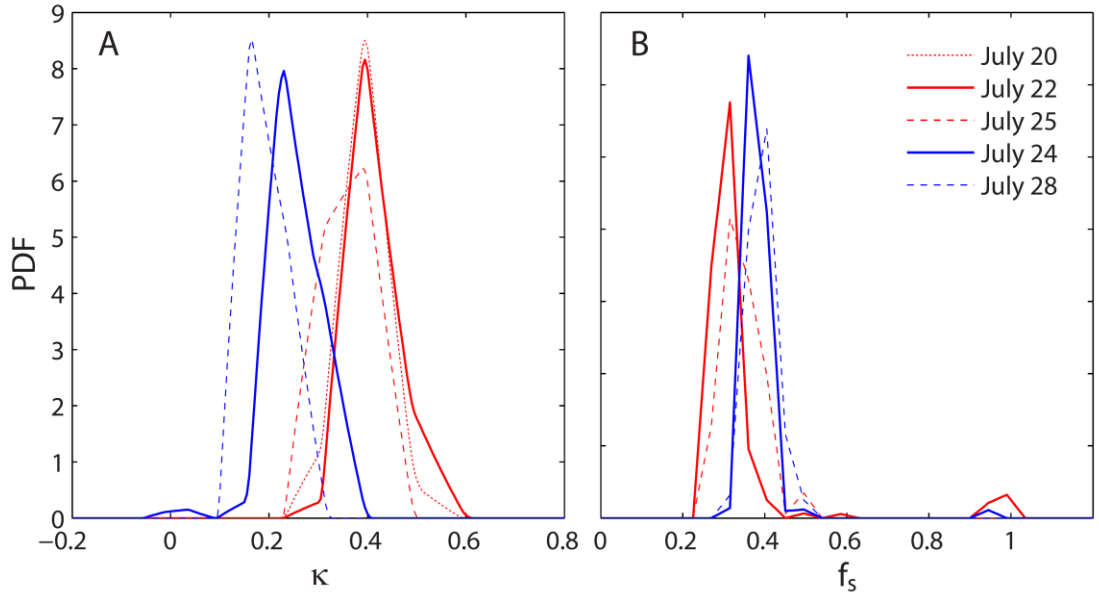

Fig. R4 (Fig. 4 in manuscript). Average κ-PDF (A) and f_s-PDF (B) of 50 nm particles during the 5 NPF events.

Other comments

Reviewer:

1. Lines 4-11 of Page 4: How many sizes did the authors scan for a given SS?

Reply:

The DMA-CCNC system is operated in a size-scanning mode. After the data inversion, the final activation ratio curve was given at 40 sizes, from about 9 to 300 nm. To make it clear, we added "The system is operated in a size-scanning mode" into the text.

Reviewer:

2. There were two methods applied to determine the hygroscopicity. How is the comparison?

Reply:

The κ derived from 50% activation ratio ($D_{P,50}$) from DMA-CCNC measurement, and derived from hygroscopic growth factor measured with HTDMA are shown in Fig. R5. Generally, κ derived with two measurements agree with each other. For larger sizes, CCNC-derived κ are higher than HTDMA-derived κ. This is probably because the κ of some secondary organic aerosols (SOA) may increase at high RH. SOA-particles were more CCN active than suggested by their sub-saturated growth factors at RH<98% (Wex et al., 2009 and references therein). We also added Fig. R5 into the supplement as a reference (Fig. S1).

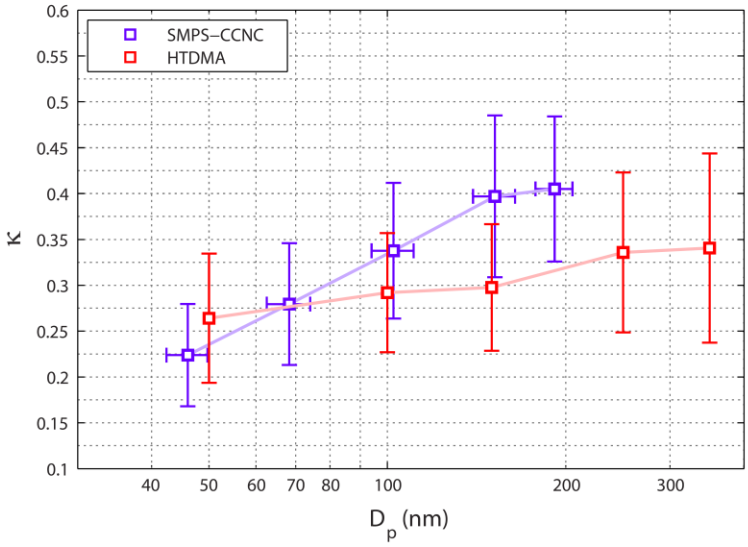

Fig. R5. Comparison of κ derived with DMA-CCNC measurement and HTDMA measurement.

Reviewer:

3. Line 20 of Page 20: the authors stated there are 10 out of 28 days associated with NPF events but only 5 days with particle growing. What parameter controls the growing process? Does the hygroscopicity of aerosols at these two cases different?

Reply:

Thanks for this comment. We realize that the statement "NPF events were observed on 10 of 28 days and clear growth of newly formed particles was observed on 5 of those days" in the manuscript is somehow inaccurate. The 10 observed NPF events during the campaign are shown in Fig. R6, R7 and R8. Actually, the 5 events shown in Fig. 2 in the manuscript are good NPF cases with very clear growth and without strong fluctuation in diameter and concentration of the nucleation mode (i.e. Class I in the classification system in Dal Maso et al., 2005). In the other 5 events, we also observed particle growth in 4 of them, which is weak and/or with strong fluctuations (i.e. Class II and undefined events in the classification system in Dal Maso et al., 2005) (Fig. R7). There is only one event which is clearly without growth (Fig. R8).

To make it clearer, we revised the statement in section 3.1 as "During our intensive field campaign, NPF events were observed on 10 of 28 days. Clear growth of nucleation mode particles without strong fluctuations in diameter or concentration (i.e. Class I of the classification system in Dal Maso et al., 2005) was observed on 5 of those days."

There are many possible parameters which may influence or interrupt the growth of new particles, for example, variations in solar radiation (cloud cover), temperature, and concentration of precursors. Moreover, NPF usually occurred inhomogeneously in horizontal and vertical scale in a region. Horizontal wind and vertical mixing may also result in fluctuations in the PNSD measured at a fixed point. As an example, we did not observe the growth of nucleation mode particles on July 16th, probably because the strong north wind blew the newly formed particles away from the area of our station (Fig. R8). With the measurement we have, it is difficult to evaluate the parameter(s) controlling the growth process.

The hygroscopicity and volatility of 50 nm particles during the 10 NPF events are also displayed in Fig. R6, R7 and R8. On August 8th, when new particles dominated 50 nm (around 14:00 LT), we can see a decrease in both $\kappa_{ave,H}$ and VFR_V. The values of $\kappa_{ave,H}$ and VFR_V are similar as those in the other 2 LH-type NPF (July 24th and 28th), so this event can be also classified as a LH-type event. For the other 4 events (July 16th, 17th, 21st and 23rd), since 50 nm was not dominated by the new particles and/or some data is missing due to instrumental issues, it is difficult to make any conclusion on the hygroscopicity and volatility of the new particles.

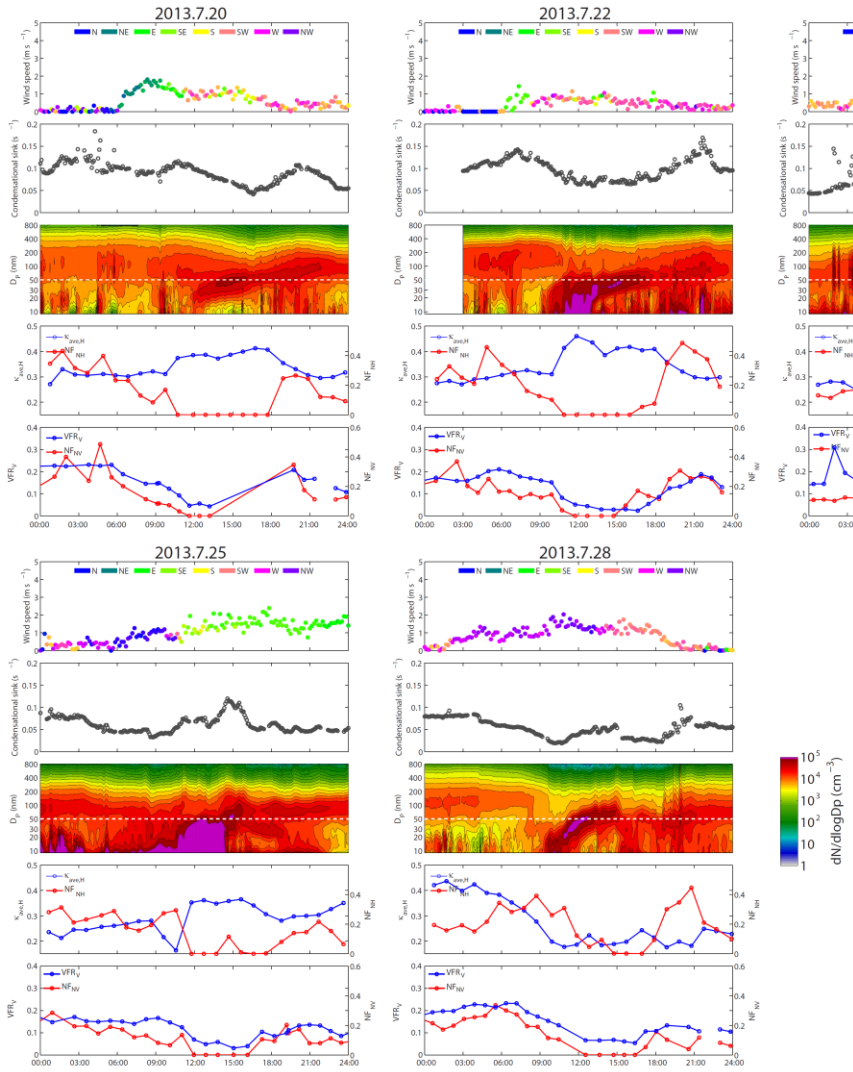

Fig. R6. Wind speed and direction, BC mass concentration, particle number size distribution, average κ of hygroscopic mode and number fraction of hydrophobic mode for 50 nm particles, volume fraction remaining of volatile mode and number fraction of non-volatile mode for 50 nm particles of the 5 NPF events with clear and smooth growth (i.e. Class I in the classification system in Dal Maso et al., 2005).

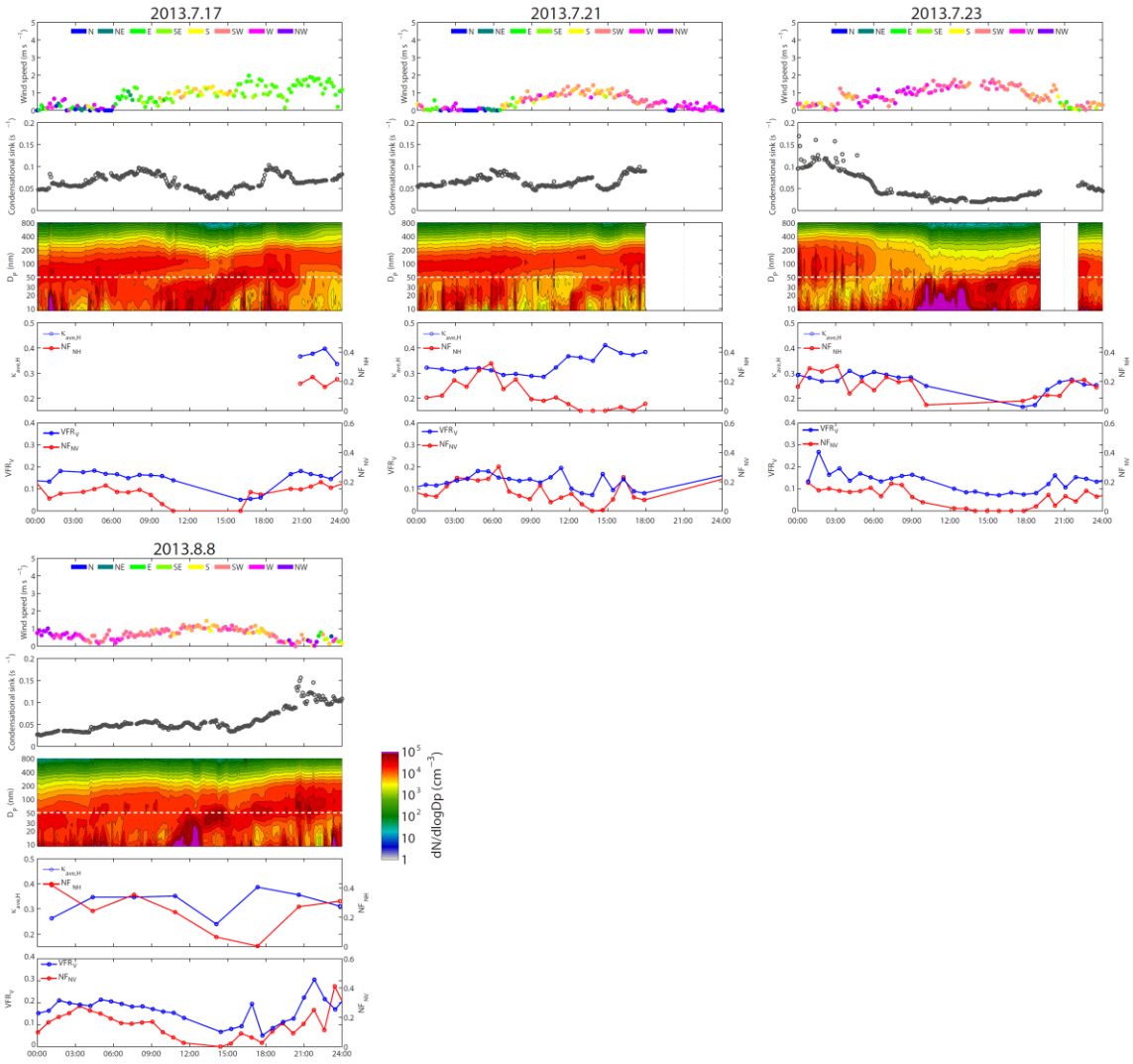

Fig. R7. Wind speed and direction, BC mass concentration, particle number size distribution, average κ of hygroscopic mode and number fraction of hydrophobic mode for 50 nm particles, volume fraction remaining of volatile mode and number fraction of non-volatile mode for 50 nm particles of the 4 NPF events with unclear growth (i.e. Class II and undefined events in the classification system in Dal Maso et al., 2005).

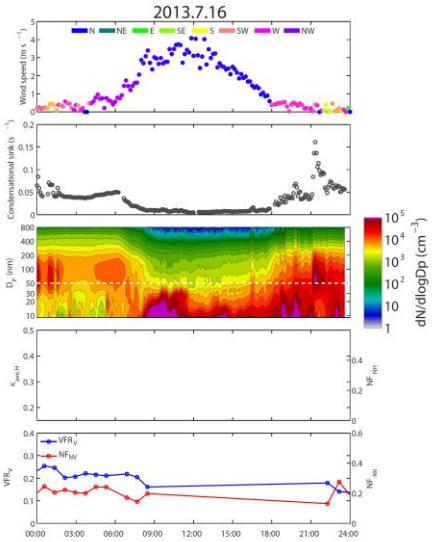

Fig. R8. Wind speed and direction, BC mass concentration, particle number size distribution, average κ of hygroscopic mode and number fraction of hydrophobic mode for 50 nm particles, volume fraction remaining of volatile mode and number fraction of non-volatile mode for 50 nm particles of the NPF events without growth.

Reviewer:

4. Because the authors focused on the NPF events, the date of Figure 4 should be the same as Figure 2.

Reply:

Figure 4 in manuscript has been replaced with a new figure of average κ-PDF and f_s-PDF of 50 nm particles during NPF, as shown as Fig. R4.

Reviewer:

5. Line 10 of Page 9: What is the average activation ratio profile the authors applied?

Reply:

The average activation ratio curve for 0.80% SS (shown as solid black line in panel A of Fig. 5 in manuscript) was applied in the calculation here. To make it clear, the sentence has been revised as "To answer this question, CCN number concentration was respectively calculated with Eq. (2) based on the campaign average activation ratio (shown as the solid black line in Fig. 5A; the calculated CCN number concentration is termed $N_{CCN,AR\text{-}ave}$), campaign average critical diameter (termed $N_{CCN,D\text{-}ave}$) and real-time activation ratio (termed $N_{CCN,ref}$) at 0.80% SS."

Reviewer:

6. The label of y axis for all SMPS figures should be Diameter (nm) not the number concentration.

Reply:

Thanks for point out the mistake. They have been corrected, as shown in Fig. R1, R2 and R3.

Reviewer:

7. The color bar for SMPS and k in Figure 2 should be provided.

Reply:

The colorbar for SMPS contour plot has been added, as shown in Fig. R3.

Reviewer:

8. There are two ticks for the right y axes of Figure 6B, 6C and 6D which should be modified.

Reply:

Thanks for the comment. The wrong ticks have been removed, as shown in Fig. R1 and R2.

Reference

Dal Maso, M., Kulmala, M., Riipinen, I., Wagner, R., Hussein, T., Aalto, P. P., and Lehtinen, K. E. J.: Formation and growth of fresh atmospheric aerosols: eight years of aerosol size distribution data from SMEAR II, Hyytial¨a, Finland, Boreal Environ. Res., 10, ¨323–336, 2005.

Ehn, M., Petäjä, T., Birmili, W., Junninen, H., Aalto, P., and Kulmala, M.: Non-volatile residuals of newly formed atmospheric particles in the boreal forest, Atmos. Chem. Phys., 7, 677-684, doi:10.5194/acp-7-677-2007, 2007.

Ma, N., Zhao, C. S., Nowak, A., Müller, T., Pfeifer, S., Cheng, Y. F., Deng, Z.Z., Liu, P. F., Xu, W. Y., Ran, L., Yan, P., Göbel, T., Hallbauer, E., Mildenberger, K., Henning, S., Yu, J., Chen, L. L., Zhou, X. J., Stratmann, F., and Wiedensohler, A.: Aerosol optical properties in the North China Plain during HaChi campaign: an in-situ optical closure study, Atmos. Chem. Phys., 11, 5959-5973, doi:10.5194/acp-11-5959-2011, 2011.

Philippin, S., Wiedensohler, A., and Stratmann, F.: Measurements of non-volatile fractions of pollution aerosols with an eight-tube volatility tandem differential mobility analyzer (VTDMA-8), J Aerosol Sci, 35, 185-203, DOI 10.1016/j.jaerosci.2003.07.004, 2004.

Wehner, B., Petäjä, T., Boy, M., Engler, C., Birmili, W., Tuch, T., Wiedensohler, A., and Kulmala, M.: The contribution of sulfuric acid and non-volatile compounds on the growth of freshly formed atmospheric aerosols, Geophys. Res. Lett., 32, L17810, doi:10.1029/2005gl023827, 2005.

Wex, H., Petters, M. D., Carrico, C. M., Hallbauer, E., Massling, A., McMeeking, G. R., Poulain, L., Wu, Z., Kreidenweis, S. M., and Stratmann, F.: Towards closing the gap between hygroscopic growth and activation for secondary organic aerosol: Part 1 – Evidence from measurements, Atmos. Chem. Phys., 9, 3987-3997, doi:10.5194/acp-9-3987-2009, 2009.

Xu, W. Y., Zhao, C. S., Ran, L., Deng, Z. Z., Liu, P. F., Ma, N., Lin, W. L., Xu, X. B., Yan, P., He, X., Yu, J., Liang, W. D., and Chen, L. L.: Characteristics of pollutants and their correlation to meteorological conditions at a suburban site in the North China Plain, Atmos. Chem. Phys., 11, 4353-4369, doi:10.5194/acp-11-4353-2011, 2011.

Yue, D. L., Hu, M., Zhang, R. Y., Wang, Z. B., Zheng, J., Wu, Z. J., Wiedensohler, A., He, L. Y., Huang, X. F., and Zhu, T.: The roles of sulfuric acid in new particle formation and growth in the mega-city of Beijing, Atmos. Chem. Phys., 10, 4953-4960, doi:10.5194/acp-10-4953-2010, 2010.

Zhang, R., Khalizov, A., Wang, L, Hu, M., and Xu, W.: Nucleation and growth of nanoparticles in the atmosphere, Chem. Rev., 112, 1957–2011, 2012.

Variation of CCN activity during new particle formation events in the North China Plain

N. Ma[1,2,4], C. S. Zhao[2,*], J. C. Tao[2], Z. J. Wu[3], S. Kecorius[1], Z. B. Wang[1,4], J. Größ[1], H. J. Liu[2], Y. X. Bian[2], Y. Kuang[2], M. Teich[1], G. Spindler[1], K. Müller[1], D. van Pinxteren[1], H. Herrmann[1], M. Hu[3], A. Wiedensohler[1]

[1]Leibniz Institute for Tropospheric Research, Leipzig 04318, Germany
[2]Department of Atmospheric and Oceanic Sciences, School of Physics, Peking University, Beijing 100871, China
[3]College of Environmental Sciences and Engineering, Peking University, Beijing 100871, China
[4]Multiphase Chemistry Department, Max Planck Institute for Chemistry, Mainz 55128, Germany

Correspondence to: C. S. Zhao (zcs@pku.edu.cn)

Abstract. The aim of this investigation was to obtain a better understanding of the variability of the cloud condensation nuclei (CCN) activity during new particle formation (NPF) events in an anthropogenically polluted atmosphere of the North China Plain (NCP). We investigated ~~the~~ size-resolved activation ratio as well as particle number size distribution, hygroscopicity and ~~chemical composition~~volatility during a ~~an~~ 4-week intensive field experiment in summertime at a regional atmospheric observatory at Xianghe. Interestingly, based on a case study, two types of NPF events were found, in which the newly formed particles exhibited either a higher or a lower hygroscopicity~~growth of the newly formed particles is was dominated by either sulfate or organic matters~~. Therefore, ~~The~~ particle CCN activity ~~therefore~~ differed significantly ~~differs~~ in those NPF events, indicating that ~~it might be difficult to find~~ a simple parameterization of particle CCN activity during NPF events over the NCP might lead to poor estimates. For ~~an~~ a more accurate estimation of the potential CCN number concentration (N_{CCN}) during NPF events, the variation of CCN activity has to be taken into account. Considering that a fixed activation ratio curve or critical diameter are usually used to calculate N_{CCN}, the influence of the variation of particle CCN activity on the calculation of N_{CCN} during NPF events was evaluated based on ~~these~~ two parameterizations. It was found that N_{CCN} might be underestimated by up to 30% if a ~~fix~~ single activation ratio curve (representative of the region and season) ~~is~~ were to be used in the calculation; and might be underestimated by up to 50% if a fixed critical diameter (representative of the region and season) ~~is~~ were used. Therefore, we suggest not using a fixed critical diameter in the prediction of N_{CCN} in NPF ~~seasons~~. If real-time CCN activity data is not available, using a proper fixed activation ratio curve can be ~~a compromising~~an alternative but compromised choice.

1 Introduction

Atmospheric nucleation and the subsequent ~~particle~~ growth of nucleated clusters, ~~(~~a new particle formation event, NPF ~~event)~~ , is frequently observed in a variety of environments around the world (Kulmala et al., 2004; Kulmala and Kerminen, 2008 and references therein)~~, which~~. This is believed to be an important source of cloud condensation nuclei (CCN). However, the contribution of homogeneous nucleation to the CCN number concentration is still not well defined~~,~~ and has therefore gained ~~a lot of~~considerable attention~~s~~ during the last decade (Kerminen et al., 2012 and references therein).

Because the size of a particle plays the most important role in determining its CCN activity (Dusek et al., 2006)~~,~~ many studies use~~d~~ the number concentration of particles larger than a ~~distinct~~critical diameter, $D_{P,cri}$ (i.e., an integral of particle number size distribution, PNSD) as a proxy ~~of~~ for the number concentration of potential CCN for a certain super saturation (SS). This method yields ~~into~~ an average relative contribution of NPF to CCN spanning from few percent to several tens of percent for different supersaturations, SS, and ~~regions~~ NPF event type (e.g. Laaksonen et al., 2005; Kuang et al., 2009; Asmi et al., 2011; Peng et al., 2014). Without a direct measurement of the CCN number concentration, such ~~kind of treatment~~parameterization is reasonable to obtain an ~~rough~~ approximation of the contribution of NPF to CCN. However, large uncertainties might be ~~included~~ incurred in those results. Only a few studies have investigated the variation of the CCN number concentration during ~~the~~ an NPF event with direct CCN measurement (e.g. Kuwata et al., 2008; Wiedensohler et al., 2009; Sihto et al., 2011).

The diameter of nucleated clusters is around 1 – 2 nm (Kulmala et al., 2007). To ~~contribute to the~~become effective CCN ~~number concentration~~, newly formed particles need to grow about 10^4 to 10^5 times in volume (i.e. ~~at least up~~ to about 30 to 50 nm, depending on cloud types). This means that the chemical composition of those particles is ~~basically~~ almost entirely determined by the condensing material. Although particle size is the parameter of primary importance, chemical composition does modify the PNSD-based CCN determination by affecting the hygroscopicity or solubility of the potential CCN particles. But this effect is only significant for particles at or slightly greater than $D_{P,cri}$. However, if the condensing vapor causing particle growth has a strong surfactant effect that lowers the water vapor accommodation coefficient or diffusion of condensed water during cloud droplet formation from the particle's surface into its volume, then the chemical composition effect on CCN fraction may extend to diameter much larger than $D_{P,cri}$. ~~Although not as important as size, particle chemical composition also plays some roles in determining its CCN activity.~~

~~-~~A number of studies have investigated the mechanism of the growth of newly formed particles. Low-volatile organic compounds are suggested to play the major role in particle growth (Kulmala et al., 1998; Kerminen et al., 2000, Wehner et al., 2005), which has been proved in many observations in different region (e.g. Laaksonen et al., 2008; Smith et al., 2010; Ehn et al., 2014~~);),~~ while sulfuric acid was also found to play an important role in the growth process (Birmili et al., 2003; Boy et al., 2005). Yue et al. (2010) found two types of NPF events in Beijing in which either sulfate compounds or organic ~~matters~~material (OM) can be the dominant species in ultrafine particles. Therefore, the CCN activity of newly formed particles may differ in different source regions and atmospheric cases, depending on the dominant process in the particles

Formatted: Superscript

Formatted: Font: Italic

Formatted: Subscript

Formatted: Font: Italic

growth. This means, the NPF may influence CCN budget not only by modifying particle number size distribution, but also by changing particle chemistry and consequently CCN activity. However, the variation of particle CCN activity during the NPF event ~~was~~ has been ~~very~~ seldom discussed in previous studies. Especially in China, no such investigation ~~was~~ has been done for regional NPF events.

Measurements of aerosol particle optical properties (Ma et al., 2011, 2012), hygroscopicity (Liu et al., 2011) and CCN activation (Deng et al., 2011) during the Haze campaign in China (HaChi) showed that the North China Plain (NCP) is one of the most anthropogenically polluted regions in the world. With abundant gas phase precursors in the NCP, NPF ~~is~~ occurs frequently ~~occurred~~ (Wu et al., 2007; Wang et al., 2013a)~~,~~ and has a clear and distinct ~~contribution~~ effect on the particle concentration (Guo et al., 2014). The high number concentration of aerosol particles in the NCP may have impacts on cloud microphysical properties and precipitation (Zhao et al., 2006a, b; Deng et al., 2009). To have a better understanding of these impacts, it is essential to have a precise parameterization of particle CCN activity in this polluted region. ~~In the~~As a first step, we have therefore undertaken to investigate and understand the contribution and influence of NPF on particle CCN activity, based on a case study in summertime in the NCP.

2 Measurements and data processing

2.1 Observational Site

During July 9th to August 8th in 2013, ~~aerosol~~ microphysical and optical properties of aerosol particles over the size range from 10 nm to 10 µm were measured at Xianghe station (39.75 N, 116.96 E, 36 m a.s.l.), a regional atmospheric observatory in the NCP about 50 km southeast from Beijing and 70 km west from Tianjin (Figure 1). The observatory is located close to a small village and about 5 km west of Xianghe city center. The surroundings are farmland and residential areas. The measurements can be assumed to be representative of the regional background aerosol of the north NCP during daytime (09:00 – 18:00 LT). From time to time, an influence of local anthropogenic emission could be identified during nighttime (18:00 – 09:00 LT). More information about the site can be found in Zhang et al. (2016).

Most of the online instruments ~~are~~ were located in a measurement container, in which the temperature was maintained at 22 °C. The inlet system consisted of a PM10 inlet (Rupprecht & Patashnick Co., Inc., Thermo, 16.67 l/min), three in-line Nafion dryers (Leibniz-Institute for Tropospheric Research, Germany; Wiedensohler et al., 2013) and an automatic absorption dryer (Leibniz-Institute for Tropospheric Research, Germany; Tuch et al., 2009) ~~based on the design by Tuch et al. (2009)~~. This set up ensured a relative humidity in the aerosol sample flow below 30%. In the measurement container, sampled aerosol was ~~fed~~ directed to separate instruments through stainless steel and/or ~~/~~conductive tubing using an isokinetic flow splitter.

2.2 Particles number size distribution

A mobility particle size spectrometer (TROPOS-type scanning mobility particle size spectrometer, SMPS; Wiedensohler et al., 2012), consisting of a Hauke-type medium differential mobility analyzer (DMA, 28 cm effective length) and a condensation particle counter (CPC Model 3772; TSI, Inc., Shoreview, MN USA), was used to measure PNSDs with mobility diameter from 9 to 800 nm with temporal resolution of 5 min. The measurements were performed in compliance with recently issued guidelines for atmospheric particle size distribution measurements (Wiedensohler et al., 2012). Data evaluation includes a multiple charge correction (Pfeifer et al., 2014), counting efficiency correction of the condensation particle counters (Wiedensohler et al., 1997), and corrections for the diffusion losses in the system and inlet tubing. The mass concentration of sub-80 nm ($m_{[9\text{-}80nm]}$) and sub-800 nm particles ($m_{[9\text{-}800nm]}$) was also calculated from the measured particle number size distribution, with a assumed particle density of 1.6 g cm^{-3}.

2.3 Size-resolved particle activation ratio

The size-resolved particle activation ratio (AR), defined as the ratio ~~between~~ of the number of particles in a defined diameter increment which can be activated instrumentally at a certain SS ~~and~~ to the total number of particles in that increment ~~at a certain diameter~~, was measured by a DMA-CCNC system. The system ~~consists~~ consisted of an electrostatic classifier (Model 3080; TSI, Inc., Shoreview, MN USA)~~,~~ coupled with a condensation particle counter (CPC Model 3772; TSI, Inc., Shoreview, MN USA)~~,~~ and a continuous-flow CCN counter (Model CCN200, Droplet Measurement Technologies, USA; Roberts and Nenes, 2005; Lance et al., 2006). The system is operated in a size-scanning mode. ~~More details about the system are given in Deng et al. (2011).~~ The monodisperse sample flow ~~of~~ from the DMA was split into two flows with flow rate of 1.0 l/min and 0.5 l/min. The CPC and CCN counter measured ~~then~~ the total particle and the CCN number concentrations ~~for a certain~~over the particle size range from ~~xx~~9 to ~~xxx~~300 nm. More details about the system are given in Deng et al. (2011). During the measurement~~,~~ ~~the SS in~~ the CCN counter was ~~circularly set to~~operated at five SS values sequentially, ~~with~~ for 20 min at~~for~~ 0.07% and 10 min each at~~for~~ 0.10%, 0.20%, 0.40% and 0.80%. Two complete size scans were ~~covered in the duration~~made during ~~of~~ each SS setting (4 scans for 0.07%), and only the last scan during each ~~supersaturation~~ SS was used since the ~~system~~ CCN counter needs ~~some~~ time for temperature stabilization ~~stabilizing the temperature~~ in the column after the SS is changed.~~changing the SS.~~ The data from CCN counter during the selected ~~period~~ final scan was matched with particle number concentration measured simultaneously by the CPC. The size-resolved particle activation ratio was then inverted using a modified algorithm based on Hagen and Alofs (1983) (Deng et al., 2011, 2012). The time resolution of a full scan (size-resolved activation ratios at 5 SS) is 1 hour. ~~Finally, the size-resolved activation ratios were available for all the 5~~five SS ~~values once per in each hour.~~ The sheath and sample flow rates were calibrated before the campaign and checked everyday.~~, as well as t~~The SS of CCN counter were calibrated before the campaign and checked at the end of the campaign with monodisperse ammonium sulfate particles (Rose et al., 2008).

Formatted: Font: Italic
Formatted: Subscript
Formatted: Font: Italic
Formatted: Superscript
Formatted: Font: Not Italic

To ~~have a~~ gain better insight into the temporal variation of CCN activity two parameters were derived, the diameter of 50% activation ratio ($D_{P,50}$) and the slope of the activation ratio curve (S_{50}) were used. S_{50} was calculated as $\frac{0.2}{\log D_{P,60} - \log D_{P,40}}$, where 0.2 is the activation ratio difference and $D_{P,40}$ and $D_{P,60}$ are the particle diameters ~~of~~ at activation ratios of 40% and 60% ~~activation ratio~~, respectively.

2.4 Particle hygroscopicity

Particle hygroscopic growth factor (f_g), defined as the ratio between the particle diameter at a certain relative humidity (RH) and the particle dry diameter, was measured with a hygroscopic tandem differential mobility analyzer (TROPOS-type HTDMA; Massling et al., 2007) at 87% RH for dry diameters ($D_{P,dry}$) of 50, 100, 150, 200, 250, 350 nm. The time resolution of the full scan covering ~~all~~ the 6 sizes was about 50 min. The probability density function of f_g (f_g-PDF) is obtained based on the measured distribution function of f_g with the TDMA inversion algorithm developed by Gysel et al. (2009). Calibration with monodisperse ammonium sulfate particles was automatically conducted every 6 hours.

A hygroscopicity parameter κ was calculated according to Petters et al. (2007):

$$\kappa = \left(f_g^3 - 1\right) \cdot \left(\frac{1}{S} \exp\left(\frac{4\sigma_{s/a} M_W}{RT\rho_W D_{P,dry} f_g}\right) - 1\right) \quad (1)$$

where S is the saturation ratio; ρ_W is the density of water; M_W is the molecular weight of water; $\sigma_{s/a}$ is the surface tension of the solution / air interface which is assumed to be equal to the surface tension of the pure water / air interface; R is the universal gas constant; and T is the temperature. The probability density function of κ (κ-PDF) was then derived and used in this study. As shown in Zhang et al. (2016), the κ-PDF usually exhibits a bi-model or tri-model shape. In this study, we simply define the particles with $\kappa > 0.1$ as hygroscopic mode particles, and the rest as nearly-hydrophobic mode particles. More details about this measurement and data processing can be found in Zhang et al. (2016). As a reference, a comparison of κ derived with SMPS-CCNC measurement and HTDMA measurement is shown in Fig. S1 in supplement.

2.5 Particle volatility

Particle shrink factor (f_v), defined as the ratio between the diameter of a particle after being heated at a certain temperature and its original diameter, was measured with a volatility tandem differential mobility analyzer (TROPOS-type VTDMA; Philippin et al., 2004) at 300 °C. The same dry particle diameters as HTDMA measurement (50, 100, 150, 200, 250, 300 and 350 nm) was selected for VTDMA measurement. The time resolution of full scans was about 50 minutes.

The VTDMA has a similar structure as the HTDMA with the only difference in the conditioning unit – the humidifier is replaced with a volatilization column, where volatile compounds would evaporate at 300 °C revealing non-volatile particles or cores (Burtscher et al., 2001). The residence time of the particles in the heating column was 0.5 s, which is sufficient to evaporate the volatile fraction of particles in a narrow size range (Philippin et al., 2004). The TDMA inversion algorithm

Formatted: Font: Not Italic
Formatted: English (U.K.)
Formatted: English (U.K.)
Formatted: Heading 3
Formatted: Font: Italic
Formatted: Font: Italic, Subscript
Formatted: English (U.S.)

developed by Gysel et al. (2009) was used for data inversion. Ambient temperature (25 °C) scans were used to correct the size shift between the two DMAs and define the width of the transfer function (Gysel et al., 2009). 203 nm PSL particles were used to calibrate the offset in sizing of the two DMAs on weekly basis.

The probability density function of f_s (**f_s-PDF) was used in this study. We simply define the particles with f_s<0.8 as non-volatile mode particles, and the rest as volatile mode particles. The volume fraction remain of volatile mode particles at 300 °C was calculated with** $VFR_V = \frac{\int_{f_s=0}^{0.8} f_s \cdot c(f_s)\,df_s}{\int_{f_s=0}^{0.8} c(f_s)\,df_s}$**, where** $c(f_s)$ **is the probability density function of f_s.**

Formatted: Font: Italic
Formatted: Font: Italic, Subscript
Field Code Changed
Formatted: Font: Not Bold
Field Code Changed

2.5 6 Particle chemical composition

A Digitel high volume (HV) DHA-80 filter sampler (Riemer, Hausen, Germany) was used to collect atmospheric particles of an aerodynamic diameter less than 10 µm (PM10) on quartz fiber filters (MK 360, Munktell, Falun, Sweden). To reduce the blank content of carbonaceous material, the filters were heated for 24 h at 105°C before sampling. After sampling the filters were stored at −20°C until usage. Samples were taken every 12 h (day time samples: 6:00 – 18:00 LT, night time samples: 18:00 LT until six on the following morning) at a flow rate of 0.5 m^3 min^{-1}.

Inorganic ions were analyzed by ion chromatography (IC690 Metrohm, Switzerland; ICS3000, Dionex, USA). Before analysis, a filter aliquot was extracted in deionized water by shaking and ultrasonication and filtered through 0.45-mm-pore-size syringe filters.

The determination of total carbon (TC) as organic carbon (OC) and elemental carbon (EC) was carried out by a thermal-optical method using the Sunset Laboratory Dual-Optical Carbonaceous Analyzer (Sunset Laboratory Inc., U.S.A.). For analyses of quartz filters the EUSAAR 2 temperature-protocol was used and a charring correction using light transmission was applied (Cavalli et al. 2010).

3 Results and discussion

3.1 New particle formation events in the NCP

NPF events ~~were~~ have been frequently observed in the north NCP. Based on a 1-year data set, Wu et al. (2007) found NPF events on 40% of measurement days in an urban background station in Beijing. At the regional atmospheric observatory and regional GAW (Global Atmosphere Watch) station Shangdianzi in the north of Beijing, the frequency of NPF day was found to be 36% based on a continuously measurement longer than 1 year (Shen et al., 2011).

During our intensive field campaign, NPF events were observed ~~during~~ on 10 ~~out~~ of 28 days, ~~, in which a~~ and Clear smooth growth of ~~newly formed particles~~nucleation mode particles without strong fluctuations in diameter or concentration (i.e.

Class I in the classification system in Dal Maso et al., 2005) ~~were found~~ was observed on 5 of those days. The time variation of particle number size distribution, κ-PDF ~~of 50 nm particles~~ and f_κ-PDF of 50 nm particles, and the mass fraction of organic matter and sulfate in PM10 during these 5 NPF days are shown in the panels in Fig ~~ure~~ 2. During the first NPF event, which occurred on July 20th, the nucleation mode did not start at the lower detection limit of our SMPS, meaning that the nucleation ~~might have taken place~~ event likely occurred upstream of our measurement site. This event was however counted as an NPF event, since the hygroscopicity and CCN activity of the nucleation mode particles during NPF events is basically determined by the growth process, which was observed on that day. It can be seen that the NPF events started in the morning on all ~~the~~ 5 days. In the first 3 cases, the newly formed particles ~~kept on growing towards~~ continued to grow through the end of the day. In the other 2 cases, ~~the~~ growth was interrupted in the afternoon.

The hygroscopicity and volatility of nanoparticles as measured by the HTDMA and VTDMA is often invoked to provide insight into the particle composition (Zhang et al., 2011).

It is interesting to ~~note~~ see in Fig ~~ure~~ 2 that the hygroscopicity of newly formed particles is largely different in the five events. On July 20th, 22nd and 25th, after the nucleation mode ~~reaching~~ grew to 50 nm, the κ-PDF at 50 nm ~~shows had~~exhibited a dominant hygroscopic mode at κ ~~of~~ around 0.4 until 18:00 LT. However, the newly formed, 50 nm, particles ~~show~~ exhibited a much lower κ on July 24th and 28th. ~~;~~ I~~i~~n the late afternoon on July 24th, the hygroscopic mode ~~of κ-PDF is~~ was located between 0.1 and 0.2. ~~;~~ O~~o~~n July 28, the average κ of hygroscopic mode ~~is~~ was also lower than 0.2. The ~~particle~~ hygroscopicity parameter κ of a particle is mainly determined by its chemical composition (Petters and Kreidenweis, 2007). Therefore, it can be assumed that the particulate matter produced during the growth process ~~is~~ was dominated by different species in different NPF events.

The difference in chemical composition of new particles was also reflected by the VTDMA measurement. Non-volatile residual at 300 °C can be found in 50 nm newly formed particles in all the five NPF events. This phenomenon was also observed in Melpitz, Germany (Wehner et al., 2005) and Hyytiälä, Finland (Ehn et al., 2007). And the non-volatile cores were presumed to be polymer-type organics (Wehner et al., 2005; Ehn et al., 2007). In our measurements, the sizes of the non-volatile cores of 50 nm new particles were however different in the five NPF events. In the event on July 20th, 22nd and 25th, the majority of 50 nm new particles exhibited a shrink factor of about 0.3; while on July 24th and 28th, the shrink factor is a slightly higher, about 0.4. This means more polymer-type organics were formed during the growth of new particles on July 24th and 28th.

In a study combining in-situ measurements and aerosol dynamic model, sulfuric acid was found to be the major contributor of the growth of newly formed particles in the north NCP, and organic compounds were also found to play a major role in some cases (Yue et al., 2010). Yue et al. (2010) classified NPF events in the north NCP into two types, i.e. sulfur-rich and sulfur-poor events, in which the growth of the new particles is respectively dominated by sulfates and organics. Observed in the same region, our measurements of particle hygroscopicity and volatility can be also well explained by the two NPF types as in Yue et al. (2010). The NPF events on July 20th, 22nd and 25th are very like the sulfur-rich type NPF, i.e., condensation and neutralization of sulfuric acid contributed most to the growth of the new particles, and resulted in a high particle

Formatted: Font: Italic

Formatted: Font: Italic, Subscript

hygroscopicity. The NPF events on July 24th and 28th are like the sulfur-poor event, i.e., condensation of organic compounds had a higher contribution to the growth, resulting in a lower particle hygroscopicity, and more polymers might be produced (Kalberer et al., 2004), resulting in a higher shrink factor

.

As a reference, ~~T~~the mass fraction of organic ~~matters~~ and sulfate compounds in PM10 obtained from offline analysis of 12-h DIGITEL HV-samples are shown in the bottom subplots of Fig~~ure~~ 2. ~~The~~ It should be noted that the ultrafine particles ~~take~~ account for only a minor fraction ~~in~~ ~~o~~fin PM10 total mass~~.~~ and the mass fractions of organics and sulfate are determined not only by the activity of secondary production, but also the long range transportation and vertical mixing. ~~However, the temporal variation of the mass fraction of a certain species in PM10 can to some extent indicate its production activity.~~ It can be seen that the average mass fraction of organics ~~OM in~~ during the daytime of July 20th, 22nd and 25th ~~is~~ was lower than the average of the previous nighttime, while the mass fraction of sulfate obviously increased (July 22nd and 25th) or at least stayed at the same level (July 20th)~~, meaning that the secondary production of sulfate is was more active than that of OM~~. And ~~T~~the opposite variation can be found on July 24th and 28th. ~~, meaning that the production of OM was more efficientgreater during the growth of the newly formed particles.~~ This is basically consistent with the measurements of particle hygroscopicity and volatility.

The possible difference in the chemical composition of new particles might be cause by several factors, e.g. the concentration of precursors and the activity of some reactions. Furthermore, these factors might be determined or influenced by other parameters, e.g. ambient temperature, radiation, air mass origin, and vertical mixing. To find out the reason of the composition variation of the new particles is out of the scope of this study, and needs some additional measurements which are not available. In the following sections, we will focus on the CCN activity of new particles in the two types of NPF event. Since we have no direct measurement of the chemical composition of ultrafine particles, to be accurate, the events on July 20th, 22nd and 25th are termed MH-type NPF (NPF with More Hygroscopic particles), while the events on July 24th and 28th are termed LH-type NPF (NPF with Less Hygroscopic particles).

~~Considering the hygroscopicity of sulfate and OM, this result is consistent with the aforementioned variation of κ-PDF in during the five events.~~

~~Our result is in agreement with Yue et al. (2010). They found that in Beijing area, condensation and neutralization of sulfuric acid contribute 45±18% to the apparent growth rate on average, and organic compounds are also an important contributor. And two types of NPF events were observed in which the growth process is was driven by either organics or sulfates.~~

3.2 Variation of CCN activity during the NPF events

Newly formed particles may grow ~~up~~ to CCN-active sizes of 50 nm in a few hours and contribute to the total CCN number concentration (e.g. Wiedensohler et al., 2009; Yue et al., 2011; Wang et al., 2013b; Wu et al., 2015). As discussed above, the hygroscopicity, volatility and chemical composition of aerosol particles might differ~~s~~ in different NPF events in the NCP. The CCN activity of aerosol particles and the CCN productivity of NPF might therefore also differ ~~in different events~~. As a

case study, ~~T~~the NPF events on July 22nd (MH-type NPF) and 24th (LH-type NPF) are selected and discussed in detail in this section~~. Considering the variation of the particle hygroscopicity and the mass fraction of sulfate and OM, we name identify these two events as sulfate-dominant NPF event and OM-dominant NPF events, respectively.~~.

3.2.1 CCN activity in MH-type ~~in sulfate-dominant NPF event~~NPF

Figure 3 illustrates details of the NPF event that occurred on July 22nd. July 22nd ~~is~~ was a hazy day with ~~the~~ average temperature, RH and wind speed of 26.1 °C, 77.5% and 0.4 ms^{-1}, respectively. The weak south-southwest wind ~~starting~~ continuing from the previous day facilitate~~d~~s the accumulation of pollutants in the region (Xu et al., 2011). The daily average BC mass concentration ~~is~~ was 6.94 μgm^{-3}, 50% higher than the average 4.66 μgm^{-3} of the entire measurement period ~~(4.66 μgm^{-3})~~.

As ~~the developing of~~ the boundary layer developed in the morning, ~~the the BC mass concentration and the~~ particulate ~~particle~~ condensational sink (~~CS,~~ Kulmala et al., 2001) and the mass concentration of BC and sub-800 nm particles ~~s~~started to decrease at 07:00 LT. The newly formed particles started to be visible in our SMPS record at around 09:00 LT. The indicatory parameters for NPF, $N_{[40\text{-}60nm]}$ and the geometric mean diameter of nucleation mode, increase in coincidence over a three-hour period. Large amount of secondary particulate matter was produced during the growth of new particles, shown as a sharp increase in sub-80 nm particle mass concentration.~~,~~ ~~and~~ The new particles ~~kcep on~~continued growing until the end of the day with an average growth rate of 6.3 nm h^{-1} (~~Figure~~ Fig. 3A). The newly formed particles reached 50 nm at around 10:30 LT, resulting in a sharp elevation of $N_{[40\text{-}60nm]}$ from about 2×10^3 cm^{-3} to 1×10^4 cm^{-3}. Correspondingly, the number fraction of nearly hydrophobic mode particles (NF_{NH}) and non-volatile mode particles (NF_{NV}) decreased from about 0.2 to 0, meaning that the newly formed particles grew to 50 nm and dominated the nuclei mode number. This can also be confirmed by the average κ-PDF and f_κ-PDF during the NPF event (Fig. 4). Both κ-PDF and f_κ-PDF exhibited narrow unimodal patterns, indicating that the majority of 50 nm particles originated from the same source, NPF. Identifying as MH type, during the NPF event, the 50 nm new particles exhibited a much higher $\kappa_{ave,H}$ than the pre-existing particles (about 0.45 vs. 0.3). As discussed in section 3.1, it is very likely that the condensation and neutralization of sulfuric acid contributed most to the growth of the new particles.

~~Correspondingly, the average κ of hygroscopic mode particles ($\kappa_{ave,H}$) increased from around 0.3 to 0.45 within 1 hour (Figure 3D). Since~~ As the newly formed particles grow ~~grew~~ up to 50 nm and become ~~dominated~~ the majority~~nuclei mode number, the number fraction of hydrophobic mode particles (NF_{NH}) decreases decreased~~ from about 0.2 to 0. ~~Such a great variation~~large decrease in particle hygroscopicity indicates that the chemical composition of 50 nm particles during the NPF event is was different from that of pre-existing ones.

~~The mass concentration and fraction of the major compounds in PM10 is shown in Figure 4. As mentioned in section 3.1, the ultrafine particles were only take a minor fraction in of PM10 total mass. However, the temporal variation of the mass fraction of different chemical compounds may provide some information about the secondary aerosol production. We can see that SO_4^{2-} takes was 21.5% of PM10 total mass concentration on average during the daytime of July 22nd (11:00 LT –~~

Formatted: English (U.S.)

Formatted: Font: Italic

Formatted: Font: Italic, Subscript

Formatted: Font: Italic

Formatted: Font: Italic, Subscript

Formatted: Font: Italic

Formatted: Font: Italic, Subscript

~~17:52 LT), which is almost double of that for~~ of ~~the night before (July 21st 18:55 LT – July 22nd 06:55 LT). This indicates that the secondary production of sulfate is~~ was ~~very active during that period, and makes~~ constituted ~~a major contribution on~~ to ~~the PM10 mass. Considering the high hygroscopicity of the newly formed particles (average κ about 0.45), it is reasonable to assume that sulfate takes~~ constitutes ~~the main mass fraction in those particles.~~

During this NPF event, an enhancement of aerosol CCN activity can be seen. As the $N_{[40\text{-}60nm]}$ ~~increases~~ increased sharply at around 10:30 LT, $D_{P,50}$ ~~decreases~~ decreased from about 46 nm to 39 nm for 0.80% SS, and decreased from about 70 nm to 60 nm for 0.40% SS (Fig~~ure~~ 3~~F~~E). The S_{50} ~~increases~~ increased from about 3.5 to 6.0 for 0.80% SS and ~~increases~~ increased from about 4 to 6 for 0.40% SS (Fig~~ure~~ 3G~~F~~), meaning that the size-resolved activation ratio curve ~~gets~~ became steeper. It is interesting that enhancement of aerosol CCN activity can also be seen for 0.20% SS, for which $D_{P,50}$ is ~~out of~~larger than the size range dominated by the newly formed particles (Fig~~ure~~ 3C). This is because ~~the secondarily produced~~ low volatility, water soluble compounds produced by gas phase reactions may condense on all particles. The CCN activity of pre-existing particles might therefore also increase.

To have a better view of particle CCN activity during the NPF event of July 22nd, three records of size-resolved activation ratio before and during the NPF event are selected and averaged (the corresponding records are marked as color-filled points in Fig~~ure~~ 3~~F~~E), as shown in Fig~~ure~~ 5. The activation ratio before the nucleation is basically the same as the campaign average ~~for~~ at all ~~the~~ three SS. However, the activation ratio curves obviously shifted towards lower size and ~~get~~ became steeper during the NPF event for SS of 0.40% and 0.80%, indicating that the particles ~~are~~ were more hygroscopic, and ~~with~~ had a narrower probability distribution of hygroscopicity compared with the pre-existing particles (Su et al., 2010).

In the nighttime after 18:00 LT, due to the collapse of the boundary layer and the increase of aerosol emission (traffic and cooking), the influence of anthropogenic emission starts to be visible in the time series of particle number size distribution (Fig~~ure~~ 3A). The newly formed particles ~~keep on growing~~grew further largely ~~contributed by the~~ through coagulation and condensation of the freshly emitted particulate and gaseous pollutants, and therefore ~~become~~ became less hygroscopic. The BC mass concentration ~~increases~~ increased significantly after 18:00 LT and ~~shows a~~ peaked ~~of~~ at about 20 μgm^{-3} at around 22:00 LT (Fig~~ure~~ 3B), resulting in an increase of the number fraction of hydrophobic mode particles (Fig~~ure~~ 3D and S2). These results indicate that in the nighttime ~~the~~ a major fraction of the particle population ~~is getting~~ became less hygroscopic, and~~-~~ that different compounds ~~are~~ were inhomogeneously distributed among particles. Accordingly, particle CCN activity varies a lot in this period (~~Figure~~ Fig. 3~~F~~E and G~~F~~). Compared with the campaign-average, the activation ratio curve in nighttime is flatter and shifted towards larger size. And the activation ratio reaches only about 80% even at the size of $D_{P,50}\times2$, which is probably due to the high concentration of externally mixed BC particles (also shown as a clear near-hydrophobic and non-volatile mode at 100 and 150 nm in Fig. S2 and S3). Considering the increasing BC mass concentration, the BC emission is very likely to play ~~the~~ a major role in the variation of CCN activity in nighttime. Condensation of insoluble organic compounds might be also responsible.

Formatted: Font: Italic

Formatted: Font: Italic

3.2.2 CCN activity in LH-type ~~OM-dominant~~ NPF ~~event~~

Figure 6 displays another NPF event that occurred on July 24th. This day ~~is~~ was relatively clean with cloudless blue sky. The daily average temperature and RH ~~is~~ were ~~respectively~~ 28.4 °C and 70.5%, respectively. The BC mass concentration stay~~eds~~ at a low level (1.74 μgm^{-3}) in daytime due to the 2 ms^{-1} northwest wind and the development of ~~the~~ a deeper boundary layer. The NPF event ~~starts~~ started at around 09:00 LT. The growth of newly formed particles ~~keep on growing~~ continued throughout the day with an average growth rate of 6.3 nm h^{-1} (Fig~~ure~~ 6A). It can be seen that $N_{[40\text{-}60nm]}$ increase~~d~~ from about 2×10^3 cm^{-3} to 1.4×10^4 cm^{-3} in a few hours, $N_{[60\text{-}80nm]}$ also increase~~d~~ during the daytime. As the newly formed particles ~~grow~~ grew ~~up~~ to 50 nm and become the majority at this size, the number fraction of nearly-hydrophobic mode and non-volatile mode particles ~~decreases~~ decreased to almost 0 within 1 hour. The κ-PDF and f_s-PDF also exhibited narrow unimodal patterns (Fig. 4). It is interesting to note that, unlike the event on July 22nd, the average κ for the hygroscopic mode of 50 nm particles ~~deceases~~ decreased a bit after the nucleation, and ~~stays~~ stayed below 0.3 for the rest of the day. ~~-~~Such low hygroscopicity of newly formed particles implies that the driving mechanism of particle growth in daytime for this event ~~is~~ was somehow different from the event on July 22nd. It very likely that sulfuric acid played a less important role in the growth process, and organics had a higher contribution, compared with the MH-type NPF. It can be also seen in Fig. 6E that VFR_V during this NPF event is higher than that during the event on July 22nd, meaning that the more polymer-type organics was produced during the growth of the new particles in this event.

~~We can see in Figure 4 that the average mass fraction of SO_4^{2-} in PM10 in the daytime (July 24th 06:03 LT – 18:03 LT) is was slightly lower than that in the previous night (July 23rd 18:03 LT – July 24th 06:03 LT). In contrast, the mass fraction of OC increases increased from 14.1% (July 23rd 18:03 LT – July 24th 06:03 LT) to 20.0% (July 24th 06:03 LT – 18:03 LT) which is nearly double the mass fraction of SO_4^{2-}. It therefore can be assumed that the condensation of lowless volatile, less hygroscopic OC plays a major role in the growth of the newly formed particles in the daytime on July 24th.~~

~~With Along with the active secondary production of OC which is less hygroscopic or even hydrophobic~~Correspondingly, no enhancement can be found in particle ~~hygroscopicity and~~ CCN activity in daytime (Figure ~~6D~~ 6F and ~~E~~G). $D_{P,50}$ for 0.20% SS even increase~~d~~ from about 110 nm to 120 nm. The average size-resolved activation ratio for 0.20%, 0.40% and 0.80% SS at selected time (marked as color-filled points in ~~Figure~~ Fig. 6~~E~~6F) are shown in ~~Figure~~ Fig. 5. ~~Different from~~In contrast to the event on July 22nd, due to the decrease of particle hygroscopicity, the average activation ratio curves shift a bit towards larger ~~size~~ diameter during the new particle formation event.

The nighttime story on July 24th is similar ~~as~~ to that on July 22nd. The increasing anthropogenic emission caused a decrease in particle hygroscopicity and CCN activity (Figure 6D, F and G). However, the activation ratio at size range of 100 – 200 nm is much lower than that in the nighttime of July 22nd (Fig. 5). This is probably because the concentration of background aerosol particles was lower on July 24th (also can be seen from the $m_{[9\text{-}800nm]}$ in panel B of Fig. 3 and 6). The relative contribution of BC particles in the evening was therefore higher, resulting in a high number fraction of externally mixed BC particles. ~~The increasing anthropogenic emission causes caused a decrease in particle hygroscopicity and CCN activity~~

Formatted: English (U.S.)
Formatted: Subscript
Formatted: Superscript
Formatted: Superscript
Formatted: Superscript
Formatted: Font: Italic

~~(Figure 6D, E and F).~~ Nocturnal nucleation also occurred on July 24th (Fig.~~ure~~ 6A), which is discussed in detail in Kecorius et al. (2015).

3.3 Influence of the varying CCN activity on the CCN prediction during NPF events

One of the aims of studying particle CCN activity is to predict the CCN number concentration (N_{CCN})~~. D~~ which is defined as the number concentration of particles which can be activated at a certain SS~~,~~; N_{CCN} can be calculated as follows:

$$N_{CCN} = \int_{\log D_P} AR(\log D_P, SS) \cdot n(\log D_P) \cdot d\log D_P \quad (2)$$

where, AR is the activation ratio function and $n(\log D_P)$ is the particle number size distribution. It can be ~~learned~~ seen from Eq. (2) that N_{CCN} is determined by both the size-resolved activation ratio and particle number size distribution. Since CCN activity mainly depends on particle size (Dusek et al., 2006), N_{CCN} is more sensitive ~~on~~ to the variation of particle number size distribution (Deng et al., 2013). Also, ~~direct measurement of~~ particle CCN activity and hygroscopicity are more difficult to measure and thus to be widely applied. Therefore, a fixed size-resolved activation ratio curve or critical diameter (normally averaged over a certain time period) is usually used when evaluating the contribution of NPF ~~on~~ to N_{CCN}. However, as discussed in Sect. 3.2, the activation ratio curve can vary largely ~~in~~ on NPF days in the NCP. Moreover, the activation ratio curve might be different ~~in~~ for different types of NPF events. The questions then arises as to ~~can~~ whether we can simply~~just~~ use an average activation ratio curve or a fixed critical diameter for NPF events, ~~or~~ and what is the possible bias if an average activation ratio curve or a fixed critical diameter is applied rather than a variable, real-time activation ratio curve. To answer this question, ~~N_{CCN}~~ CCN number concentration was respectively calculated with ~~eq~~Eq. (2) based on the campaign average activation ratio ~~–~~(shown as the solid black line in Fig. 5A; the calculated CCN number concentration is termed $N_{CCN,AR\text{-}ave}$), campaign average critical diameter (termed $N_{CCN,D\text{-}ave}$) and real-time activation ratio (termed $N_{CCN,ref}$) at 0.80% SS. The real-time particle number size distribution was used in the calculation. The campaign average critical diameter for a certain SS ($D_{P,cri}$) was chosen as follows: first~~ly~~, $D_{P,cri}$ was calculated for each data record by solving

$$N_{CCN,ref} = \int_{\log D_{P,cri}}^{\log D_{P,max}} n(\log D_P) d\log D_P \quad (3)$$

where, $D_{P,max}$ is the maximum diameter of the measured particle number size distribution; then the geometric average of $D_{P,cri}$ for the whole period was calculated and used. The calculated $D_{P,cri}$ is 55.3, 80.6 and 114.9 nm for 0.80%, 0.40% and 0.20% SS, respectively. Without direct measurement of N_{CCN}, the N_{CCN} calculated with real-time activation ratio ($N_{CCN,ref}$) was taken as the reference value. The relative difference between ~~N_{CCN} calculated with campaign average activation ratio / critical diameter and the reference value during the two NPF days~~ $N_{CCN,AR\text{-}ave}$ and $N_{CCN,ref}$ (termed CCNbiasA), and between $N_{CCN,D\text{-}ave}$ and $N_{CCN,ref}$ (termed CCNbiasB), was then evaluated. CCNbiasA and CCNbiasB were respectively calculated as

Formatted: Font: Italic

$$CCNbiasA = \frac{N_{CCN,AR-ave} - N_{CCN,ref}}{N_{CCN,ref}} \quad (4)$$

$$CCNbiasB = \frac{N_{CCN,D-ave} - N_{CCN,ref}}{N_{CCN,ref}} \quad (5)$$

On July 22nd (~~sulfate-dominant NPF event~~MH-type NPF), as the ~~growing of the~~ newly formed particles grew, N_{CCN} at 0.80% SS ~~increase doubly~~ doubled during the daytime, from about 1.3×10^4 to 2.5×10^4 cm^{-3}. ~~Since sulfate dominates the particle growth, t~~The CCN activity of aerosol particles increases during the NPF. As shown ~~before~~in Fig 5, the activation ratio curve ~~got~~ was steeper and shifted towards smaller size compared with the campaign average curve. ~~$N_{CCN,AR-ave}$~~ CCNbiasA ~~is~~ is therefore respectively about -20%, -15% and -10% ~~lower than $N_{CCN,ref}$~~ for SS of 0.80%, 0.40% and 0.20% in the daytime. On July 24th (~~OM-dominant NPF event~~LH-type NPF), ~~since OM contributes more to the growth of the particles than sulfate on the growth of the particles,~~ the activation ratio curve during particle growth is very similar ~~as~~ to the campaign average (0.80% SS), or even moves a bit to ~~the~~ larger size in the afternoon (0.40% and 0.20% SS, Fig. 5 ~~Figure 6~~). The ~~relative difference between $N_{CCN,AR-ave}$ and $N_{CCN,ref}$~~CCNbiasA for 0.80% SS during daytime is about -8%, which is much less than the event on~~ease of~~ July 22nd. For 0.40% and 0.20% SS, $N_{CCN,AR-ave}$ is even ~~much~~ higher than $N_{CCN,ref}$ in the afternoon.

When using the average $D_{P,cri}$, the calculated $N_{CCN,D-ave}$ is lower than $N_{CCN,ref}$ in both of these two NPF events. ~~The relative differences between $N_{CCN,D-ave}$ and $N_{CCN,ref}$~~CCNbiasB are respectively about -40%, -30% and -10% for 0.80%, 0.40% and 0.20% SS in the afternoon of July 22nd, and -35%, -40% and 10% for the three SS in the afternoon of July 24th.

To give a more general result, ~~the relative difference between $N_{CCN,AR-ave}$ (and also $N_{CCN,D-ave}$) and $N_{CCN,ref}$~~CCNbiasA and CCNbiasB were calculated for the entire measurement period. Its overall frequency distribution and the 2--dimensional frequency distribution ~~at different~~as a function of time of day are shown in Fig~~ure~~ 7.

It can be seen in Fig~~ure~~ 7A that when using the average activation ratio, the majority of ~~the biases in the calculated N_{CCN}~~CCNbiasA are located between -0.1 and 0.1, meaning that the relative bias of $N_{CCN,AR-ave}$ is lower than 10% in most cases. It can be seen from the contour plot that large minus biases, ranging from -0.1 to -0.3, are all located between 12:00 and 18:00 LT. The large minus biases are caused by the increase ~~of CCN activity, resulted from the increase~~ of ~~sulfate mass fraction~~particle hygroscopicity in MH-type NPF event as discussed in section 3.2.1. Therefore, it can be concluded that in the NCP, the bias of N_{CCN} calculated with an average activation ratio may vary between -30%,0 to 10%30% during NPF evnets~~,~~ depending on the type of ~~the~~ NPF ~~events~~; while the bias is mainly within ±10% in daytime ~~in~~ of non-NPF days. It should be noted that this conclusion is based on "using an average activation ratio curve which is representative of the period and area studied". Using an inappropriate activation ratio curve (e.g. an average for another season or another region) may result in higher bias in calculated N_{CCN}.

The frequency distribution of the relative difference between $N_{CCN,D-ave}$ calculated with the average critical diameter and $N_{CCN,ref}$ is shown in ~~fig~~Fig. 7B. It can be seen that the overall frequency distribution is broader than that of $N_{CCN,AR-ave}$ but the majority of the ~~samples~~ relative bias still locates between -0.1 and 0.1. However, a long tail can be seen on the left side. The

Field Code Changed

Field Code Changed

Formatted: Font: Italic

Formatted: Font: Italic

Formatted: Font: Italic

Formatted: Font: Italic

Formatted: Font: Italic

Formatted: Font: Italic

Formatted: Font: Italic

underestimation of N_{CCN} in NPF events is clearer in the contour plot: large body of samples locates at relative difference between -0.1 to -0.5 in the afternoon. This indicates that to use an average $D_{P,cri}$ may result in a larger underestimation of calculated N_{CCN} during NPF events in the NCP. This is because using such a stepwise size-resolved activation ratio overestimates N_{CCN} at $D_P > D_{P,cri}$ and underestimates N_{CCN} at $D_P < D_{P,cri}$. If real-time PNSD and activation ratio curve are similar as the average ones, those overestimation and underestimation may compensate. However, during NPF events, the activation ratio curve may shift towards lower size (in MH-type NPF) and particle number concentration in ultrafine size range increases significantly. The underestimation of N_{CCN} in the left side of $D_{P,cri}$ is therefore much higher than the overestimation in the right side of $D_{P,cri}$, and resulting in a large negative CCNbiasB. Therefore, applying a fixed critical diameter in the calculation of N_{CCN} ~~might~~ may result in an underestimation up to 50% in NPF events in the NCP. We should also note that the critical diameter used here is actually "the best estimation" which derived from the samples used also in the test. Assuming an arbitrary critical diameter may result in even larger bias in the estimation of N_{CCN}.

It is also worth to note that in both fig. 7A and B, there are a group of samples locates at relative difference between 0.1 and 0.3 in the evening, meaning that the N_{CCN} calculated with the average activation curve or critical diameter may sometimes be overestimated by up to 30% in the evening. As discussed in previous sections, this overestimation is basically caused by the increase of (nearly) hydrophobic matters, mostly BC, in the nocturnal boundary layer. Although BC comes from local anthropogenic emission, such an increase in BC concentration in the evening is actually a regional phenomenon, which was also observed in other studies in the NCP (e.g. Ma et al., 2011; Cheng et al., 2009). In the NCP, due to the very dense population and the developing industry and agriculture, the villages and cities are densely distributed in the region. The BC emitted from residential area in the evening may diffuse to the area around and causes an increase of the regional background of BC concentration.

3.4 Discussion

During NPF events, nucleation creates a large number of nuclei particles. The contribution of the NPF to N_{CCN} is mainly determined by the consequent growth processes, i.e. coagulation and condensation which enlarge the particles to ~~CCN~~ the size range where they readily act as atmospheric CCN. As discussed ~~before~~above, the chemical composition of particles might change during these processes. In other words, besides enlarging the particles to CCN size range, those processes might also modify the particle CCN activity in varying degrees, depending on the chemical and physical ~~cases~~composition of the atmosphere.

Two case studies are shown in sections 3.2.1 and 3.2.2~~,~~; both include a NPF event defined by a pronounced "banana pattern" in the time series of PNSD. But the CCN activity of the newly formed particles was found to be ~~largely~~ significantly different. Measurements of particle hygroscopicity and ~~chemical composition~~volatility suggest that the growth of the newly formed particles in the daytime ~~is~~ was likely to be ~~respectively dominated by sulfate and OM in the two cases~~driven by different species, ~~which~~ resultings in different levels of CCN activity at a given size and SS. This means that in the NCP, the CCN activity of newly formed particles during NPF events might be largely different. For example, during the ~~sulfate~~

Formatted: Font: Italic
Formatted: Subscript
Formatted: Font: Italic
Formatted: Subscript
Formatted: Font: Italic
Formatted: Subscript
Formatted: Font: Italic
Formatted: Subscript
Formatted: Font: Italic

~~dominant dominated~~MH-type NPF event on July 22nd, the activation ratio curve shows a steeper ~~shape~~ slope with a lower $D_{P,50}$ than the campaign average in the afternoon; while during the ~~OM dominant~~LH-type NPF event on July 24th, the activation ratio curve in the afternoon is basically similar ~~as~~ to the campaign average. These are only two selected cases. There might be also cases ~~dominated by sulfate even more~~with even more hygroscopic particles than ~~that for~~on July 22nd, or with ~~dominated by OM more than that~~even less hygroscopic particles than ~~for~~ on July 24th, or cases in between. Unfortunately, without ~~more~~ detailed chemical analysis of the nuclei mode particles, it is not possible to parameterize ~~impossible to get any clue of~~ the event type from the evolution of PNSD alone which is basically the only way to define a NPF event. It thus might be difficult to find a ~~simple~~ parameterization of size-resolved CCN activity for NPF events in the NCP which is appropriate for all cases.

For accurate estimation of N_{CCN} during a NPF event, we should not only focus on the increase of particle number concentration in certain size ranges. The variation of particle CCN activity should be also taken into account. However, we can only get this information from direct measurement CCN activity, or measurements of hygroscopicity or chemical composition, which are all difficult to be widely applied. Therefore an average activation ratio curve or even a fixed critical diameter ~~were~~ have usually been used when evaluating the contribution of NPF ~~on~~ to N_{CCN} (e.g. Laaksonen et al., 2005; Kuang et al., 2009; Asmi et al., 2011; Peng et al., 2014). From the discussion in section 3.3 we learned that the bias of the estimated N_{CCN} during NPF events ~~ranges from about 0~~can be up to 30% ~~in NPF event~~ if a fixed activation ratio curve (best estimation, representative of the region and season) is used. Using a fixed critical diameter is likely to result in larger underestimation of N_{CCN}. The bias can be up to 50% during NPF events. In daytime without NPF, the bias of estimated N_{CCN} can be limited within 10% if either a proper fixed activation ratio curve or critical diameter is used. ~~As a conclusion~~Thus, we suggest not using a fixed critical diameter in the prediction of N_{CCN} in NPF seasons. If real-time CCN activity data is not available, using a proper fixed activation ratio curve can be a compromising choice.

As an important source of aerosol particles, NPF events are ~~is~~ very likely to have a ~~great~~ major contribution ~~on~~ to the ~~amount~~ number of CCN. Due to the complexity of the nucleation and growth processes and the inhomogeneous spatial distribution of nucleation and consequent growth, at least in the NCP, this contribution has not been well addressed. Wehner et al. (2010) found that NPF might occur at higher altitudes in the residual layer as well as in the mixed or mixing boundary layer. This means NPF might be even more important in CCN budget than we ~~expected~~expect from ground based measurements. More cases of NPF with measurements of particle chemical composition and microphysical properties are therefore needed to better address its role. It would be also interesting to have ~~some~~ vertically resolved CCN measurements.

Our measurements only cover a period of about one month. The average activation ratio is proved to be good enough in the estimate of CCN number concentration in non-NPF periods. It is therefore worth to have a long-term (i.e. longer than one year) measurements of size-resolved activation ratio to provide a precise parameterization of CCN activity in different season or airmass types which can be used to estimate CCN number concentration with lower uncertainty.

Formatted: Font: Italic

Formatted: Subscript

4 Conclusion

To study the variation of particle CCN activity during NPF events in the NCP, size-resolved activation ratio as well as other particle physical and chemical properties were measured ~~in~~ during a 1-month field campaign at a regional station in the north NCP.

~~New particle formation~~NPF events were observed ~~in~~ on 10 ~~days~~ out of 28 days, in which clear and smooth growth of newly formed particles were found ~~in~~ on 5 days. In different NPF events, ~~the~~ hygroscopicity and volatility of newly formed particles was found to be ~~largely significantly~~largely different, suggesting that the particle growth might be dominated by different species. Two NPF events, MH-type and LH-type NPF, were selected for case studies~~, in which sulfate and or organic matters are respectivelycompounds were dominant, respectively, responsible for the growth of the newly formed particles~~. The size-resolved activation ratio curves during the ~~sulfate-dominated~~MH-type NPF event showed a steep shape with lower $D_{P,50}$ than the campaign average; while the activation ratio curves during the ~~OM-dominated~~LH-type event ~~are~~ were basically similar ~~as~~ to the campaign average. This means that during NPF in the NCP, the CCN activity of newly formed particles was different during these two events; the aerosol present during the LH-type event was less active as CCN for a given diameter and supersaturation. ~~This means that during NPF in the NCP, the CCN activity of newly formed particles might be largely different.~~

To see the influence of assuming a constant CCN activity in the calculation of N_{CCN} in the NCP, N_{CCN} was calculated with the campaign average activation ratio curve and critical diameter, and then compared with the reference values. The bias of the estimated N_{CCN} ~~ranges from about 0 to~~during NPF events can be up to 30% ~~in NPF event~~ if a fixed activation ratio curve is used. Using a fixed critical diameter is likely to result in larger underestimation of N_{CCN}. The bias can be up to 50% during NPF events. In daytime without NPF, the bias of estimated N_{CCN} can be limited within 10% if either a proper fix activation ratio curve or critical diameter is used.

We can learn from this study that for the accurate estimation of N_{CCN} during NPF events, one should not only focus on the increase of particle number concentration in certain size ranges. The variation of CCN activity should be also taken into account. It might be difficult to find a simple parameterization of size-resolved CCN activity for NPF events in the NCP, since it may vary a lot from case to case. Without real-time CCN activity data, a proper fixed activation ratio curve or critical diameter can be used to calculated N_{CCN} for non-NPF daytime. But large ~~uncertainty~~ uncertainties might appear in predicted the N_{CCN} for NPF event, especially ~~in case of using~~if a fixed critical diameter is used.

Formatted: Font: Not Italic

Formatted: Font: Not Italic

Formatted: Font: Italic

Acknowledgment

This work is supported by the National Science Foundation of China under Grant No. 41590872, the project Sino German Science Center No. GZ663, and the EU project BACCHUS No. 603445.

Reference

Asmi, E., Kivekäs, N., Kerminen, V.-M., Komppula, M., Hyvärinen, A.-P., Hatakka, J., Viisanen, Y., and Lihavainen, H.: Secondary new particle formation in Northern Finland Pallas site between the years 2000 and 2010, Atmos. Chem. Phys., 11, 12959-12972, doi:10.5194/acp-11-12959-2011, 2011.

Birmili, W., Berresheim, H., Plass-Dülmer, C., Elste, T., Gilge, S., Wiedensohler, A., and Uhrner, U.: The Hohenpeissenberg aerosol formation experiment (HAFEX): a long-term study including size-resolved aerosol, H_2SO_4, OH, and monoterpenes measurements, Atmos. Chem. Phys., 3, 361-376, doi:10.5194/acp-3-361-2003, 2003.

Boy, M., Kulmala, M., Ruuskanen, T. M., Pihlatie, M., Reissell, A., Aalto, P. P., Keronen, P., Dal Maso, M., Hellen, H., Hakola, H., Jansson, R., Hanke, M., and Arnold, F.: Sulphuric acid closure and contribution to nucleation mode particle growth, Atmos. Chem. Phys., 5, 863-878, doi:10.5194/acp-5-863-2005, 2005.

Burtscher, H., Baltensperger, U., Bukowiecki, N., Cohn, P., Huglin, C., Mohr, M., Matter, U., Nyeki, S., Schmatloch, V., Streit, N., and Weingartner, E.: Separation of volatile and non-volatile aerosol fractions by thermodesorption: instrumental development and applications, J Aerosol Sci, 32, 427-442, Doi 10.1016/S0021-8502(00)00089-6, 2001.

Cavalli, F., Viana, M., Yttri, K. E., Genberg, J., and Putaud, J.-P.: Toward a standardised thermal-optical protocol for measuring atmospheric organic and elemental carbon: the EUSAAR protocol, Atmos. Meas. Tech., 3, 79-89, doi:10.5194/amt-3-79-2010, 2010.

Cheng, Y. F., Berghof, M., Garland, R. M., Wiedensohler, A., Wehner, B., Müller, T., Su, H., Zhang, Y. H., Achtert, P., Nowak, A., Pöschl, U., Zhu, T., Hu, M., and Zeng, L. M.: Influence of soot mixing state on aerosol light absorption and single scattering albedo during air mass aging at a polluted regional site in northeastern China, J. Geophys. Res., 114, D00G10, doi:10.1029/2008JD010883, 2009.

Deng, Z. Z., Zhao, C. S., Zhang, Q., Huang, M. Y., and Ma, X. C.: Statistical analysis of microphysical properties and the parameterization of effective radius of warm clouds in Beijing area, Atmos. Res., 93, 888–896, 2009.

Deng, Z. Z., Zhao, C. S., Ma, N., Liu, P. F., Ran, L., Xu, W. Y., Chen, J., Liang, Z., Liang, S., Huang, M. Y., Ma, X. C., Zhang, Q., Quan, J. N., Yan, P., Henning, S., Mildenberger, K., Sommerhage, E., Schäfer, M., Stratmann, F., and Wiedensohler, A.: Size-resolved and bulk activation properties of aerosols in the North China Plain, Atmos. Chem. Phys., 11, 3835-3846, doi:10.5194/acp-11-3835-2011, 2011.

Deng, Z. Z., Zhao, C. S., Ma, N., Zhang, Q., Huang, M. Y.: A Method for Measuring Aerosol Activation Ratios with High Size Resolution, Acta Scientiarum Naturalium Universitatis Pekinensis, 48(3), 2012 (in Chinese).

Deng, Z. Z., Zhao, C. S., Ma, N., Ran, L., Zhou, G. Q., Lu, D. R., and Zhou, X. J.: An examination of parameterizations for the CCN number concentration based on in situ measurements of aerosol activation properties in the North China Plain, Atmos. Chem. Phys., 13, 6227-6237, doi:10.5194/acp-13-6227-2013, 2013.

Formatted: English (U.K.)

Formatted: Indent: Left: 0 cm, First line: 0 cm

Formatted: English (U.S.)

Formatted: Font: Not Bold

Formatted: Font: Not Bold

Dusek, U., Frank, G. P., Hildebrandt, L., Curtius, J., Schneider, J., Walter, S., Chand, D., Drewnick, F., Hings, S., Jung, D., Borrmann, S., and Andreae, M. O.: Size matters more than chemistry for cloud-nucleating ability of aerosol particles, Science, 312(5778), 1375–1378, 2006.

Ehn, M., Petäjä, T., Birmili, W., Junninen, H., Aalto, P., and Kulmala, M.: Non-volatile residuals of newly formed atmospheric particles in the boreal forest, Atmos. Chem. Phys., 7, 677-684, doi:10.5194/acp-7-677-2007, 2007.

Ehn, M., Thornton, J. A., Kleist, E., Sipila, M., Junninen, H., Pullinen, I., Springer, M., Rubach, F., Tillmann, R., Lee, B., LopezHilfiker, F., Andres, S., Acir, I.-H., Rissanen, M., Jokinen, T., Schobesberger, S., Kangasluoma, J., Kontkanen, J., Nieminen, T., Kurten, T., Nielsen, L. B., Jorgensen, S., Kjaergaard, H. G., Canagaratna, M., Maso, M. D., Berndt, T., Petaja, T., Wahner, A., Kerminen, V.-M., Kulmala, M., Worsnop, D. R., Wildt, J., and Mentel, T. F.: A large source of low-volatility secondary organic aerosol, Nature, 506, 476–479, 2014.

Guo, S., Hu, M., Zamora, M. L., Peng, J., Shang, D., Zheng, J., Du, Z., Wu, Z., Shao, M., and Zeng, L.: Elucidating severe urban haze formation in China, P. Natl. Acad. Sci. USA, 111, 17373–17378, 2014.

Gysel, M., McFiggans, G. B., and Coe, H.: Inversion of tandem differential mobility analyzer (TDMA) measurements, J. Aerosol Sci., 40, 134–151, doi:10.1016/j.jaerosci.2008.07.013, 2009.

Hagen, D. E. and Alofs, D. J.: Linear inversion method to obtain aerosol size distributions from measurements with a differential mobility analyzer, Aerosol Sci. Technol., 2, 465–475, 1983.

Kecorius, S., Zhang, S., Wang, Z., Größ, J., Ma, N., Wu, Z., Ran, L., Hu, M., Wang, P., Ulevičius, V., and Wiedensohler, A.: Nocturnal aerosol particle formation in the North China Plain, Lith. J. Phys., 55, 44–53, 2015.

Kerminen, V.-M., Virkkula, A., Hillamo, R., Wexler, A. S., and Kulmala, M.: Secondary organics and atmospheric cloud condensation nuclei production, J. Geophys. Res., 105, 9255–9264, 2000.

Kerminen, V.-M., Paramonov, M., Anttila, T., Riipinen, I., Fountoukis, C., Korhonen, H., Asmi, E., Laakso, L., Lihavainen, H., Swietlicki, E., Svenningsson, B., Asmi, A., Pandis, S. N., Kulmala, M., and Petäjä, T.: Cloud condensation nuclei production associated with atmospheric nucleation: a synthesis based on existing literature and new results, Atmos. Chem. Phys., 12, 12037-12059, doi:10.5194/acp-12-12037-2012, 2012.

Kuang, C., McMurry, P., and McCormick, A.: Determination of cloud condensation nuclei production from measured new particle formation events, Geophys. Res. Lett., 36, L09822, doi:10.1029/2007JD009253, 2009.

Kulmala, M., Toivonen, A., Mäkelä, J. M., and Laaksonen, A.: Analysis of the growth of nucleation mode particles observed in Boreal forest, Tellus, 50B, 449–462, 1998.

Kulmala, M., Dal Maso, M., Mäkelä, J. M., Pirjola, L., Väkevä, M., Aalto, P., Miikkulainen, P., Hämeri, K., and O'Dowd, C. D.: On the formation, growth and composition of nucleation mode particles, Tellus, 53B, 479–490, 2001.

Kulmala, M., Vehkamäki, H., Petäjä, T., Dal Maso, M., Lauri, A., Kerminen, V.-M., Birmili, W., and McMurry, P. H.: Formation and growth rates of ultrafine atmospheric particles: A review of observations, J. Aerosol Sci., 35, 143–176, 2004.

Formatted: English (U.S.)

Kulmala, M., Riipinen, I., Sipilä, M., Manninen, H. E., Petäjä, T., Junninen, H., Dal Maso, M., Mordas, G., Mirme, A., Vana, M., Hirsikko, A., Laakso, L., Harrison, R. M., Hanson, I., Leung, C., Lehtinen, K. E. J., and Kerminen, V.-M.: Towards Direct Measurement of Atmospheric Nucleation, Science, 318, 89–92, 2007.

Kulmala, M. and Kerminen, V.-M.: On the formation and growth of atmospheric nanoparticles, Atmos. Res., 90, 132–150, doi:10.1016/j.atmosres.2008.01.005, 2008.

Kuwata, M., Kondo, Y., Miyazaki, Y., Komazaki, Y., Kim, J. H., Yum, S. S., Tanimoto, H., and Matsueda, H.: Cloud condensation nuclei activity at Jeju Island, Korea in spring 2005, Atmos. Chem. Phys., 8, 2933-2948, doi:10.5194/acp-8-2933-2008, 2008.

Laaksonen, A., Hamed, A., Joutsensaari, J., Hiltunen, L., Cavalli, F., Junkermann, W., Asmi, A., Fuzzi, S., and Faccini, M. C.: Cloud condensation nucleus production from nucleation events at a highly polluted region, Geophys. Res. Lett., 32, L06812, doi:10.1029/2004GL022092, 2005.

Laaksonen, A., Kulmala, M., O'Dowd, C. D., Joutsensaari, J., Vaattovaara, P., Mikkonen, S., Lehtinen, K. E. J., Sogacheva, L., Dal Maso, M., Aalto, P., Petäjä, T., Sogachev, A., Yoon, Y. J., Lihavainen, H., Nilsson, D., Facchini, M. C., Cavalli, F., Fuzzi, S., Hoffmann, T., Arnold, F., Hanke, M., Sellegri, K., Umann, B., Junkermann, W., Coe, H., Allan, J. D., Alfarra, M. R., Worsnop, D. R., Riekkola, M. -L., Hyötyläinen, T., and Viisanen, Y.: The role of VOC oxidation products in continental new particle formation, Atmos. Chem. Phys., 8, 2657-2665, doi:10.5194/acp-8-2657-2008, 2008.

Lance, S., Medina, J., Smith, J. N., and Nenes, A.: Mapping the operation of the DMT Continuous Flow CCN counter, Aerosol Sci. Technol., 40, 242–254, 2006.

Liu, P. F., Zhao, C. S., Göbel, T., Hallbauer, E., Nowak, A., Ran, L., Xu, W. Y., Deng, Z. Z., Ma, N., Mildenberger, K., Henning, S., Stratmann, F., and Wiedensohler, A.: Hygroscopic properties of aerosol particles at high relative humidity and their diurnal variations in the North China Plain, Atmos. Chem. Phys., 11, 3479-3494, doi:10.5194/acp-11-3479-2011, 2011.

Ma, N., Zhao, C. S., Nowak, A., Müller, T., Pfeifer, S., Cheng, Y. F., Deng, Z.Z., Liu, P. F., Xu, W. Y., Ran, L., Yan, P., Göbel, T., Hallbauer, E., Mildenberger, K., Henning, S., Yu, J., Chen, L. L., Zhou, X. J., Stratmann, F., and Wiedensohler, A.: Aerosol optical properties in the North China Plain during HaChi campaign: an in-situ optical closure study, Atmos. Chem. Phys., 11, 5959-5973, doi:10.5194/acp-11-5959-2011, 2011.

Ma, N., Zhao, C. S., Müller, T., Cheng, Y. F., Liu, P. F., Deng, Z. Z., Xu, W. Y., Ran, L., Nekat, B., van Pinxteren, D., Gnauk, T., Müller, K., Herrmann, H., Yan, P., Zhou, X. J., and Wiedensohler, A.: A new method to determine the mixing state of light absorbing carbonaceous using the measured aerosol optical properties and number size distributions, Atmos. Chem. Phys., 12, 2381-2397, doi:10.5194/acp-12-2381-2012, 2012.

Massling, A., Leinert, S., Wiedensohler, A., and Covert, D.: Hygroscopic growth of sub-micrometer and one-micrometer aerosol particles measured during ACE-Asia, Atmos. Chem. Phys., 7, 3249-3259, doi:10.5194/acp-7-3249-2007, 2007.

Peng, J. F., Hu, M., Wang, Z. B., Huang, X. F., Kumar, P., Wu, Z. J., Guo, S., Yue, D. L., Shang, D. J., Zheng, Z., and He, L. Y.: Submicron aerosols at thirteen diversified sites in China: size distribution, new particle formation and corresponding contribution to cloud condensation nuclei production, Atmos. Chem. Phys., 14, 10249-10265, doi:10.5194/acp-14-10249-2014, 2014.

Petters, M. D. and Kreidenweis, S. M.: A single parameter representation of hygroscopic growth and cloud condensation nucleus activity, Atmos. Chem. Phys., 7, 1961-1971, doi:10.5194/acp-7-1961-2007, 2007.

Pfeifer, S., Birmili, W., Schladitz, A., Müller, T., Nowak, A., and Wiedensohler, A.: A fast and easy-to-implement inversion algorithm for mobility particle size spectrometers considering particle number size distribution information outside of the detection range, Atmos. Meas. Tech., 7, 95-105, doi:10.5194/amt-7-95-2014, 2014.

Philippin, S., Wiedensohler, A., and Stratmann, F.: Measurements of non-volatile fractions of pollution aerosols with an eight-tube volatility tandem differential mobility analyzer (VTDMA-8), J Aerosol Sci, 35, 185-203, DOI 10.1016/j.jaerosci.2003.07.004, 2004.

Roberts, G. C. and Nenes, A.: A continuous-flow streamwise thermal-gradient CCN chamber for atmospheric measurements, Aerosol Sci. Technol., 39, 206–221, 2005.

Rose, D., Gunthe, S. S., Mikhailov, E., Frank, G. P., Dusek, U., Andreae, M. O., and Pöschl, U.: Calibration and measurement uncertainties of a continuous-flow cloud condensation nuclei counter (DMT-CCNC): CCN activation of ammonium sulfate and sodium chloride aerosol particles in theory and experiment, Atmos. Chem. Phys., 8, 1153-1179, doi:10.5194/acp-8-1153-2008, 2008.

Shen, X. J., Sun, J. Y., Zhang, Y. M., Wehner, B., Nowak, A., Tuch, T., Zhang, X. C., Wang, T. T., Zhou, H. G., Zhang, X. L., Dong, F., Birmili, W., and Wiedensohler, A.: First long-term study of particle number size distributions and new particle formation events of regional aerosol in the North China Plain, Atmos. Chem. Phys., 11, 1565-1580, doi:10.5194/acp-11-1565-2011, 2011.

Sihto, S.-L., Mikkilä, J., Vanhanen, J., Ehn, M., Liao, L., Lehtipalo, K., Aalto, P. P., Duplissy, J., Petäjä, T., Kerminen, V.-M., Boy, M., and Kulmala, M.: Seasonal variation of CCN concentrations and aerosol activation properties in boreal forest, Atmos. Chem. Phys., 11, 13269-13285, doi:10.5194/acp-11-13269-2011, 2011.

Smith, J. N., Barsanti, K. C., Friedl, H. R., Ehn, M., Kulmala, M., Collins, D. R., Scheckman, J. H., Williams, B. J., and McMurry, P. H.: Observations of aminium salts in atmospheric nanoparticles and possible climatic implications, P. Natl. Acad. Sci. USA, 107, 6634– 6639, 2010.

Su, H., Rose, D., Cheng, Y. F., Gunthe, S. S., Massling, A., Stock, M., Wiedensohler, A., Andreae, M. O., and Pöschl, U.: Hygroscopicity distribution concept for measurement data analysis and modeling of aerosol particle mixing state with regard to hygroscopic growth and CCN activation, Atmos. Chem. Phys., 10, 7489-7503, doi:10.5194/acp-10-7489-2010, 2010.

Formatted: English (U.S.)

Tuch, T. M., Haudek, A., Müller, T., Nowak, A., Wex, H., and Wiedensohler, A.: Design and performance of an automatic regenerating adsorption aerosol dryer for continuous operation at monitoring sites, Atmos. Meas. Tech., 2, 417-422, doi:10.5194/amt-2-417-2009, 2009.

Wang, Z. B., Hu, M., Wu, Z. J., and Yue, D. L., Reaserch on the formation mechanism of new particles in the atmosphere, Acta Chim. Sinica, 71, 519–527, 2013a.

Wang, Z. B., Hu, M., Sun, J. Y., Wu, Z. J., Yue, D. L., Shen, X. J., Zhang, Y. M., Pei, X. Y., Cheng, Y. F., and Wiedensohler, A.: Characteristics of regional new particle formation in urban and regional background environments in the North China Plain, Atmos. Chem. Phys., 13, 12495-12506, doi:10.5194/acp-13-12495-2013, 2013b.

Wehner, B., Petäjä, T., Boy, M., Engler, C., Birmili, W., Tuch, T., Wiedensohler, A., and Kulmala, M.: The contribution of sulfuric acid and non-volatile compounds on the growth of freshly formed atmospheric aerosols, Geophys. Res. Lett., 32, L17810, doi:10.1029/2005gl023827, 2005.

Wehner, B., Berghof, M., Cheng, Y. F., Achtert, P., Birmili, W., Nowak, A., Wiedensohler, A., Garland, R. M., Pöschl, U., Hu, M., and Zhu, T.: Mixing state of nonvolatile aerosol particle fractions and comparison with light absorption in the polluted Beijing region, J. Geophys. Res., 114, D00G17, doi:10.1029/2008JD010923, 2009.

Wiedensohler, A., Orsini, D., Covert, D. S., Coffmann, D., Cantrell, W., Havlicek, M., Brechtel, F. J., Russell, L. M., Weber, R. J., Gras, J., Hudson, J. G., Litchy, M.: Intercomparsion study of the size-dependent counting efficiency of 26 condensation particle counters, Aerosol Sci. Technol., 27, 224–242, 1997.

Wiedensohler, A., Cheng, Y. F., Nowak, A., Wehner, B., Achtert, P., Berghof, M., Birmili, W., Wu, Z. J., Hu, M., Zhu, T., Takegawa, N., Kita, K., Kondo, Y., Lou, S. R., Hofzumahaus, A., Holland, F., Wahner, A., Gunthe, S. S., Rose, D., Su, H., and Poschl, U.: Rapid aerosol particle growth and increase of cloud condensation nucleus activity by secondary aerosol formation and condensation: A case study for regional air pollution in northeastern China, J. Geophys. Res., 114, D00G08, doi:10.1029/2008JD0101884, 2009.

Wiedensohler, A., Birmili, W., Nowak, A., Sonntag, A., Weinhold, K., Merkel, M., Wehner, B., Tuch, T., Pfeifer, S., Fiebig, M., Fjaraa, A. M., Asmi, E., Sellegri, K., Depuy, R., Venzac, H., Villani, P., Laj, P., Aalto, P., Ogren, J. A., Swietlicki, E., Williams, P., Roldin, P., Quincey, P., Huglin, C., Fierz-Schmidhauser, R., Gysel, M., Weingartner, E., Riccobono, F., Santos, S., Gruning, C., Faloon, K., Beddows, D., Harrison, R., Monahan, C., Jennings, S. G., O'Dowd, C. D., Marinoni, A., Horn, H. G., Keck, L., Jiang, J., Scheckman, J., McMurry, P. H., Deng, Z., Zhao, C. S., Moerman, M., Henzing, B., de Leeuw, G., Loschau, G., and Bastian, S.: Mobility particle size spectrometers: harmonization of technical standards and data structure to facilitate high quality long-term observations of atmospheric particle number size distributions, Atmos. Meas. Tech., 5, 657–685, doi:10.5194/amt- 5-657-2012, 2012.

Wiedensohler, A., Birmili, W., Putaud, J. P., and Ogren, J.: Recommendations for Aerosol Sampling, Aerosol Science: Technology and Applications, John Wiley & Sons, Ltd, 45-59, 2013.

Wu, Z., Hu, M., Liu, S., Wehner, B., Bauer, S., Maßling, A., Wiedensohler, A., Petäjä, T., Dal Maso, M., Kulmala, M.: New particle formation in Beijing, China: Statistical analysis of a 1-year data set, J. Geophys. Res., 112, D09209, doi:10.1029/2006JD007406, 2007.

Wu, Z. J., Poulain, L., Birmili, W., Größ, J., Niedermeier, N., Wang, Z. B., Herrmann, H., and Wiedensohler, A.: Some insights into the condensing vapors driving new particle growth to CCN sizes on the basis of hygroscopicity measurements, Atmos. Chem. Phys., 15, 13071-13083, doi:10.5194/acp-15-13071-2015, 2015.

Xu, W. Y., Zhao, C. S., Ran, L., Deng, Z. Z., Liu, P. F., Ma, N., Lin, W. L., Xu, X. B., Yan, P., He, X., Yu, J., Liang, W. D., and Chen, L. L.: Characteristics of pollutants and their correlation to meteorological conditions at a suburban site in the North China Plain, Atmos. Chem. Phys., 11, 4353-4369, doi:10.5194/acp-11-4353-2011, 2011.

Yue, D. L., Hu, M., Zhang, R. Y., Wang, Z. B., Zheng, J., Wu, Z. J., Wiedensohler, A., He, L. Y., Huang, X. F., and Zhu, T.: The roles of sulfuric acid in new particle formation and growth in the mega-city of Beijing, Atmos. Chem. Phys., 10, 4953-4960, doi:10.5194/acp-10-4953-2010, 2010.

Yue, D. L., Hu, M., Zhang, R. Y., Wu, Z. J., Su, H., Wang, Z. B., Peng, J. F., He, L. Y., Huang, X. F., Gong, Y. G., and Wiedensohler, A.: Potential contribution of new particle formation to cloud condensation nuclei in Beijing, Atmos. Environ., 45, 6070–6077, 2011.

Zhang, R., Khalizov, A., Wang, L, Hu, M., and Xu, W.: Nucleation and growth of nanoparticles in the atmosphere, Chem. Rev., 112, 1957–2011, 2012.

Zhang, S. L., Ma, N., Kecorius, S., Wang, P. C., Hu, M., Wang, Z. B., Größ, J., Wu, Z. J., and Wiedensohler, A.: Mixing state of atmospheric particles over the North China Plain, Atmos. Environ., 125, 152-164, 2016.

Zhao, C., Tie, X., Brasseur, G., Noone, K. J., Nakajima, T., Zhang, Q., Zhang, R., Huang, M., Duan, Y., Li, G., and Ishizaka, Y.: Aircraft measurements of cloud droplet spectral dispersion and implications for indirect aerosol radiative forcing, Geophys. Res. Lett., 33, L16809, doi:10.1029/2006gl026653, 2006a.

Zhao, C., Tie, X., and Lin, Y.: A possible positive feedback of reduction of precipitation and increase in aerosols over Eastern Central China, Geophys. Res. Lett., 33, L11814, doi:10.1029/2006gl025959, 2006b.

Figure 1.: Map of the ~~NCP~~North China Plain. The observational site is marked as a red point. Urban areas are marked in yellow. The green line denotes the contour line of 500 m a.s.l., which can be considered as the natural boundary of the NCP.

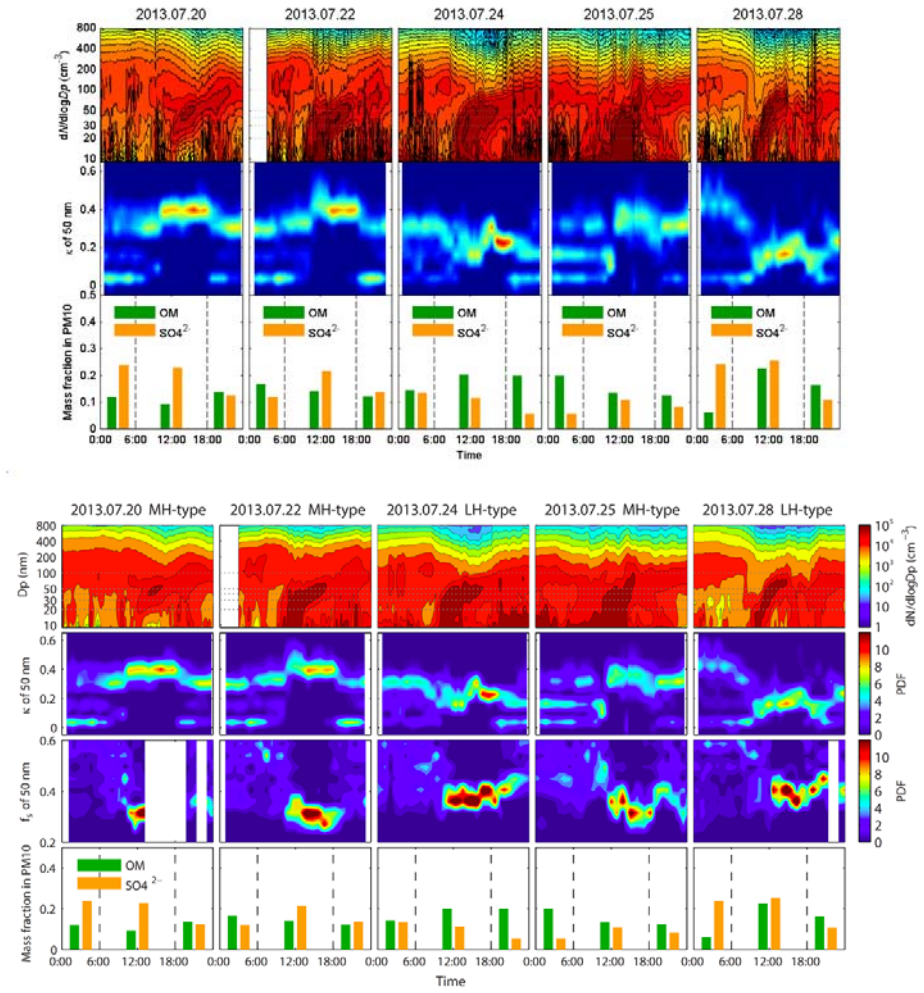

Figure 2. 5 NPF events observed during the campaign period. Subplots show the time series of particles number size distribution ~~(upper)~~, κ-PDF of 50 ~~nm particles (middle),~~ and f_s-PDF of 50 nm particles, and mass fraction of organics ~~matters~~ and sulfate from PM10 HV-sample analysis ~~(lower)~~.

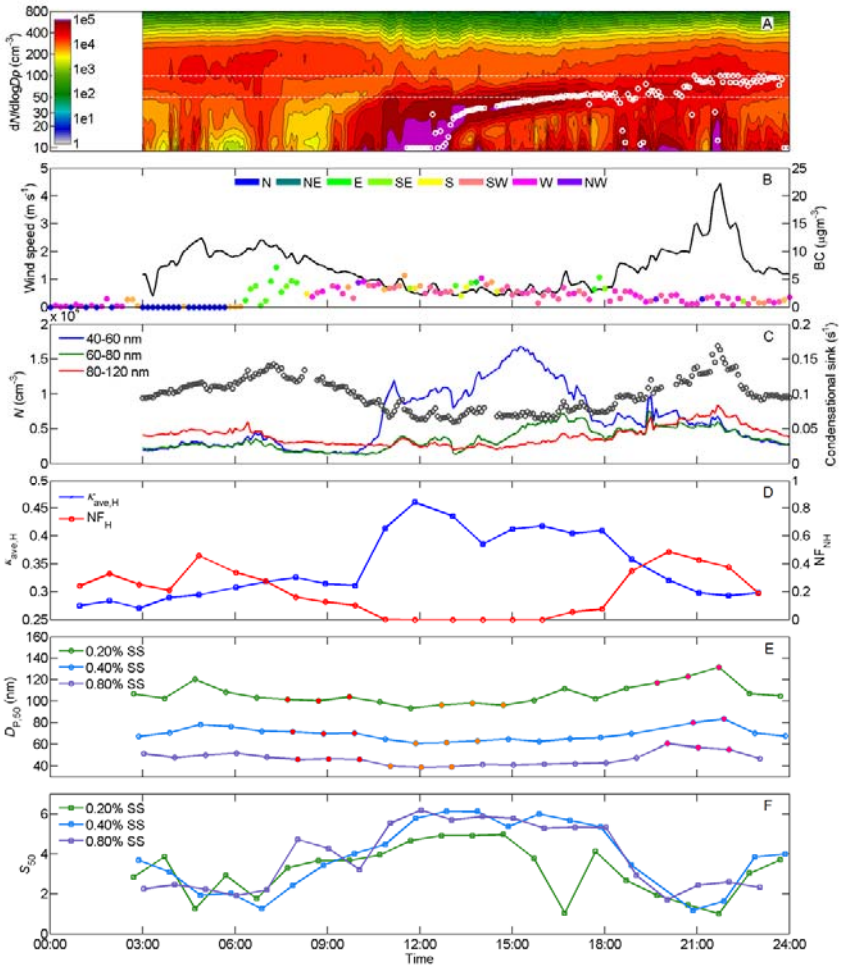
A
dN/dlogDp (cm-3)
1e5
1e4
1e3
1e2
1e1
1
B
N NE E SE S SW W NW
Wind speed (m s-1)
BC (μgm-3)
C
40-60 nm
60-80 nm
80-120 nm
N (cm-3)
x 10^4
Condensational sink (s-1)
D
λ'ave,H
NFH
λave,H
NFNH
E
0.20% SS
0.40% SS
0.80% SS
Dp,50 (nm)
F
0.20% SS
0.40% SS
0.80% SS
Ss0
00:00
03:00
06:00
09:00
12:00
15:00
18:00
21:00
24:00
Time

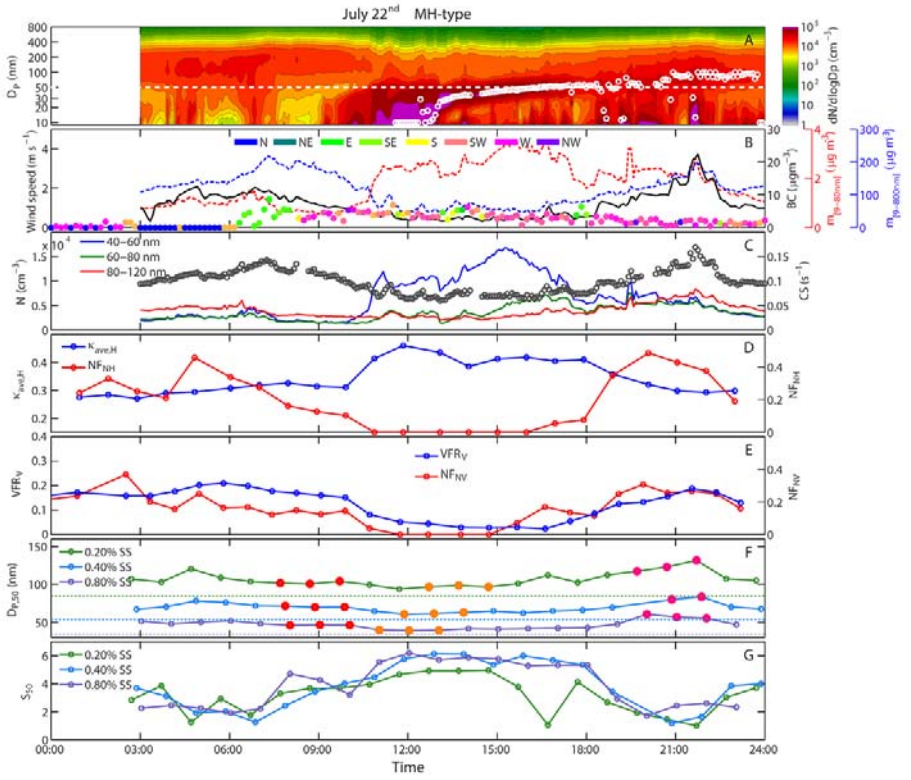

Figure 3. MH-type NPF event ~~of~~ on July 22nd. ~~(A)~~ Time series of (A) particle number size distribution and geometric mean diameter of nucleation mode ~~(A)~~, (B) wind speed/direction and ~~BC~~ the mass concentration of BC, sub-80 nm and sub-800 nm particles ~~(B)~~, (C) condensational sink (CS) and number concentration of particles in defined size ranges ~~and condensational sink (C)~~, (D) average κ of hygroscopic mode and number fraction of nearly- hydrophobic mode for 50 nm particles ~~(D)~~, (E) volume fraction remaining of volatile mode and number fraction of non-volatile mode for 50 nm particles, (~~E~~F) $D_{P,50}$ for 0.20%, 0.40% and 0.80% SS ~~(E)~~, as well as (~~F~~G) S_{50} for the three SS. The dashed lines in panel F show the theoretical critical diameters for ammonium sulfate at the three SS. ~~(F) on July 22nd.~~ Points filled with color in ~~subplot~~ panel ~~E~~ G show the records selected to calculate the average size-resolved activation ratio shown in Fig~~ure~~ 5.

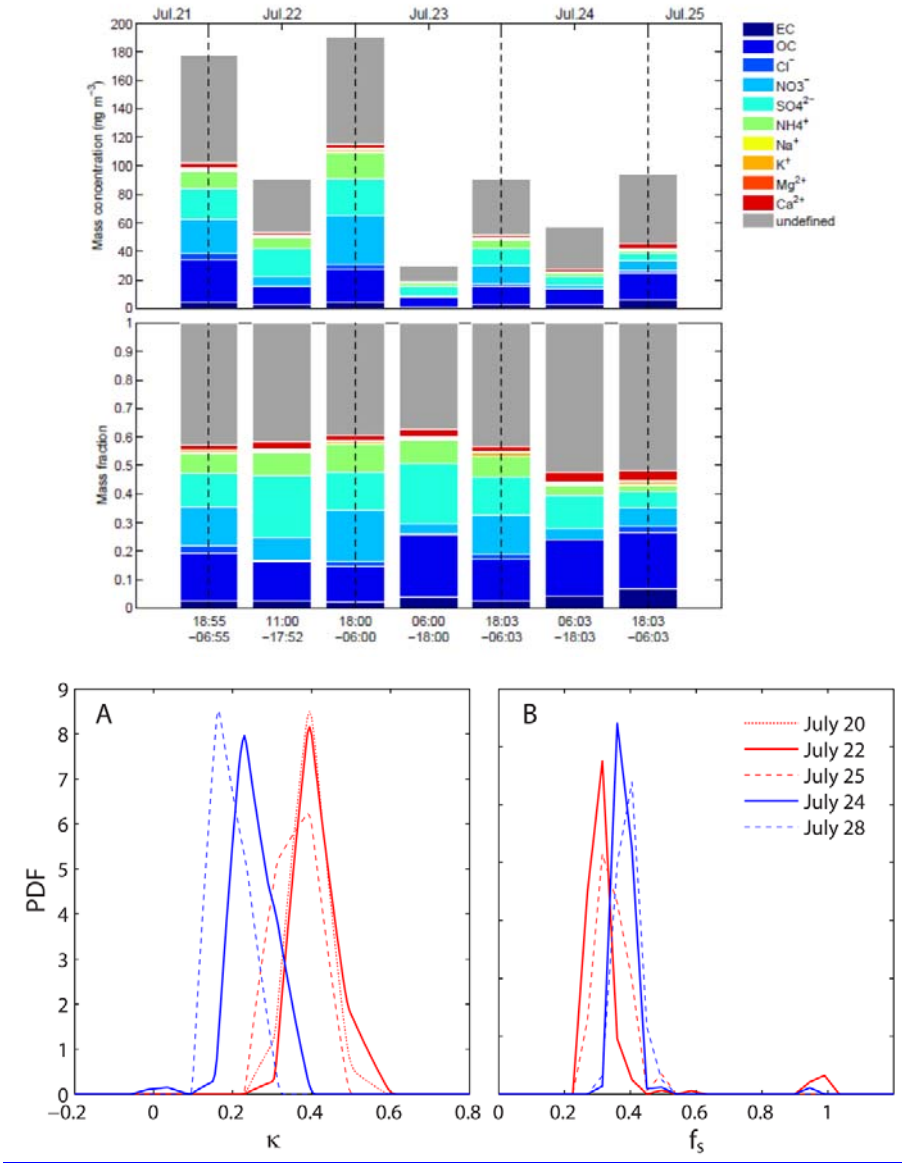
Jul.21
Jul.22
Jul.23
Jul.24
Jul.25
Mass concentration (ng m^{-3})
Mass fraction
EC
OC
Cl$^-$
NO3$^-$
SO4^{2-}
NH4$^+$
Na$^+$
K$^+$
Mg^{2+}
Ca^{2+}
undefined
18:55 −06:55
11:00 −17:52
18:00 −06:00
06:00 −18:00
18:03 −06:03
06:03 −18:03
18:03 −06:03
A
B
PDF
κ
f_s
July 20
July 22
July 25
July 24
July 28

Figure 4. Average κ-PDF (A) and f_s-PDF (B) of 50 nm particles during the 5 NPF events.~~Mass concentration and mass fraction of chemical compounds in PM10 during the two NPF events~~

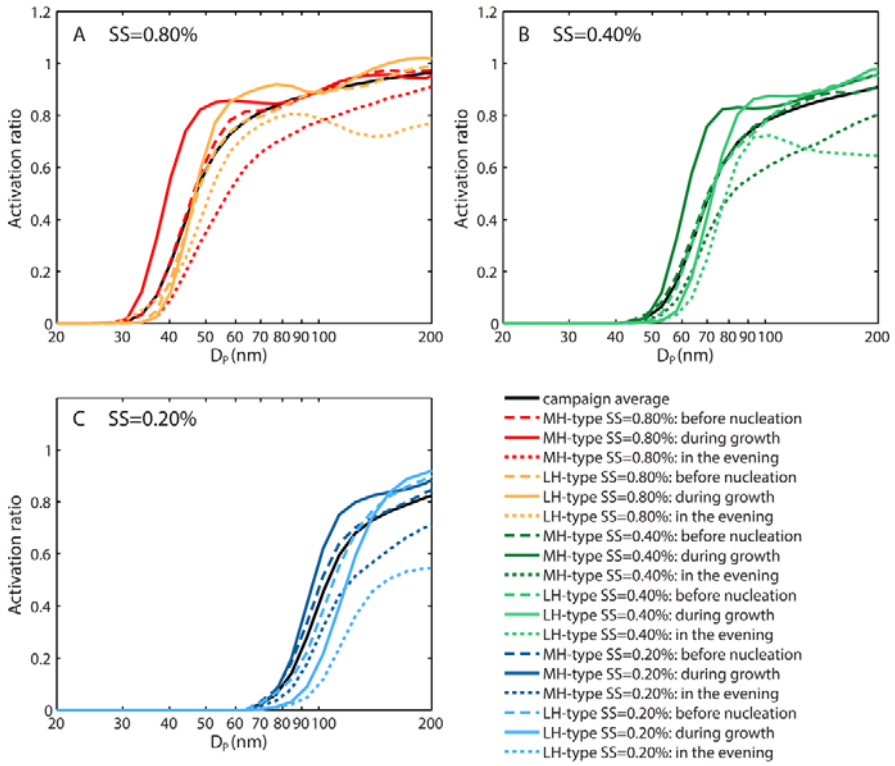
A SS=0.80%
B SS=0.40%
C SS=0.20%
Activation ratio
Dp (nm)
campaign average
MH-type SS=0.80%: before nucleation
MH-type SS=0.80%: during growth
MH-type SS=0.80%: in the evening
LH-type SS=0.80%: before nucleation
LH-type SS=0.80%: during growth
LH-type SS=0.80%: in the evening
MH-type SS=0.40%: before nucleation
MH-type SS=0.40%: during growth
MH-type SS=0.40%: in the evening
LH-type SS=0.40%: before nucleation
LH-type SS=0.40%: during growth
LH-type SS=0.40%: in the evening
MH-type SS=0.20%: before nucleation
MH-type SS=0.20%: during growth
MH-type SS=0.20%: in the evening
LH-type SS=0.20%: before nucleation
LH-type SS=0.20%: during growth
LH-type SS=0.20%: in the evening

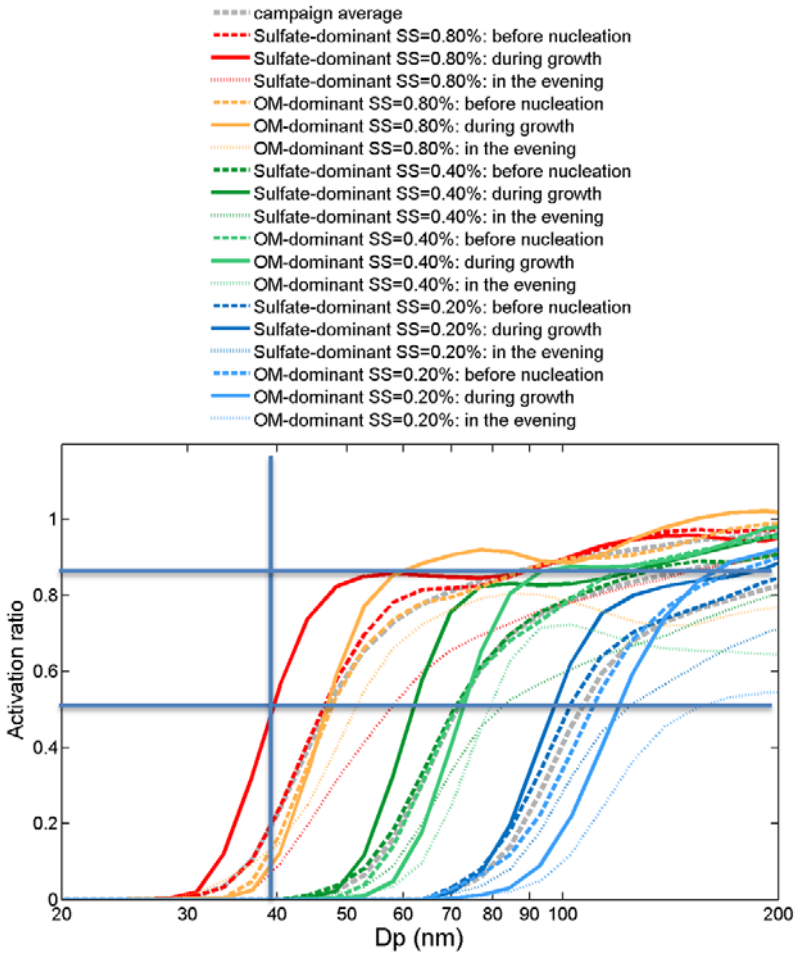

Figure 5. Average size-resolved activation ratio for the selected time periods on July 22nd and 24th

Formatted: Font: (Asian) +Body Asian (宋体)

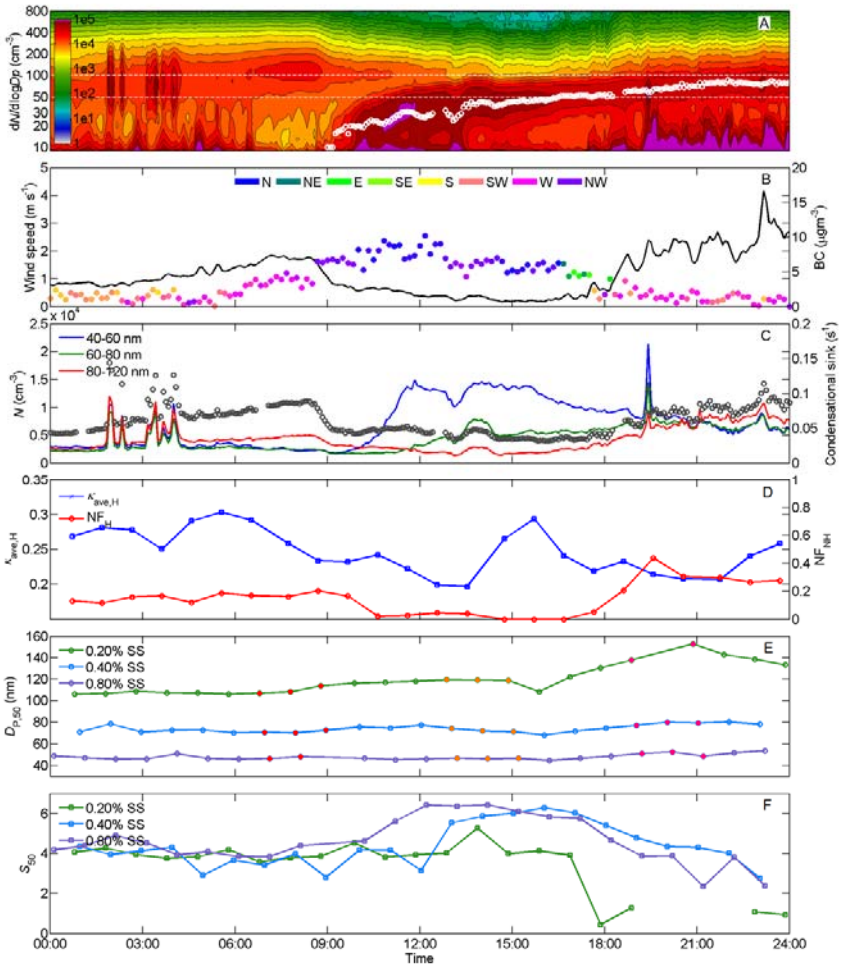
A
dW/d log Dp (cm-3)
1e5
1e4
1e3
1e2
1e1
1
B
N NE E SE S SW W NW
Wind speed (m s-1)
BC (μgm-3)
C
x 10^4
40-60 nm
60-80 nm
80-120 nm
N (cm-3)
Condensational sink (s-1)
D
κave,H
NFH
κave,H
NFNH
E
0.20% SS
0.40% SS
0.80% SS
Dp,50 (nm)
F
0.20% SS
0.40% SS
0.80% SS
S50
00:00
03:00
06:00
09:00
12:00
15:00
18:00
21:00
24:00
Time

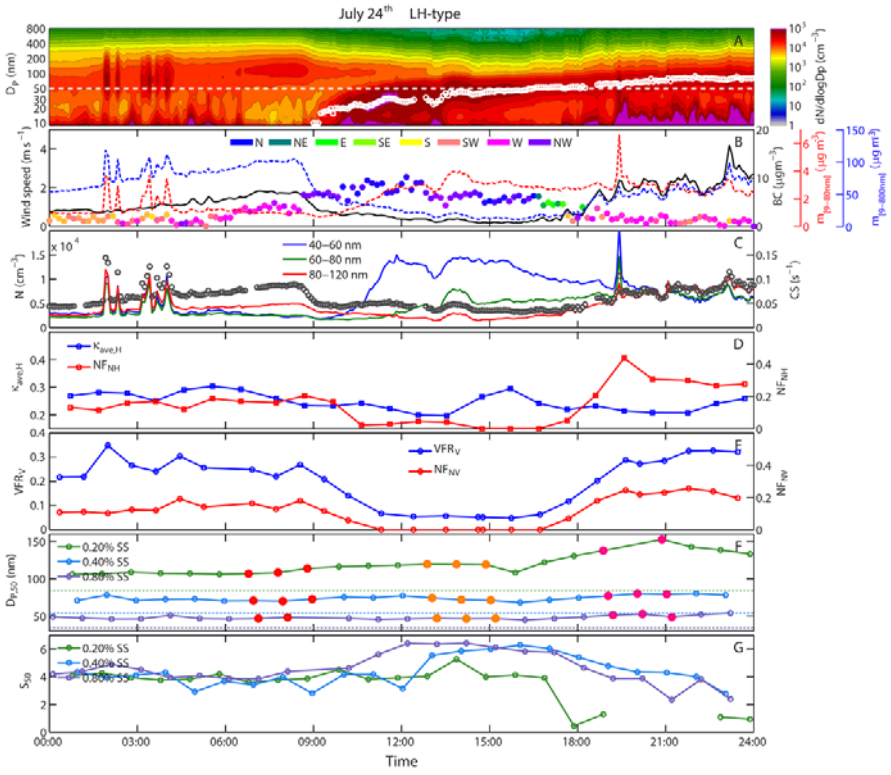

Figure 6. LH-type NPF event on July 24th. Time series of (A) particle number size distribution and geometric mean diameter of nucleation mode, (B) wind speed/direction and the mass concentration of BC, sub-80 nm and sub-800 nm particles, (C) condensational sink (CS) and number concentration of particles in defined size ranges, (D) average κ of hygroscopic mode and number fraction of nearly-hydrophobic mode for 50 nm particles, (E) volume fraction remaining of volatile mode and number fraction of non-volatile mode for 50 nm particles, (F) $D_{P,50}$ for 0.20%, 0.40% and 0.80% SS, as well as (G) S_{50} for the three SS. The dashed lines in panel F show the theoretical critical diameters for ammonium sulfate at the three SS. Points filled with color in panel G show the records selected to calculate the average size-resolved activation ratio shown in Fig. 5.~~Time series of particle number size distribution and geometric mean diameter of nucleation mode (A), wind speed/direction and BC mass concentration (B), number concentration of particles in defined size ranges and condensational sink (C), average κ of hygroscopic mode and number fraction of hydrophobic mode for 50 nm particles (D), $D_{P,50}$ for 0.20%, 0.40% and 0.80% SS (E), as well as S_{50} for the three SS (F) on July 24th. Points filled with color in subplot E show the records selected to calculate the average size-resolved activation ratio shown in Figure 5.~~

Formatted: Superscript

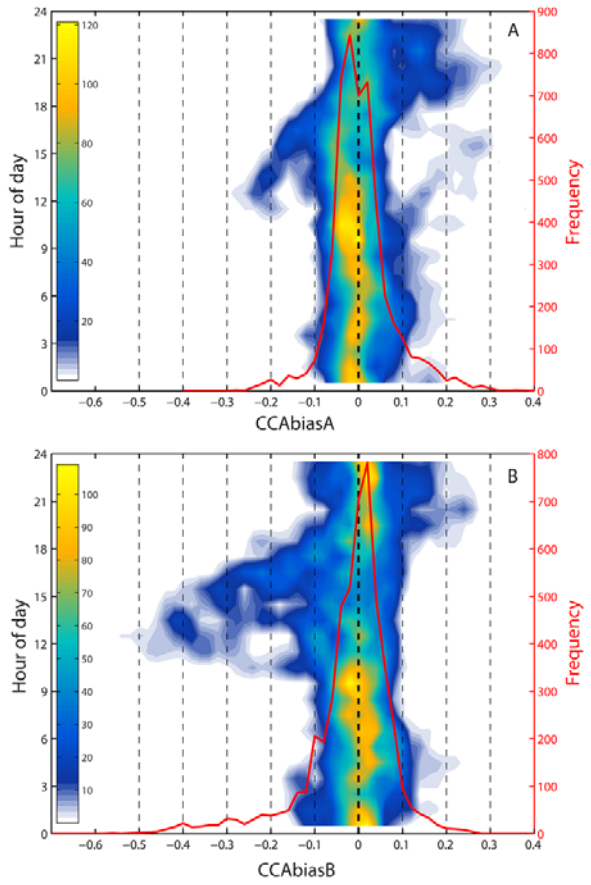
A
Hour of day
Frequency
CCAbiasA
B
Hour of day
Frequency
CCAbiasB

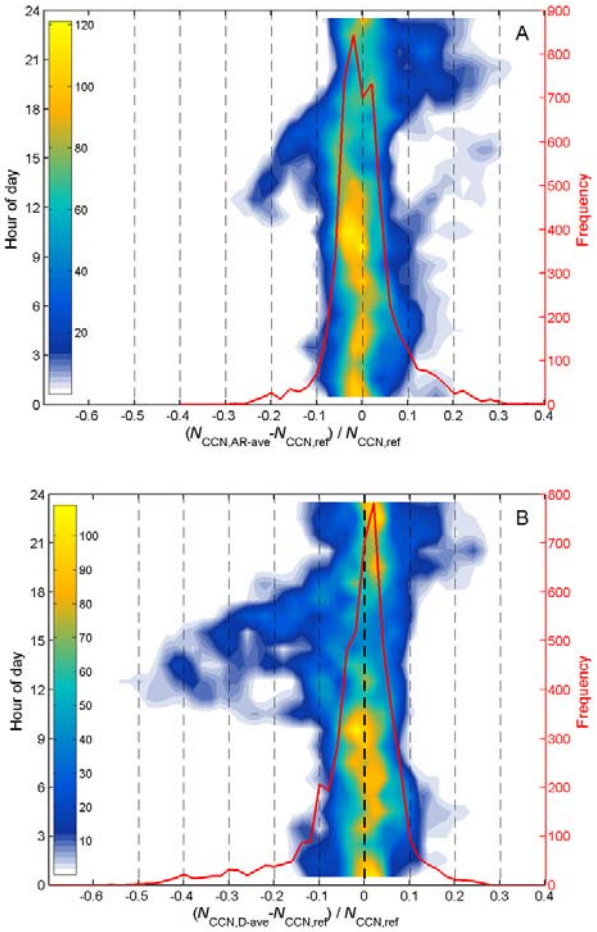

Figure 7. 2-dimensional frequency distribution (number of occurrences per interval of CCNbias and time of day, shown as contour plot) and overall frequency distribution (number of occurrences per interval of CCNbias, shown as red line) of CCNbiasA (panel A) and CCNbiasB (panel B) for the entire campaign period

~~Frequency distribution at different time of day and overall frequency distribution of the relative difference between $N_{CCN,ave}$ and $N_{CCN,real}$, and between $N_{CCN,Defi}$ and $N_{CCN,real}$~~